Generating a new electrochemical biosensing platform *via* the FTacV interrogation of a chemically and biologically functionalised gold immobilised SHIRT protein

Matthew John Weatherill

MSc by research

University of York

Chemistry

December 2024

Abstract

Biological sensors play a vital role in modern healthcare, as demonstrated by the COVID-19 pandemic. These sensors function using biorecognition elements to bind to a target analyte. *Streptococcus* High Identity Repeat Tandem (SHIRT) proteins are a group of proteins that display an impressive thermal and chemical stability, and therefore have promise as a protein scaffold which can be functionalised to produce new biorecognition elements for biosensing. The challenge in harnessing SHIRT proteins for biosensor development is finding a cheap, scalable method to detect analyte binding. This work tackles this problem by devising a strategy utilizing a chemical biology toolkit to: (1) make SHIRT redox active by labelling the protein with viologen molecules, and (2) immobilise the labelled protein onto an electrode surface for electrochemical investigations. Electrochemical characterisation of viologen-SHIRT conjugates was done using cyclic voltammetry and Fourier transformed alternating current voltammetry (FTacV). The kinetic resolution of fast electron transfer processes enabled by FTacV means that the viologen-protein electrochemistry can be interrogated in air instead of the oxygen free environments normally required. It was concluded that a more stable protein-electrode “film” is formed when viologen labelled-SHIRT is immobilised on a gold electrode *via* a C-terminal di-cysteine amino acid motif, compared to an N-terminal thiol-labelling strategy. Finally, using the method developments devised, a SH3 binding derivative of SHIRT was designed and purified and the biosensing capabilities of a viologen-labelled conjugate were proven by the observation of an electrochemical analyte-binding titration curve.

Table of Contents

List of abbreviations

2PCA	2-pyridinecarboxaldehyde
ac	Alternating current
BDD	Boron doped diamond
dCV	Direct current cyclic voltammetry
DET	Direct electron transfer
DMF	Dimethylformamide
DMSO	Dimethylsulfoxide
E. coli	*Escherichia coli*
ESI	Electrospray ionisation
EV	Ethyl viologen
FT	Fourier transform
FTacV	Fourier transformed alternating current voltammetry
GC	Glass carbon
GOx	Glucose oxidase
HIRTD	High identity repeat tandem domain
HPLC	High-performance liquid chromatography
IMAC	Immobilised-metal affinity chromatography
IR	Infrared
LB	Lysogeny broth
LC-MS	Liquid chromatography-mass spectroscopy
LFT	Lateral flow test
LPA	Lipoic acid
MS	Mass spectrometry
NHS	*N*-hydroxysuccinimide
NMR	Nuclear magnetic resonance
PAGE	Polyacrylamide gel electrophoresis
PBS	Phosphate buffered saline
PFV	Protein film voltammetry
PG	Pyrolytic graphite
SCE	Saturated calomel electrode
SDS	Sodium dodecyl sulfate
SHE	Standard hydrogen electrode
SHIRT	*Streptococcus* high identity repeat tandem
SMB	Small molecule binding

TLC	Thin layer chromatography
UV-Vis	Ultraviolet-visible
2PCA	2-pyridinecarboxaldehyde

Tables and figures

Acknowledgements

“Non est ad astra mollis e terris via.” - Seneca

The past year has been a formative experience for me, I’ve learnt so much, made many mistakes and it wouldn’t have been possible without the support of those around me. Firstly, I would like to acknowledge my supervisors Prof. Alison Parkin, Dr Christopher Spicer and Dr Michael Plevin for their role in enabling this opportunity and allowing for me to refine my scientific skills. I also want to thank the chemistry department at the University of York as a whole, especially the support staff who ensure research can be carried out smoothly. This is extended to my colleagues in the biology department at the University of York, especially to Dr Rachael Cooper who helped collect data and kindly donated protein for this project.

I would also like to extend my gratitude to those that I have worked alongside during my time at B block, you’ve all been so welcoming and allowed me to learn more about fields I had never worked in before. I’d specifically like to mention Dr Natalia Baranska, an exemplary electrochemist and all-around scientist, and Dr Nicholas Yates, a fantastic synthetic chemist able to overcome any technical problem. You were both wonderful, giving guidance and support that made me feel more confident in my own ability and for that I am thankful. Of course, I would be amiss if I didn’t mention the Parkin/Willems office, you’ve all improved my time at York, through the conversations (and laughs) we had that were often the highlight of my day and for the constant support you all have given me, I will miss not being able to work alongside you all. I want to particularly thank Alice Hewson, Morgan Batiste-Simms, Lucy Hudson, Greg McNeil, Connor Miles, Dr Lloyd Murphy, Tom Ramsey, Ella Reid and Alex Robertson, you’ve all influenced me positively in one way or another.

Finally, I am blessed to have had a loving and supportive family throughout the previous year. You taught me to work hard, to be resilient through hardship and to never lose perspective on the truly important aspects of life. I want to thank you for your constant presence and the guidance you’ve given which kept me on track until the end of this MRes.

Author Declaration

I, Matthew John Weatherill, declare that this thesis is a presentation of original work, and I am the sole author. Due to the nature of the interdisciplinary work reported, some experiments were conducted in collaboration with other researchers, such contributions are acknowledged. The work described was performed under the supervision of Prof. Alison Parkin, Dr Christopher Spicer, and Dr Michael Plevin at the University of York. This work has not previously been presented for a degree or other qualification at this University or elsewhere. All sources are acknowledged as references.

1 Biosensor technology

Biosensors are a staple of modern diagnostics, as exemplified by the recent growth in in-line diabetic blood glucose sensors and during the COVID-19 pandemic. Biosensors also play a critical role in water and waste monitoring,[1] and forensic testing. Biosensors circumvent the requirement for centralised laboratories, specialised equipment, and specialists who undertake repetitive work.[2] In healthcare settings they enable faster diagnosis for diseases and rapid monitoring of patients' health. Conventionally, many commercial sensors require the use of animal-derived antibodies, as well as suffering from a lack of binding specificity, leading to false-results.[3]

One of the most common type of biosensors are lateral flow tests (LFT's). These biosensors work *via* antigens (analyte) present in a sample binding to antibodies which are attached to nanoparticles (biorecognition element). The antigen/antibody-nanoparticles flow to a test strip which contains an antibody specific to the antigen of interest; if binding occurs, this causes a colour change at the test line (signal detection). The sample continues to flow to the control line where an antibody binds to the antibodies on the nanoparticles, this is an indication the test is functioning properly (**Figure 1**). Changing the identity of the antibodies allows for LFT's to be configured for the detection of a range of different analytes.[4]

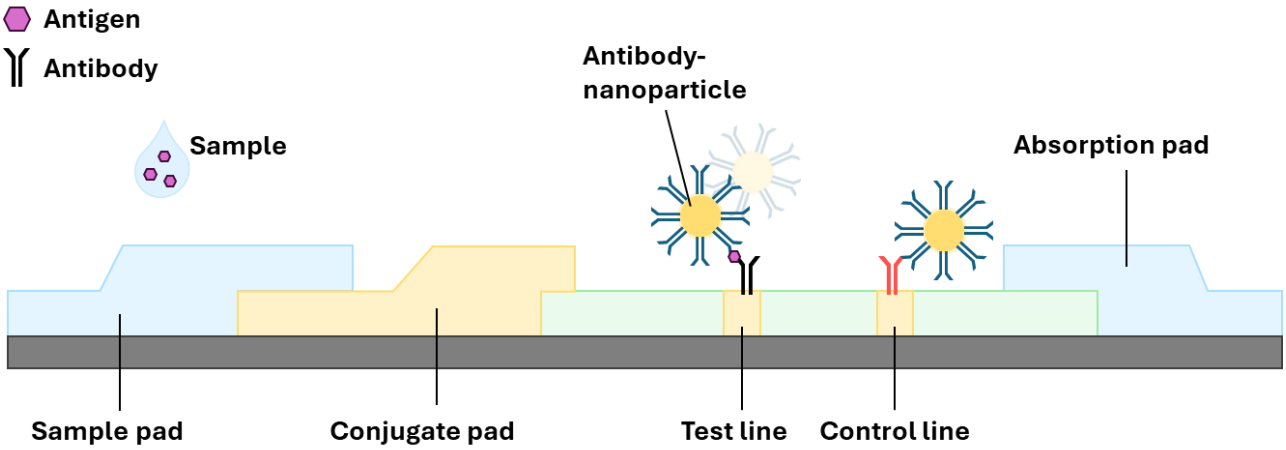

Figure 1 A generic lateral flow test (LFT). Sample is adsorbed by the sample pad and flows towards the end of the test (absorption pad) using capillary action.

The COVID-19 pandemic, where over three billion lateral flow tests (LFT's) were performed throughout 2022,[5] has led to a greater emphasis on self-testing and reporting. LFT's highlight some of the best qualities of biosensors, being a low-cost platform that's accessible and simple to use.[4] A limitation of the LFT technology is the fact that tests aren't quantitative, giving simple positive or negative test results.

1.1 Electrochemical biosensors

Electrochemical biosensors are analytical devices that convert an analyte-binding response into an electrical signal. Electrochemical sensors have come a long way over the past sixty years, being first invented by L. Clark and C. Lyons in 1965 for the detection of oxygen in blood samples.[6] In 1975 the first commercial electrochemical biosensor was developed by Yellow Spring Instruments to measure glucose levels, and throughout the 80's and 90's great progress was achieved to develop the technology further, resulting in the modern in-line continuous monitoring sensors seen today.[7,8]

The basic form of an electrochemical biosensor consists of a biological receptor having an affinity for a specific analyte; a detector known as a transducer converts physiochemical events into a current or voltage response. A signal processor then can amplify and interpret the electrical signal to produce a useable result.[2] Critically while LFT typically report a binary result, electrochemical biosensors are normally designed to quantitatively analyse the concentration of the target analyte.

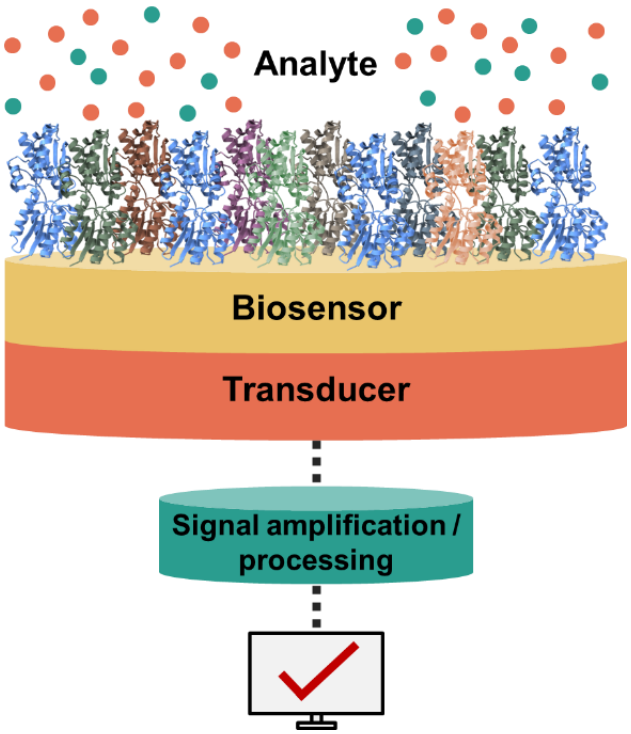

Figure 2: The generic structure of an electrochemical biosensor. Analyte binds to a recognition site, causing a physical change that's detected, via an electrochemical response at the transducer. This is then amplified into a useable signal.

Broadly, electrochemical biosensors can be subcategorised as either utilising amperometric or voltammetric biosensing methods. Amperometric sensing works by looking at the current at a fixed potential. Often this current arises from electron flux related to the oxidation or reduction of a target molecule or metabolite; the current response is therefore directly related to the concentration of analyte. Voltammetric detection looks at the current response over a changing potential window and can therefore enable more complex data processing to correct for baseline drift. These two methods can also serve as a basis for more complex techniques.[9,10] This thesis explores the utility of using Fourier transformed alternating current voltammetry (FTacV) as a electrochemical biosensing method.

1.1.1 Electrochemical biosensor biorecognition elements

The primary aim of this work is to explore the functionalisation and electrochemical interrogation of a new type of protein scaffold to work out the feasibility of developing a new electrochemical biosensor platform. It is therefore important to take into consideration the properties of existing biorecognition elements commonly used in electrochemical biosensors.

Antibodies are Y-shaped proteins that are used by the immune system to identify and elicit an immune response against a variety of antigens such as proteins, polysaccharides and nucleic acid sequences from bacteria and viruses.[11,12] In commercial biosensor technology antibodies against specific target antigens are typically derived from the serum of animals, which is incompatible with some moral belief systems. In electrochemical antibody biosensors, the antibody recognition element is commonly immobilised onto a conducting surface, and an external redox mediator (eg. $K_3[Fe(CN)_6]$) is added in solution, which can freely exchange electrons with the working electrode. When antigen binding occurs, the electron exchange between the redox mediator and electrode is hindered, resulting in a slower rate of electron transfer and a correspondingly decreased electrical current. Electrical impedance spectroscopy (EIS) is often used to measure the resistance to charge transfer which quantifies how “easy” it is for electrons to transfer between mediator and electrode, due to the inverse relationship between current and resistance.[13]

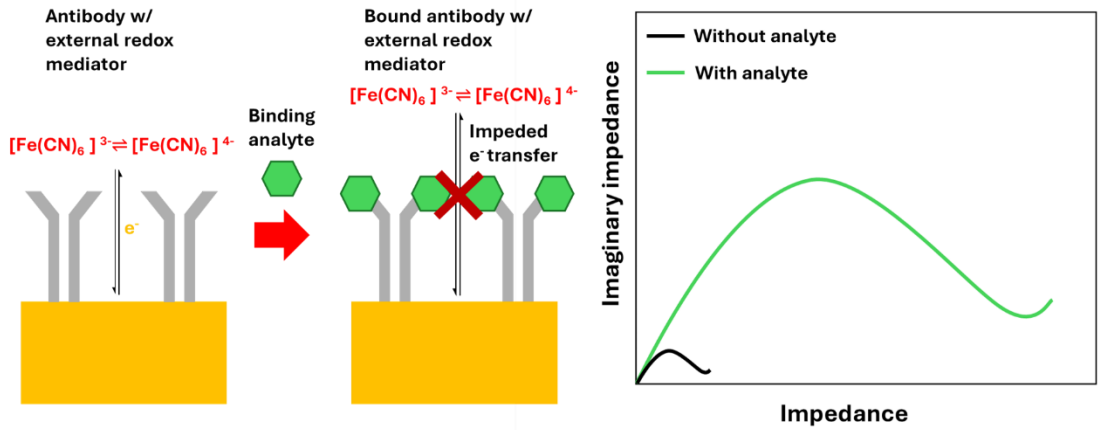

Figure 3 Example of an antibody electrochemical biosensor. (Left) The unbound antibody allows for unimpeded reduction/oxidation of the solution phase redox mediator. When analyte binding to the electrode-immobilised antibody occurs, the redox mediator is blocked from transferring electrons to/from the working electrode due to bound substrate blocking the electrode surface. (Right) An example Nyquist plot generated by EIS measurements. The impedance increases due to the analyte binding.

Aptamers are short DNA, RNA or peptide sequences that are designed *via* high-throughput screening to selectively bind to target molecules with high affinity.[14] In electrochemical aptamer biosensors, the aptamer molecular recognition element is often modified with a redox mediator molecule added at the opposite end of the aptamer sequence to the electrode immobilisation site.[15] When analyte binding occurs, the aptamer folds, bringing the redox molecule closer to the electrode surface giving rise to a greater current response because the rate of electron transfer increases as the distance between the redox mediator and electrode decreases, this is often detected using a voltammetric method (***Figure 4***).

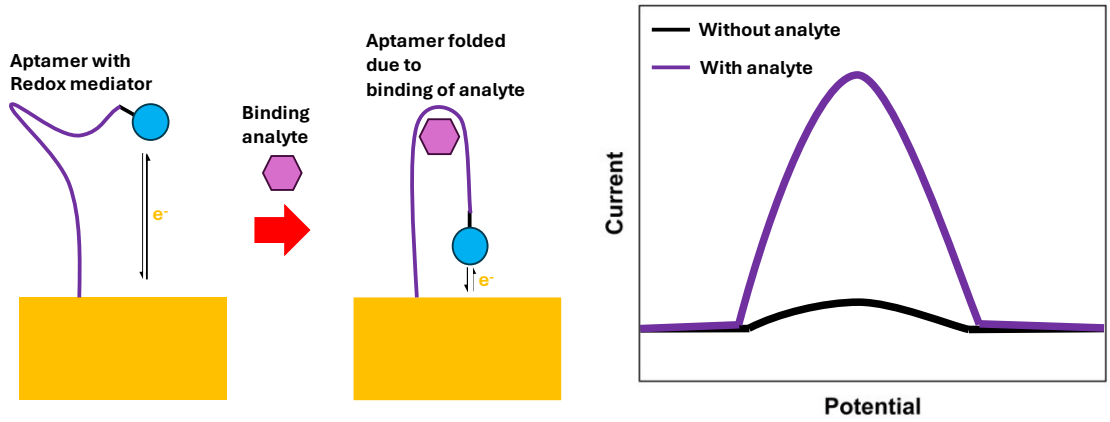

Figure 4 Example of an aptamer biosensor. (Left) The redox mediator on the aptamer is away from the electrode surface when the aptamer is in an unbound state. When analyte binding occurs, the aptamer folds and the redox mediator is brought closer to the electrode surface, this causes an increase in the current associated with electron transfer between the electrode and the mediator molecule (right).

Aptamers serve to potentially replace the more traditional use of antibodies in biosensors. This is desirable because antibodies are only applicable as bioreceptors to substances that elicit an immune response, reducing the number of potential targets and making the detection of small organic molecules particularly challenging.[16,17] Antibodies are more susceptible to environmental degradation under external stresses such as extreme pH, temperature and salt concentration, with aptamers often having extended shelf-lives compared to antibodies developed for binding of the same analyte.[18–20] One disadvantage of aptamers is that RNA aptamers suffer from degradation by nucleases in biological fluids, reducing their half-life and effectiveness.[21] Also, aptamers are susceptible to misfolding in non-aqueous solvents, meaning some industrial applications can't be pursued.[22]

1.2 High Identity Tandem Repeat Domains

1.2.1 *Streptococcus* High Identity Repeat Tandem proteins (SHIRT)

Streptococcus gordonii (*S. gordonii)* is a gram-positive, non-pathogenic bacteria found in the oral cavity as part of the typical human biofilm.[23] *S. gordonii* has been studied due to its ability to survive fluctuations in local environmental conditions and its opportunistic tendencies when spreading to non-oral sites; it has been associated with infective endocarditis, colonising the heart valves following dental procedures that cause oral bleeding.[24,25]

The surface adhesion proteins produced by *S. gordonii* play an integral role in biofilm formation. One *S. gordonii* surface adhesin protein, Sgo_0707, is a 1643 amino acid long sequence that consists of several subunits: a leader peptide, a unique N-terminal unit, a unique C-terminal unit, a LPXTF sorting motif, and a high identity repeat tandem domain (HIRTD) (***Figure 5***).[26] Tandem repeat domains are sequences with multiple, covalently attached, adjacent domains which share similar structure, ranging from a single amino acid repeat to domains consisting of hundreds of residues.[27] *Streptococcus* high identity repeat tandem (SHIRT) domains are a specific class of HIRTDs found in *Streptococcus* species. Repeated SHIRT domains regulate the distance between *S. gordonii* and the surface to which the bacteria is attached, and they are suggested to play a *in vivo* role in infection *via* the evasion of host immune systems.[28] Between repeated SHIRT domains in Sgo_0707, 90-100% of the sequence identity is conserved. [29]

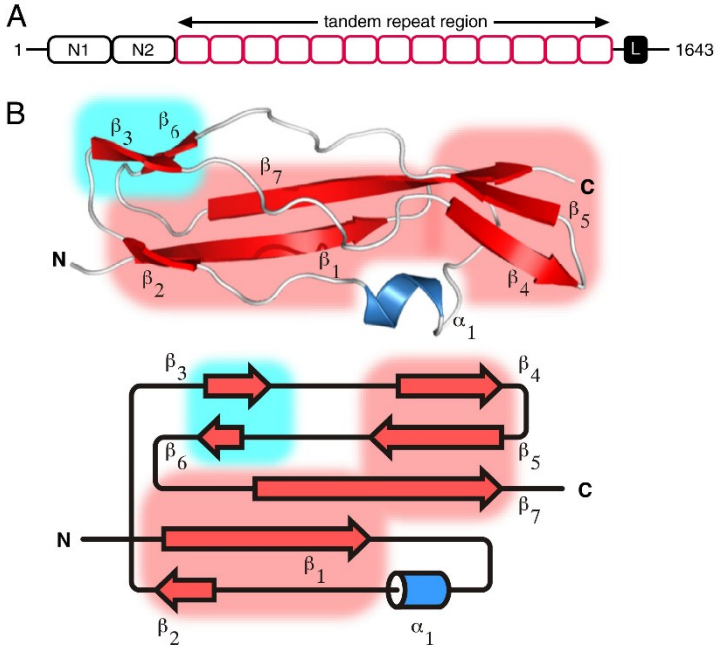

Figure 5 Scheme of Sgo_0707 showing (A) the N-terminal adhesion domains (N1 and N2), tandem repeat domains (red) and C-terminal cell-wall crosslinking motif (black box "L"). (B) HIRTD Sgo_0707 domain structure and topology. Figure reproduced from F. Whelan et al.[28]

High identity repeat tandem protein domains are rare in nature, and this is attributed to the idea that it should be unfavourable due to the high likelihood of misfolding between domains on separate repeat units causing aggregation.[30] Conversely, SHIRT monomers and dimers display high stability with: (i) a thermal transition point of 75.6 ˚C, (ii) a high refolding efficiency of ~90 % after being heat-cycled to thermal denaturation ten times, and (iii) wide-ranging solvent stability, being able to withstand buffers with high salt concentration (>3 M NaCl) and tolerating high percentages of organic solvents (~50% organic solvent).[31] An isolated SHIRT monomer protein displays an elongated rod-like structure with a unique topology where the C and N-termini that are spatially opposite to one another.

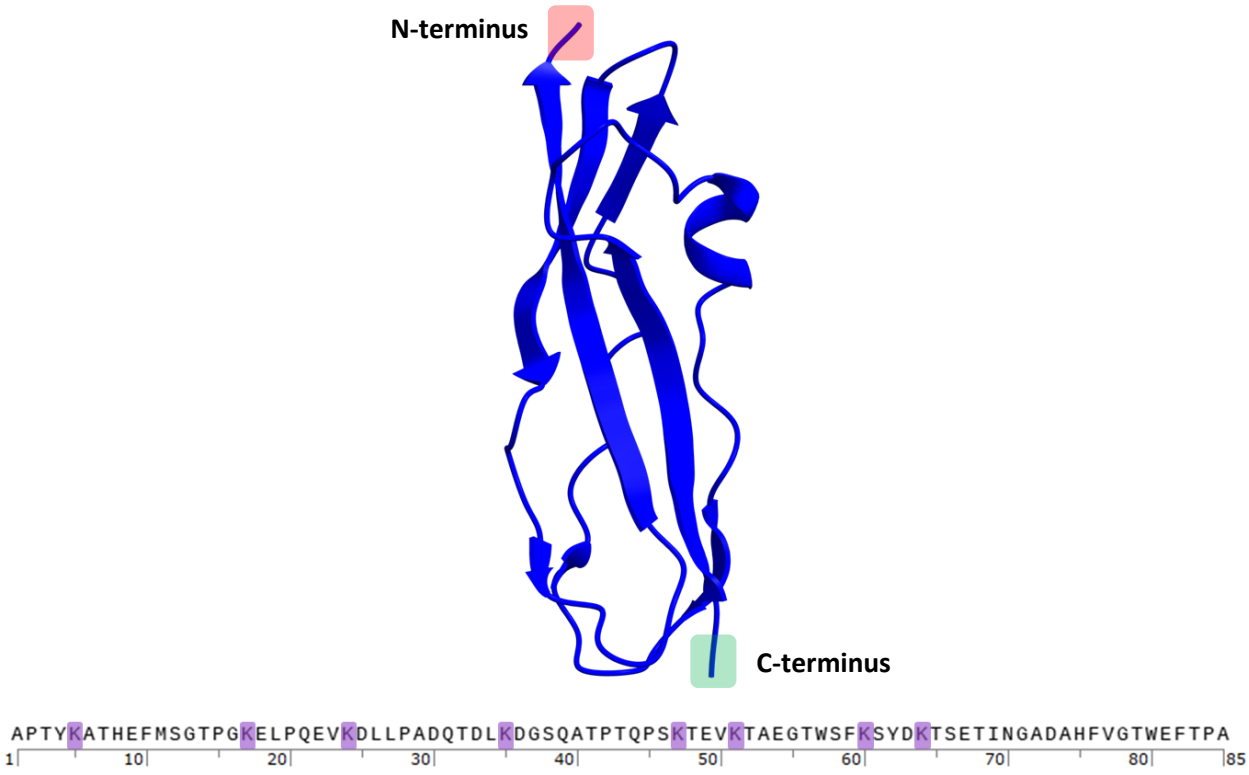

Figure 6 (Top) Single domain of SHIRT protein crystal structure 7AVH with C- (Red) and N- (Yellow) termini highlighted. (Bottom) Amino acid sequence of SHIRT with lysine residues highlighted in purple. PDB DOI: https://doi.org/10.2210/pdb7AVH/pdb

The Plevin group at York have been investigating the possible use of SHIRT as a scaffold for developing new biosensor biorecognition elements: the native high structural stability suggests it would be suitable for applications in industrial biotechnology under harsh chemical environments such as those which persist in biofuel production plants;[32] unlike antibodies, the development of new SHIRT analyte-binding constructs would not require animal testing.[33] Recent developments in the Plevin lab at York include site-directed mutagenesis to insert peptide loops onto the outside of SHIRT structures to enable protein binding. SRC Homology

3 domains (SH3) are a small protein domain associated with signal cascades and implicated in the development of multiple diseases and are of interest due to the development of aSH3 binding loop variant of SHIRT, with SH3 binding being proven with surface plasmon resonance (SPR) and quartz crystal microbalance with dissipation monitoring (QCM-D) evidence.[34] In these experiments, protein immobilisation onto a solid-state material was facilitated *via* the introduction of a C-terminal di-cystine amino acid (CGGC) motif. The Plevin group have also designed and constructed SHIRT proteins containing small organic molecule internal binding pockets, with nuclear magnetic resonance (NMR) evidence proving successful indole binding in these small molecule binding constructs.

The limitation in the ongoing SHIRT research is that the current methods for the detection of analyte binding (NMR, SPR, QCM-D) are expensive and not mobile, requiring centralised specialised equipment, with a low throughput and a requirement for specialised operators. Therefore, the aim of this project is to develop a cheap, rapid and scalable method for the detection of analyte-binding to SHIRT-based biorecognition elements.

1.3 Electrochemically active proteins

Throughout nature, proteins make use of redox-active centres to facilitate electron transfer in biological processes including respiration,[35] photosynthesis,[36] metabolism, signalling cascades[37] and chemical catalysis.[38] It's estimated about half of all proteins are metalloproteins,[39,40] and several classes of metal centres (e.g. hemocyanin's copper site and ferredoxin's iron-sulphur cluster) can facilitate electron transfer as well as several organic cofactors (e.g. NADH/NAD^+ and quinones).[41] The thermodynamics and kinetics of electron-transfer to/from a protein-confined redox centre is dependent on the structure of the cofactor, with electron tunnelling thought to occur through the protein structure.[42] Because of the biological importance of protein electron-transfer, bioelectrochemical techniques have been developed as a mechanistic toolkit. The aim of this project is to explore if an electrochemically active version of SHIRT can be created to enable the electrochemical detection of analyte binding.

1.3.1 Design strategy for redox active SHIRT

Over the past couple of decades, significant efforts have been made to develop artificial redox proteins that have high structural stability and tuneability.[42] In these studies, heme centres and other metallic electron transfer sites are typically engineered into a computationally designed protein scaffold to generate a so-called “artificial” protein.[43,44] Such approaches can require the use of multiple plasmids in a heterologous fashion to ensure correct metal cofactor incorporation. *De novo* design is complex, with the necessary computational tools for designing artificial protein metal scaffolds still under active development.[45,46] Therefore, it was determined that this project would attempt to make a redox-active SHIRT *via* the chemical labelling of a purified SHIRT protein instead of *in vivo* incorporation of biological redox cofactors. This chemical labelling approach also seemed a more straightforward way to develop the existing Plevin group SHIRT-analyte binding protein designs into an electrochemical biosensor.

1.4 Protein film electrochemistry

Since the aim of this project is to try and develop a SHIRT-based electrochemical biosensor *via* production of a redox-labelled SHIRT construct, the methods of detecting protein electron transfer must be considered. In protein film electrochemistry, protein is immobilised onto a working electrode surface, removing diffusion factors associated with solution measurements. There are two key types of measurements used in this thesis and the general theory of these methods is outlined below.

1.4.1 Cyclic voltammetry (CV)

Cyclic voltammetry (CV) is one of the most widely used electrochemical experiment types. In CV, the applied potential at the working electrode is linearly swept with respect to time, going between two potentials, E_{start} and $E_{reverse}$ (***Figure 7***). The rate at which this potential is changed is known as the scan rate (υ). Prior to any measurement, the potential is often held at E_{start} for a period of time to ensure the system is at equilibrium.

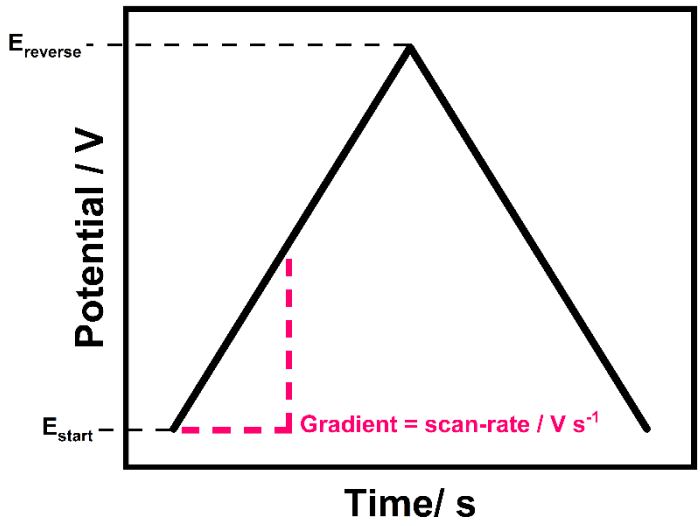

Figure 7 Potential waveform that is applied to the working electrode during a cyclic voltammetry experiment. Gradient line showing scan-rate is shown in red.

Throughout a CV experiment, the current that flows at the working electrode is plotted against the potential that is applied, producing a graph known as a cyclic voltammogram. The current is made up of two contributions: (i) the capacitive (non-Faradaic) current, caused by the net movement of ions in solution towards or away from the electrode surface, and (ii) the Faradaic current, due to a species donating or withdrawing electrons from the electrode. For an electrode covered with a film of redox-active protein, any redox-active sites undergoing reversible redox chemistry would give a corresponding reductive peak (negative current) and oxidative peak (positive current). Such Faradaic current signals are often isolated from the non-Faradaic current *via* a baseline subtraction, as shown in **Figure *8***.

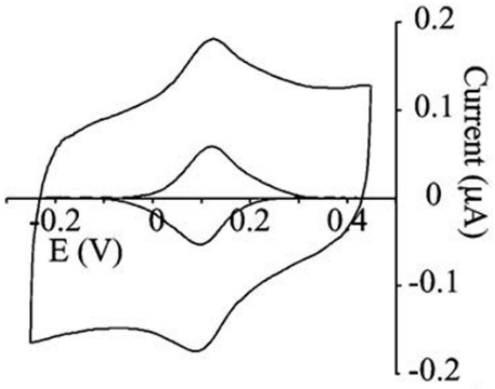

Figure 8 CV response of azurin from Pseudomonas aeruginosa on a gold electrode modified with decanethiol. The total current response is shown by the larger signal, and the baseline-subtracted Faradaic-only are the peaks centred about the zero-y-axis line. Figure is reproduced from Biochimica et Biophysica Acta – Bioenergetics, Volume 1757, J. Hirst, pages 225-239, 2006, with permissions from Elsevier. Any further inquiries/permissions regarding this figure should be directed to Elsevier.

1.4.1.1Analysing protein film CV under thermodynamic control

For a redox protein immobilized onto an electrode surface the origin of the peak-like shape of the electron transfer (Faradaic) current signal can be derived from the Nernst equation. First, the surface confined electron transfer process is defined as in **Equation 1**.

$$Ox_{(immob.)} + ne^-_{(electrode)} \underset{k_{(ox)}}{\overset{k_{(red)}}{\rightleftharpoons}} Red^{n-}_{(immob.)} \qquad \textit{Equation 1}$$

$Ox_{(immob.)}$ = Oxidised species of the immobilized redox couple.
$Red^{n-}_{(immob.)}$ = Reduced species of the immobilized redox couple.
n = Number of electrons transferred.
$e^-_{(electrode)}$ = Electron that originates from the electrode.
$k_{(ox)}$ = Rate constant for oxidation of reduced species.
$k_{(red)}$ = Rate constant for reduction of oxidised species.

Current is proportional to the rate of change of concentration of the charged species at the surface of the electrode and because the species of interest is immobilised there is no mass transport to account for, resulting in **Equation 2**.[47]

$$i = -nFA\frac{d\Gamma_{Red^{n-}_{(immob.)}}}{dt} = nFA\frac{d\Gamma_{Ox_{(immob.)}}}{dt}$$ ***Equation 2***

$i =$ Current at the electrode / A
$n =$ Number of electrons transferred by redox couple.
$F =$ Faraday's constant / C s^{-1} mol^{-1}
$A =$ Electrode surface area
$\Gamma =$ Surface concentration
$t =$ Time / s
$Ox_{(immob.)} =$ Oxidised species of the immobilized redox couple.
$Red^{n-}_{(immob.)} =$ Reduced species of the immobilized redox couple.

At sufficiently slow scan rates, it can be assumed that the redox reaction is at equilibrium, and therefore the ratio of oxidised to reduced species at each applied potential can be described by the Nernst equation, **Equation 3.**

$$E_{app} = E^0_{(Ox/Red)} - \left(\frac{RT}{nF}\right) ln\left(\frac{\Gamma_{Red^{n-}_{(immob.)}}}{\Gamma_{Ox_{(immob.)}}}\right)$$ ***Equation 3***

E_{app} Electrode potential / J C^{-1}
$E^0_{(Ox/Red)} =$ Standard potential for redox couple / J C^{-1}

Equation 4 can be stated as:

$$\Gamma_{Total_{(immob.)}} = \Gamma_{Red^{n-}_{(immob.)}} + \Gamma_{Ox_{(immob.)}}$$ ***Equation 4***

Substituting **Equation 4** into **Equation 3** yields **Equation 5**.

$$\Gamma_{Red^{n-}_{(immob.)}} = \frac{\Gamma_{Total_{(immob.)}}}{1 + e^{\left(nF(E - E^0_{(Ox/Red)})/RT\right)}}$$ ***Equation 5***

When **Equation 5** is substituted into **Equation 2**, this gives **Equation 6**

$$i = \upsilon\left(\frac{n^2F^2A\Gamma_{total}}{RT}\right)\left(\frac{e^{\left(\frac{nF\left(E - E^0_{(Ox/Red)}\right)}{RT}\right)}}{\left[1 + e^{\left(\frac{nF\left(E - E^0_{(Ox/Red)}\right)}{RT}\right)}\right]^2}\right)$$ ***Equation 6***

$\upsilon =$ Scan rate / J C^{-1} s^{-1}

Thus, for an ideal protein-film system under equilibrium conditions the peak current is proportional to the square of the number of electrons involved (n^2) and scan rate (υ).

1.4.1.2 Analysing protein film CV under kinetic control

At sufficiently fast scan rates, a CV experiment will no longer be under thermodynamic control. For a protein film doing electron transfer, an increasing separation of redox peaks with increasing scan rate is observed. The redox peak position is typically analysed using an equation derived from the Butler-Volmer equation and first defined by Laviron (**Equation 7**).[48,49] Thus, for a surface immobilised redox protein, a plot of $E_p - E^0$ against ln(υ), can be used to determine the charge-transfer coefficient (α) and rate constant (k^0).

$$E_p = E^0_{(Ox/Red)} \pm \left(\frac{RT}{n\alpha F}\right) ln\left(\frac{n\alpha F v}{k^0 RT}\right) \qquad \textit{Equation 7}$$

$E_p =$ Electrode potential of peak anodic/cathodic peak / J C^{-1}
$E^0_{(Ox/Red)} =$ Standard potential for redox couple / J C^{-1}
$i =$ Current at the electrode / A
$n =$ Number of electrons transferred by redox couple.
$R =$ Gas constant / J mol^{-1} K^{-1}
$T =$ Temperature / K
$F =$ Faraday's constant / C s^{-1} mol^{-1}
$\alpha =$ Charge-transfer coefficient
$k^0 =$ Formal rate constant / s^{-1}
$\upsilon =$ Scan rate / J C^{-1} s^{-1}

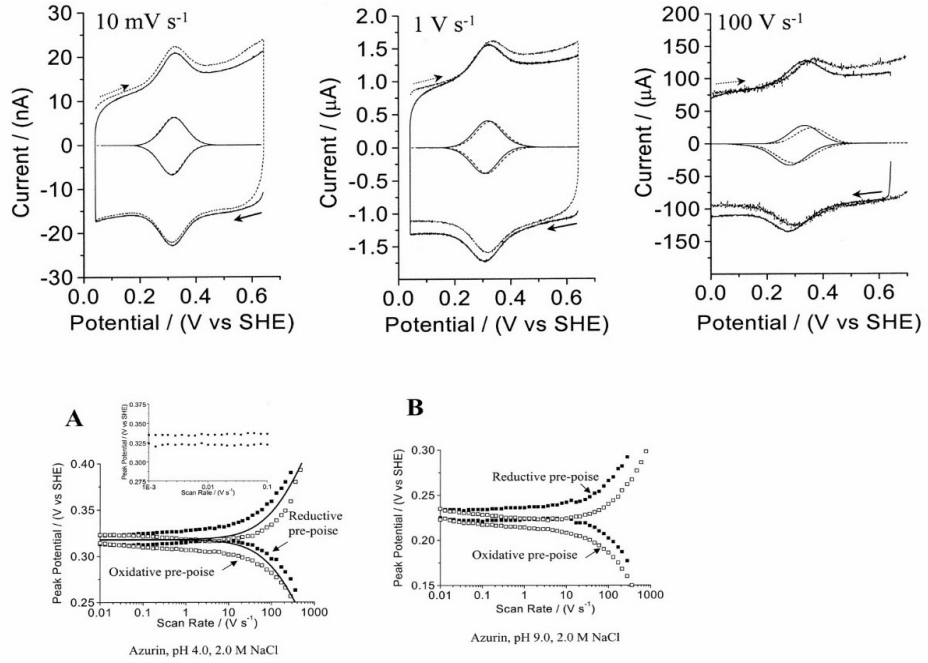

Figure 9 (Top) CV's of a protein film of the blue-copper protein azurin measured at different scan rates. The total current response and the extracted Faradaic-only background subtracted data is shown. (Bottom) Corresponding plots of peak potential positions as a function of log scan-rate, known as a "trumpet plot", from azurin experiments measured at different pH's.). This figure was reproduced from F. A. Armstrong, et al.[49]

1.4.2 Large amplitude Fourier transformed alternating current voltammetry (FTacV)

Fourier transformed alternating current voltammetry (FTacV) is a relatively new electrochemical method that the Parkin group at York are developing for bioelectrochemistry as an alternative method to CV. [50–57]

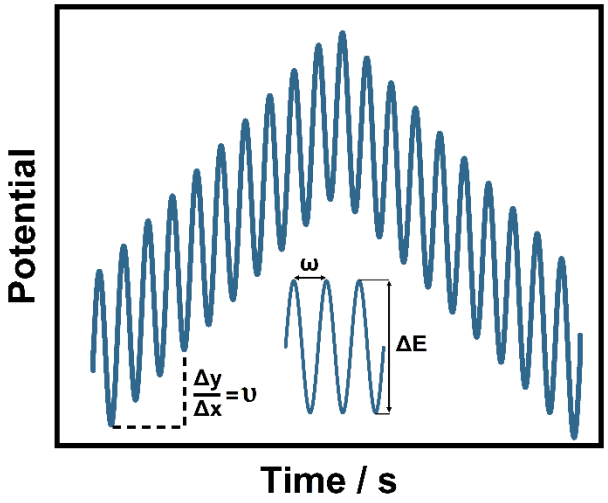

Figure 10 Potential waveform that is applied to the working electrode during a FTacV experiment. An experimentalist must select the frequency (ω) and amplitude (ΔE) of the superimposed sinusoid wave of FTacV as well as the linear scan-rate (υ) and potential range of the cyclic linear ramp.

FTacV functions by the superimposition of a typical CV linear potential-time waveform with a sinusoidal waveform (**Figure 10**).[58] The technique retains the linear scan-rate (υ) and potential window ($E_{start} \rightarrow E_{reverse}$) parameters seen in CV; the frequency (ω) and amplitude (ΔE) of the sine wave are additional experimental parameters. The method works because the large amplitude of the sine wave induces a non-linear current response which is recorded and then Fourier-transformed (FT), generating a power-spectrum representing the current contributions at linearly scaled integer-multiples of the input sinusoid frequency.[59] Band selection of regions containing real current responses are picked and individually inverse Fourier-transformed (iFT) producing current-time outputs called the n^{th} harmonic dependant on the integer scaling factor (n) applied to the inputted frequency (ω).[59] **Figure 29** in **Section 2.3.4** illustrates this. FTacV can be analysed to extract thermodynamic information, shown by the potential where electron-transfer occurred, and kinetic information, derived from the relationship between the signal intensity and harmonic frequency. FTacV allows for the separation of non-Faradaic processes from Faradaic ones, and the Faradaic current contributions can be further separated to discriminate between rapid redox (e.g. reversible electron transfer from proteins)

and slow redox processes (e.g. O_2 reduction).[51] This signal separation is possible because slow electron processes (e.g. non-Faradaic current) can keep up with the underlying "slow" linear potential ramp, but not the sinusoidal wave, due to it being too rapid a change for the processes to respond to. Fast electron processes can keep up with both the "slow" linear potential ramp and the rapid potential change of the sinusoidal oscillation, meaning only current response from rapid electron transfer processes contributes to the higher harmonics.

1.5 Summary and aims

The aim of this Master's project was to use bioconjugation techniques to attach a redox mediator to SHIRT, to turn it into an artificial redox protein, so that electrochemical measurements can be used to detect analyte binding to SHIRT constructs which have been developed by the Plevin group to selectively bind to SH3 proteins. To enable this, it was necessary to immobilise the redox-active SHIRT onto an electrode surface; I therefore also investigated strategies to immobilise SHIRT directly onto gold electrodes. Data are presented that provides evidence for immobilization of redox-active SHIRT onto gold surfaces *via* both the C- and N-terminus. Finally, utilising a redox-labelled SH3 binding mutant of SHIRT and a novel FTacV strategy, the first electrochemical biosensor SHIRT measurements were performed.

2 Viologen modified SHIRT and immobilization onto gold surfaces

2.1 Introduction

This chapter describes initial investigations into (i) functionalization of 'wild type' *Streptococcus* High Identity Repeat Domain (SHIRT) protein monomers to produce redox-active SHIRT, and (ii) comparison of the effectiveness of two possible electrode-immobilisation strategies.

2.1.1 Redox-labelling SHIRT

As described earlier (Section 1.2), SHIRT proteins are thought to perform a purely structural role in nature and therefore do not naturally incorporate either a chromophore or redox-active cofactor. The modification of a protein with redox active molecules to allow for electrochemical detection has little precedence in the literature, however, there are a substantial number of chemical biology methods to enable site selective covalent ligation to protein amino acids, and these can be adapted to install a redox functionality. Furthermore, as outlined in Chapter 1, in the aptamer electrochemical biosensor field the redox labelling of nucleic and amino acid sequences is commonly used to develop electrochemical biosensors.[60,61]

2.1.2 Amino-acid targeted ligation

There is an extensive list of strategies for residue-selective bioconjugation to amino acids.[62–69] The commonly targeted functional groups include amines, $-NH_2$ (lysine, N-terminus); carboxylic acids, -COOH (aspartic acid, glutamic acid, C-terminus); thiols, -SH (cysteine); and aldehydes, -CHO (created by oxidation). Deciding which amino acid to modify is dependent on the prevalence, position and the functionality that is desired from the bioconjugation. In this project, SHIRT has been modified with redox labels *via* reaction with surface lysine residues.

2.1.3 Lysine bioconjugation

Lysine is a convenient and well-studied residue that has been selected for bioconjugation method development due to the high nucleophilicity of the amine functional group and the abundance of this amino acid on the surface of proteins.[70] However, lysine targeting can prove problematic if regioselective conjugation is required, and amino acid replacement is regularly used in lysine targeting studies to engineer protein sequences that contain low amounts of lysine.[71,72] One of the most popular lysine bioconjugation coupling reactions utilises *N*-hydroxy succinimide (NHS) or sulfo-NHS activated esters reacting with lysine to produce a highly stable amide bond. For sulfo-NHS, the sulfonate improves water solubility (***Figure 11***).[73,74] Side reactions with the N-terminus are controlled using the lower pKa (≈ 6-8) of the N-terminal α-amino group compared to lysines ε-amino group (pKa ≈ 10).[75,76]

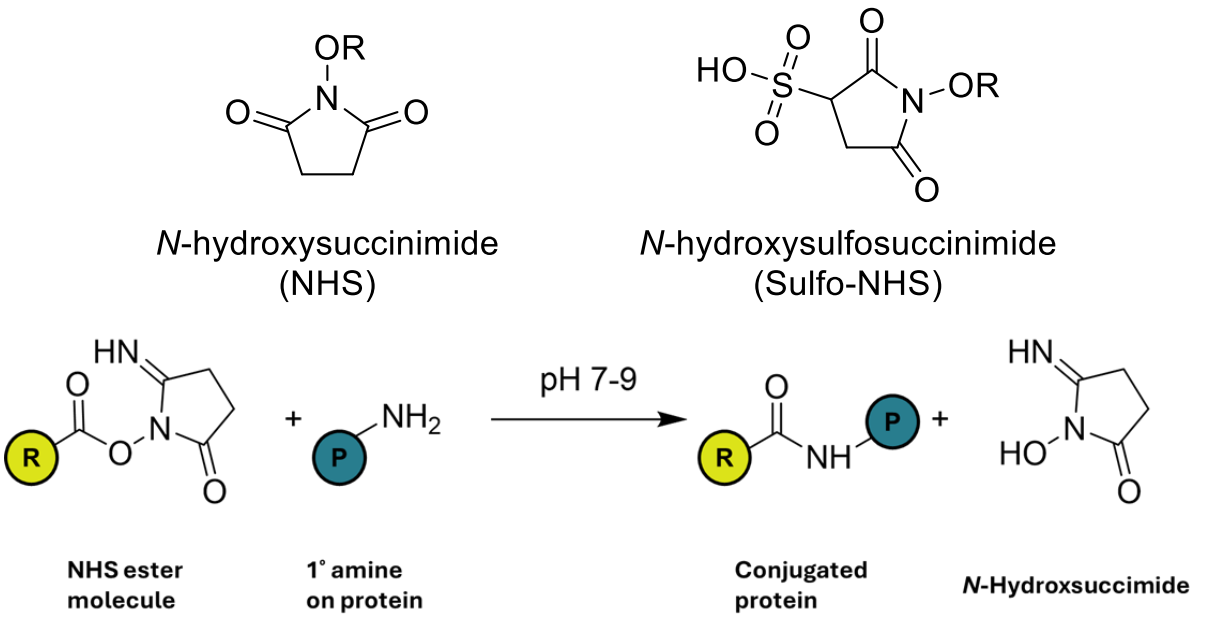

Figure 11 (Top) (left) Generic structure of N-hydroxysuccinimide (NHS) and (right) N-hydroxysulfosuccinimide (Sulfo-NHS). (Bottom) NHS reaction for chemical conjugation to a protein primary amine, R = linker attached to NHS ester, P = protein or molecule with primary amine.

This reaction was suitable for labelling SHIRT with redox molecules because of the number of surface lysine residues in the structure, as illustrated in ***Figure 12***.

Figure 12 Structure and sequence of SHIRTr3. Lysine residues are numbered and highlighted in purple in the sequence.

2.1.4 Viologen redox labels

Redox mediators have widespread use in battery and catalysis applications.[77–79] Ferrocene and quinone are popular redox mediators, however, viologen molecules were selected for use in this project because they display rapid electron transfer, are stable in the oxidised and reduced forms, and can be readily modified at the N-alkyl tail groups.[80] Conversely, ferrocene is not photo-stable,[81,82] and quinone redox chemistry is highly pH sensitive.[83] As seen in ***Figure 13***, a possible challenge to using viologens for biosensing is that they can be re-oxidised by oxygen. The way that FTacV can mitigate this issue is explored in ***Section 2.3.6.2***.

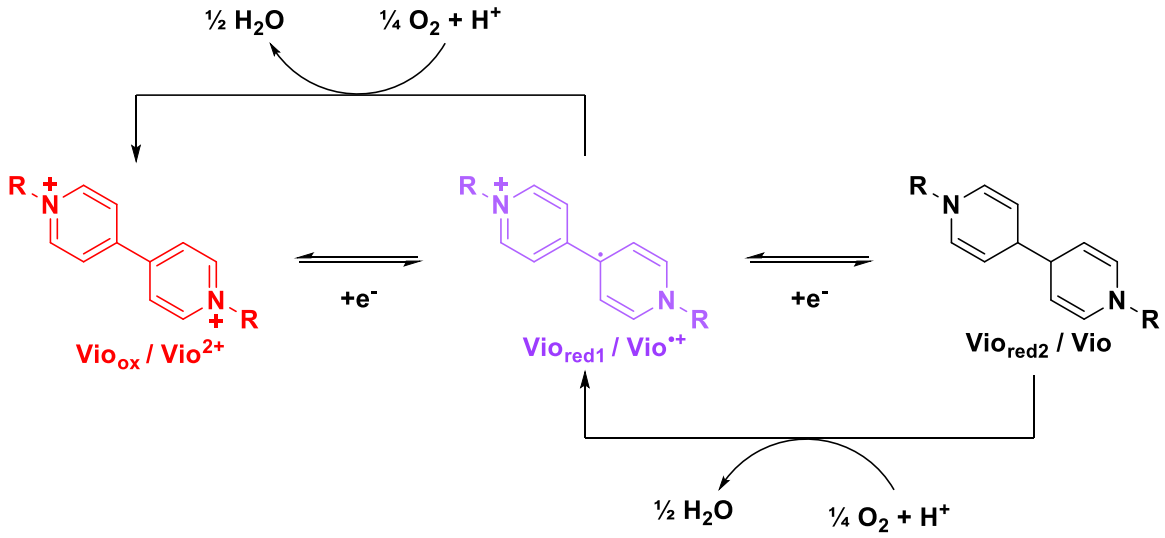

Figure 13 The two-step redox chemistry of a generic viologen molecule. Colours represent the typically observed colour for each state: Vio^{2+} (Red/Yellow), $Vio^{\bullet+}$(Violet/Blue), and Vio (Colourless).

Viologens are coloured in both reduced states, typically being violet in the radical cation (Vio_{red1}, $Vio^{\bullet+}$) state, and weakly coloured in the neutral (Vio_{red2}) state. The oxidised di-cation form (Vio_{ox}, V^{2+}) can appear slightly yellow in low concentrations, but is typically described as colourless.[84] Because a change in viologen oxidation state is readily detectable by eye, this family of molecules have been used as redox active electrochromes in assays.[85]

The formal redox potential of the viologens is modulated by the nature of the R group on the tertiary nitrogen atoms (***Figure 13***). In comparison to paraquat (R = CH_3), the elongation of an alkyl chain to C_2H_5 or C_3H_7 will decrease the formal redox potential and the addition of an electron withdrawing group (aromatic ring, alcohol, etc.) will increase the formal redox potential. Interconnection of pyridine rings can lead to both a decrease in formal redox potential (diquat) or an increase formal redox potential (triquat).[86]

Bioconjugation of a viologen based activated ester was done previously to metmyoglobin, accelerating the rate at which reduction of metmyoglobin occurred.[79] However, beyond this very little literary precedence could be found for viologen based bioconjugation. In the Parkin group, Dr Natalia Baranska designed and synthesised an ethyl viologen NHS ester molecule in order to label an iron-transport protein as part of her PhD work on artificial metalloenzymes.[87] Using modified literature procedures,[86] Dr Baranska's synthetic strategy starts from 4'4-bipyridine (***Scheme 2***). Step one uses a Menshutkin reaction to convert one of the tertiary amines in the dipyridine rings to a quaternary iodide salt via S_N2 substitution. In the second step, the isolated product is then taken, and the remaining tertiary nitrogen is alkylated using 6-bromohexanoic acid *via* the same reaction as the first step. In the third step, the carboxylic acid product is converted into its activated NHS ester form.

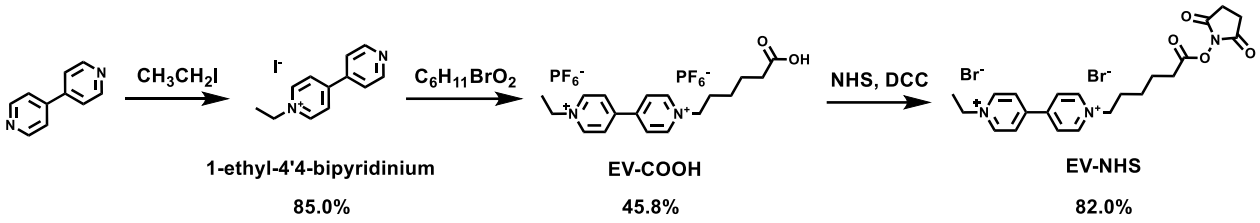

Scheme 1 The synthesis of N-hydroxysuccinimide functionalised viologen conjugate EV-NHS designed by Dr Baranska.

2.1.5 Surface immobilisation utilising the C-terminus

In protein film voltammetry, carbon-based electrodes such as pyrolytic graphite (PG) and glassy carbon (GC) have been popular because the negatively charged carboxylate groups on these carbon materials facilitates the adsorption of proteins with positively charged amino acids on their surfaces.[88–91] This would be problematic in this study, because the aim is to detect selective binding of SH3 protein to a peptide loop on SHIRT's surface, rather than non-specific binding of any protein to the carbon electrode surface. Therefore, to try and minimise non-specific electrode-binding to the SH3 analyte, I have used gold electrodes. This is also advantageous because, as described earlier, the Plevin group have already developed an approach for immobilising SHIRT onto gold using a di-cysteine C-terminal binding motif. A SHIRT mutant (referred to hereon as CGGC.SHIRT) was supplied by Dr Rachael Cooper. ***Figure 14*** shows the CGGC.SHIRT mutant with the C-terminal cystine anchoring motif for covalent bond formation to gold highlighted in green and the N-terminus of the protein highlighted in red.

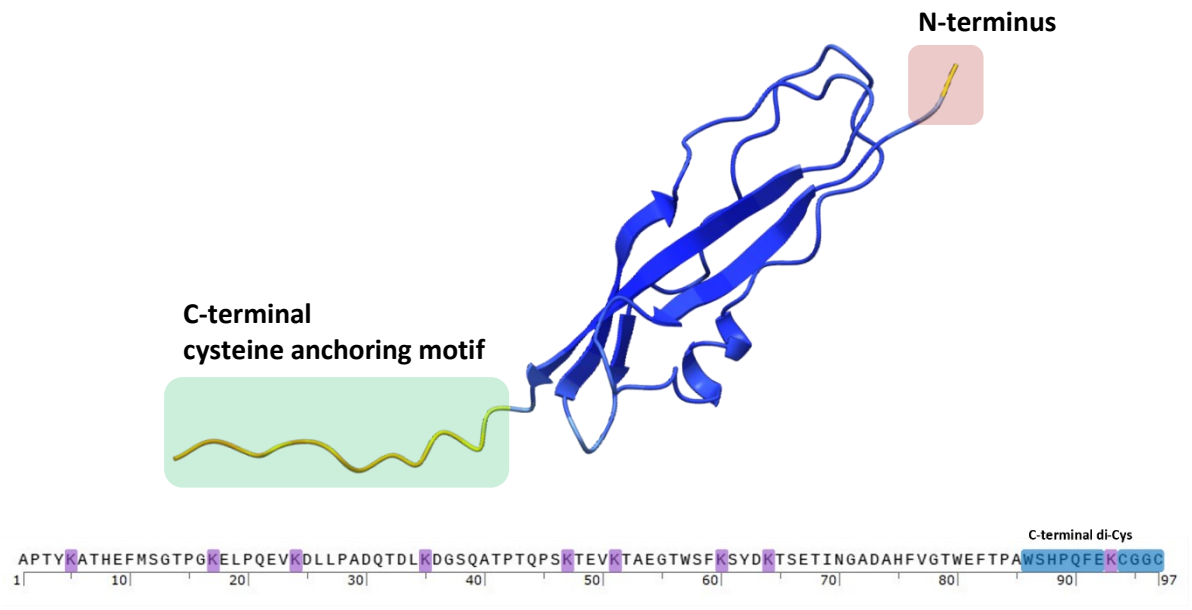

Figure 14 (Top) AlphaFold structure of CGGC.SHIRT with the C-terminal di-cysteine anchoring motif highlighted in green and the N-terminus highlighted in red. (Bottom) Sequence for CGGC.SHIRT with lysine residues highlighted in purple and the CGGC binding motif in blue.

2.1.6 N-terminal specific ligation

In SHIRT the C and N-terminal are on spatially opposite sides of the protein, as illustrated in ***Figure 14***. It is established in chemical biology literature, particularly in recent work conducted by the Spicer group at York, that conjugation of non-acetylated protein N-termini using 2-pyridinecarboxylaldehyde (2PCA) reagents is an effective, targeted and almost universal strategy for the installation of bio-orthogonal handles onto proteins.[64,92] 2PCA reagents are able to specifically target the N-terminus amine instead of lysine residues through the cyclisation of an intermediary imine *via* the nucleophilic attack of a neighbouring amide, forming a cyclic imidazolidinone (***Figure 15***).[93] Lipoic acids are a naturally occurring antioxidant produced by the body and have previously been used for immobilisation of proteins onto gold surfaces.[94–96]

I therefore aimed to synthesise a lipoic acid derivative of 2PCA to selectively bond to the N-terminus of SHIRT to provide a strategy for thiol-gold protein immobilisation that would create an electrode-SHIRT configuration that is “upside-down” relative to the C-terminus di-Cys immobilised configuration. The reason for exploring both N- and C-terminal immobilisation was to ensure that regardless of the viologen redox label(s) location, I would have an immobilisation strategy that proved capable of placing the electron-transfer labels within proximity of the electrode surface to facilitate rapid electron-transfer.

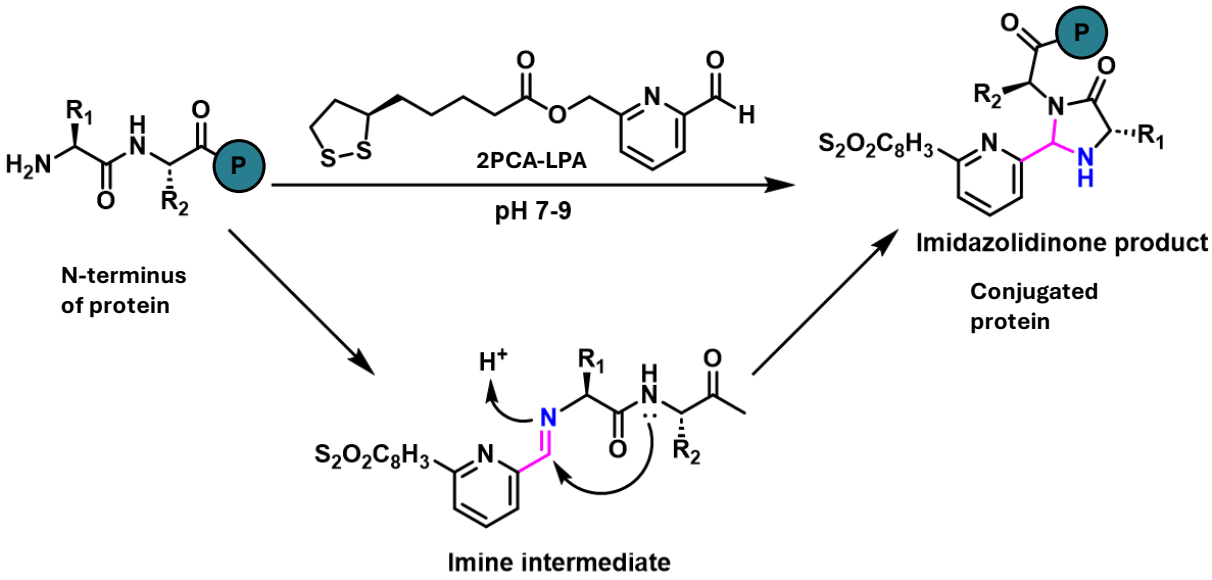

Figure 15 Reaction scheme for 2PCA reagents showing the formation of an imidazolidinone via an imine intermediate. P = protein or molecule.

2.2 Chapter aims

To explore the feasibility of developing a SHIRT-based electrochemical biosensor a strategy for both the redox labelling and the site-selective immobilization of SHIRT on an electrode is required. The following experiments aim to:

- Demonstrate a viable strategy for the targeted functionalization of lysine residues using a viologen derived NHS ester.
- Design and optimize a lipoic acid 2PCA reagent to enable SHIRT to be immobilized on gold surfaces *via* the N-terminus.
- Compare N-terminal immobilisation to C-terminal immobilisation achieved using a di-Cys amino acid motif.

2.3 Results and discussion

2.3.1 Synthesis and characterisation of ethyl viologen activated ester

As described in ***Section 5.1.3***, Dr Baranska's synthetic strategy for synthesising the activated ester viologen molecule, EV-NHS, was to first convert one of the tertiary amines in the dipyridine rings of the starting material to a quaternary iodide salt via SN2 substitution. This first step proceeded to high yields. In the second step, functionalisation of the second nitrogen of the starting material using 6-bromohexanoic acid, Dr Baranska's prior work showed that this synthesis of the carboxylic acid product was relatively slow and low yielding (~5 – 10%). My initial experiments following this synthetic scheme correlated with this: the bromine salt product was distinctively difficult to isolate due to its poor solubility in organic solvents and due to its vulnerability to hydrolysis, meaning isolation utilising lyophilisation resulted in mixtures of the product and initial starting material.

This synthetic step was improved by working with Dr Nick Yates to develop a counter-ion exchange method which improved the yield of the second step to ~45%, making use of a PF_6^- counter-ion which allowed aggregation of the molecule from an aqueous solution yielding a purer, more stable product and simplified purification.

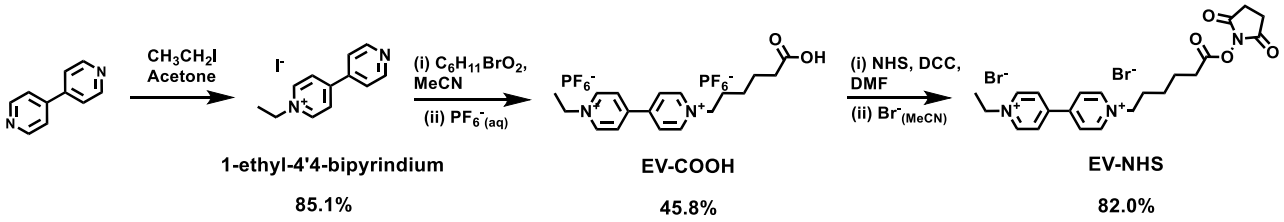

Scheme 2 Optimised synthesis of N-hydroxysuccinimide functionalised viologen conjugate EV-NHS.

In the last step of the EV-NHS synthesis, the carboxylic acid product is converted into its activated ester form in a high yielding reaction using the coupling reagent N,N'-dicyclohexylcarbodiimide (DCC). The characterisation of the reaction products was done utilising MS, NMR and FT-IR, as detailed in ***Section 5.1.3***.

2.3.2 Solution voltammetry of ethyl viologen

Solution voltammetry investigations were conducted to serve as a basis for parameter selection for later electrochemical investigations on viologen-labelled SHIRT. These experiments were conducted using a standard three-electrode setup, as described in ***Section 5.2.*** First, solution CV was conducted on the ethyl viologen carboxylic acid precursor (EV-COOH), since hydrolysis of the NHS-ester in the electrolyte solution would lead to the formation of this product. The voltammetry showed the expected solution CV 'duck' within the expected region seen for viologens at ~ -400 mV vs SHE.[97]

To emulate bioconjugation to SHIRT, a 1 mM solution of L-lysine was reacted with a 1 mM solution of EV-NHS for an hour, and the electrochemistry of the crude reaction mixture was measured, resulting in ***Figure 16B.*** Modification was also quantified using trypsin digestion followed by MALDI, as seen in ***Section 2.3.3.3***. There is a shift in midpoint potential when the conjugate is covalently bonded to lysine. This is to be expected since substituents on a redox centre changes electrostatic interactions, solvent accessibility, and the electronic nature of the molecule. This behaviour of shifting midpoint potential as a function of molecular functionalisation has been seen in the literature previously. [79,98–101] It is anticipated that the reaction will have generated a range of products since both the N-terminal amine and the amine sidechain of lysine will have been able to form an amide bond *via* reaction with EV-NHS. Using an N-terminal protected lysine would ensure exclusive reaction between the activated ester and the side chain amine group. However, the results of this proof-of-concept

experiment validates the hypothesis that binding of a protein analyte to the viologen-labelled SHIRT may also be detectable by changes in the viologen redox chemistry.

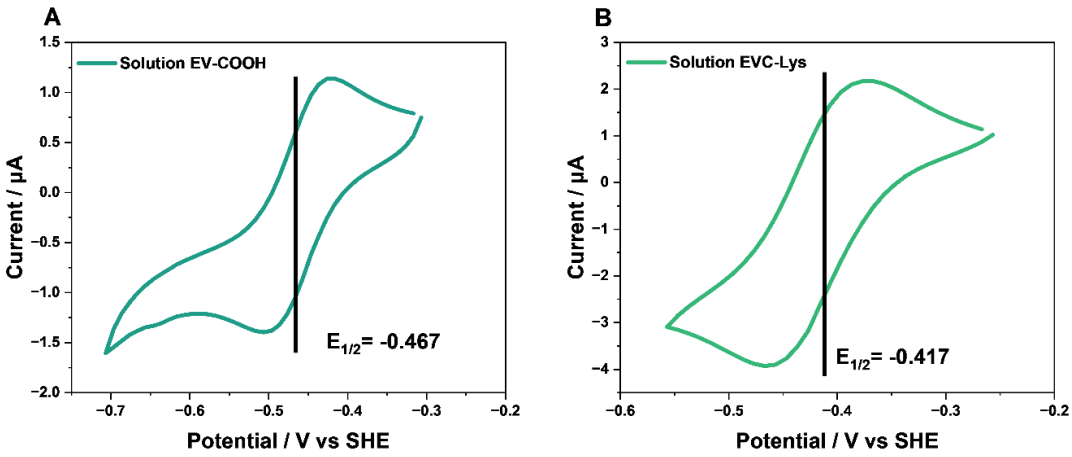

Figure 16 Gold disk work electrode cyclic voltammograms for solution voltammetry of (A) ethyl viologen conjugate EV-COOH, and (B) crude bioconjugation product of reaction between lysine and EV-NHS. The midpoint potentials are labelled at –467 mV (A) and -417 mV (B). Experiments were conducted in pH 7.5 buffer (100 mM sodium phosphate, 150 mM NaCl) at 25 °C under a N_2 atmosphere. A platinum wire counter electrode and Ag/AgCl (3 M KCl) reference electrode were used. All experiments were starting from the most negative potential.

2.3.3 Bioconjugation of 'WT' SHIRT with redox mediator and SDS-PAGE analysis

To evaluate the relationship between the amount of activated-ester viologen and conversion of lysine on SHIRT, bioconjugation experiments were run using different EV-NHS to 'wild type' (no C-terminal di-Cys sequence) SHIRT ratios and SDS-PAGE analysis was conducted, as shown in ***Figure 17***. The viologen-modified SHIRT protein is visible as a band between the 10 kDa and 15 kDa marker. Conversely, in the control lanes of the gels the unmodified SHIRT can be seen as a band at the 30 kDa marker despite a molecular weight of 9.5 kDa. This has been consistently observed by our collaborators in the Plevin group and is attributed to the SHIRT protein's rod-like structure and ability to refold even after being boiled in SDS. It is assumed that the addition of the positively charged oxidised viologen groups adds sufficient charge to assist in SHIRT running through the gel. These results pointed to 100 equivalents of EV-NHS to protein being sufficient for the complete modification of SHIRT, and these reaction conditions were used to generate all "SHIRT.EV" conjugates tested throughout the rest of this Thesis.

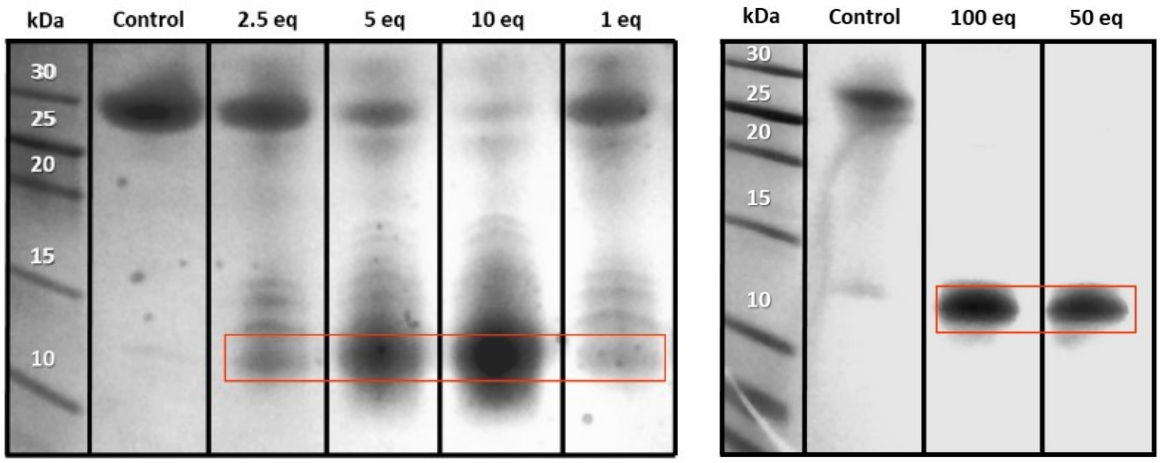

Figure 17 16.5% Tris-Tricine gels with a SDS-PAGE molecular weight low range standard ladder in the left lane, a "control" lane of unmodified SHIRT, and the products of experiments using different equivalents of EV-NHS to SHIRT, as designated. Red boxes show the modified protein band

2.3.3.1 Testing the feasibility of using UV-vis to determine the extent of SHIRT-viologen labelling

Having established that a 100-fold excess of EV-NHS seemed to yield a single viologen-SHIRT product, UV-vis was explored as a method for estimating the labelling efficiency. As in the solution voltammetry, the carboxylic acid viologen molecule, EV-COOH, was used as a proxy of the activated ester, EV-NHS, because of the vulnerability of the activated ester to hydrolysis. The UV-vis spectra of EV-COOH showed a peak in absorption at 260 nm (***Figure 18***). The extinction coefficient at 260 nm was calculated as ε_{260} = 7640 M^{-1} cm^{-1} and this compares to the literature value of 20700 M^{-1} cm^{-1} for methyl viologen.[102]

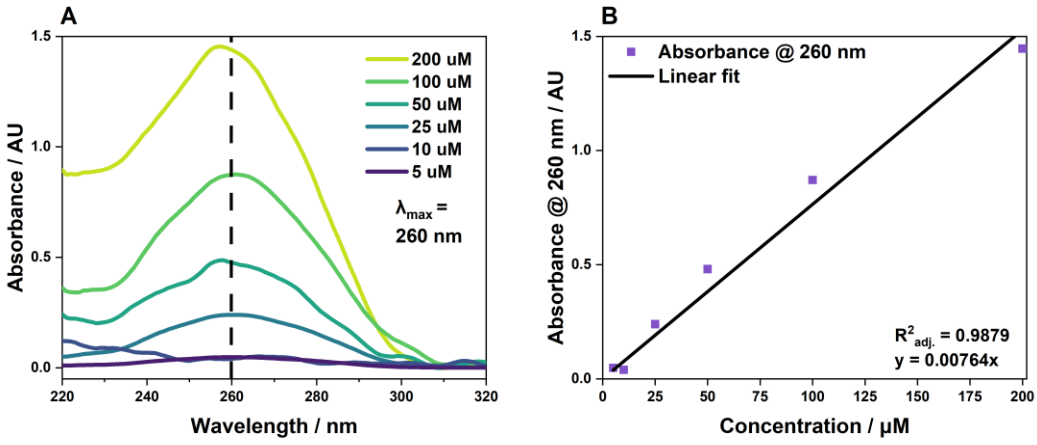

Figure 18 (A) UV-vis spectra (220 - 320 nm) of EV-COOH (pH 7.5, PBS, rt) at varying concentrations (5 µM – 200 µM), showing λ_{max} = 260 nm. (B) Measurement of the molar extinction coefficient for EV-COOH at 260 nm (ε_{260}). The molar extinction coefficient was calculated using the slope of the line of best fit.

UV-Vis spectroscopy is commonly used to determine protein concentrations, utilizing the absorption of aromatic residues at 280 nm. The UV-vis of wild type SHIRT is shown in ***Figure 19*** and using Expasy's ProtParam tool the molar extinction coefficient of SHIRT at 280 nm was calculated as ε_{280} = 13980 M^{-1} cm^{-1} based on the sequence.

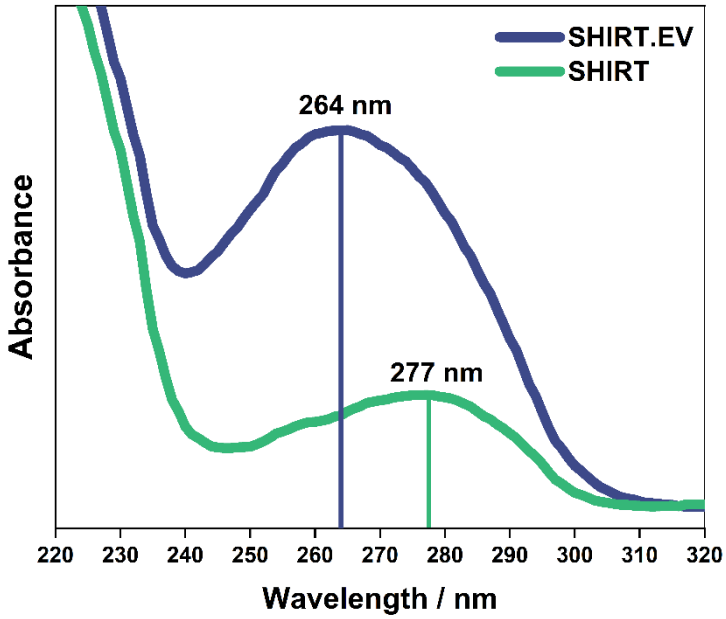

Figure 19 UV-vis spectra of 5 μM SHIRT and SHIRT.EV demonstrating the difference EV^{2+} causes to the absorbance spectrum of the protein.

The overlap between the oxidised viologen molecule (Vio^{2+}) UV absorption and SHIRT's UV absorption is shown in ***Figure 19*** which overlays the spectra of wild type SHIRT and the product of a SHIRT-viologen conjugation experiment (SHIRT.EV). To estimate the extent of lysine conjugation to viologen, the UV-vis spectra of SHIRT.EV was modelled as a linear combination of the separate spectra of SHIRT and EV-COOH, this was done in Microsoft excel using a linear regression model. The result of this deconvolution is ***Figure 20***. Using the absorption of the EV-COOH component at 260 nm and ε_{260} from ***Figure 20*** quantifies the amount of viologen in the SHIRT.EV spectra as 128 μM. Equally, using the absorption of the SHIRT component at 280 nm yields a protein concentration of 45 μM. The ratio of [SHIRT]:[EV] was therefore estimated as 1:7.

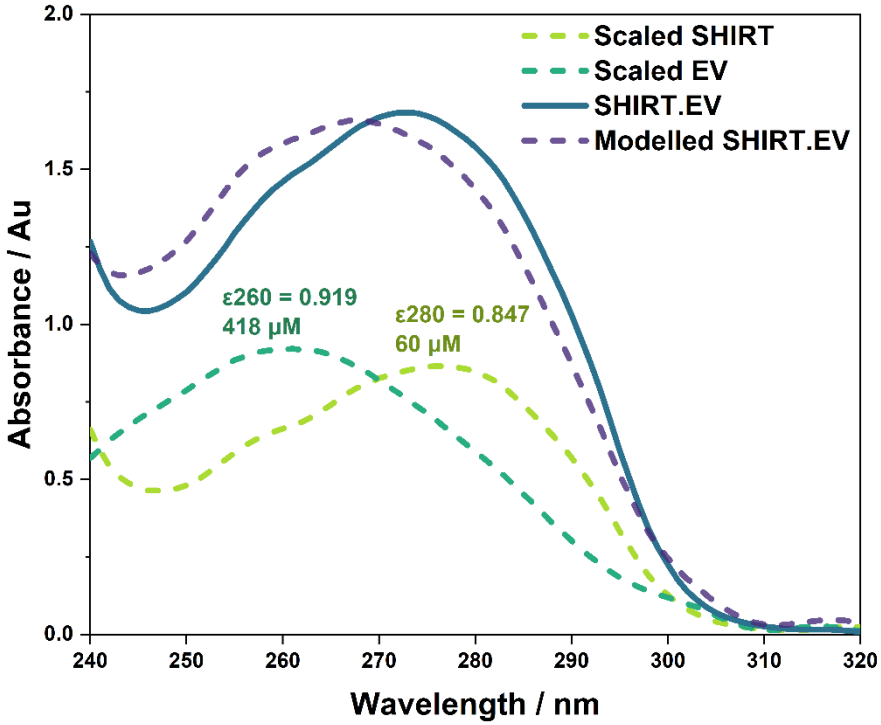

Figure 20 UV-Vis spectra of 100 µM SHIRT.EV (concentration determined by Bradford assay) and modelled SHIRT.EV with values calculated using scalar factors applied to 100 µM solutions of SHIRT and EV-COOH.

Singly reduced viologen molecules, $EV^{+\cdot}$, have an absorbance at ~395 nm and ~600 nm, and doubly-reduced molecules, EV, have an absorbance of ~500 nm, both beyond the spectral range at which SHIRT absorbs.[80,102] Therefore the possibility of producing chemically reduced SHIRT.EV was probed to determine if a simpler UV-vis method could be developed to estimate the ratio of protein to viologen in the conjugate samples. These experiments all proved unsuccessful due to rapid oxidation of the samples by oxygen (results not shown).

2.3.3.2 Protein NMR analysis to determine the extent of SHIRT-viologen labelling

In preliminary work Dr N. Barnaska conducted a ^{15}N protein NMR experiment to determine the extent of viologen conjugation to lysine. A HSQC spectrum in ***Figure 21*** displays the results of the experiment where eight new peaks were observed and attributed to the conjugation of EVC-NHS to the lysine amino acid residues. The experiment however was unable to be used to determine whether total conversion of each residue had occurred.

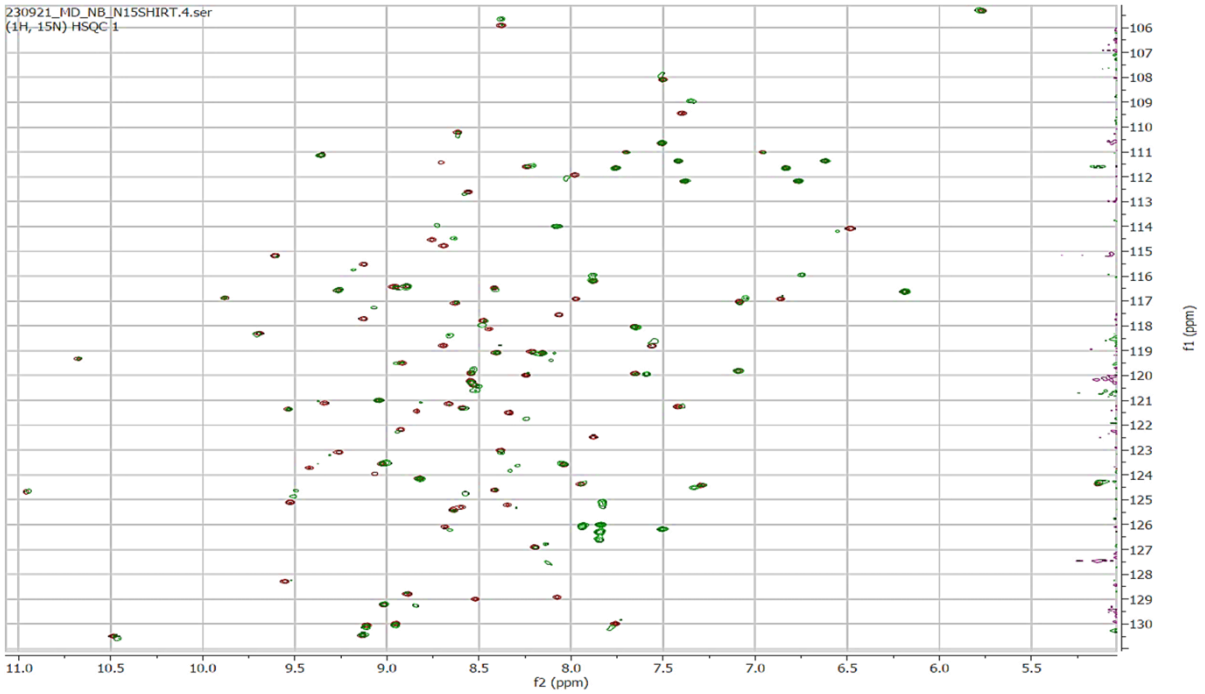

Figure 21 2D HSQC NMR experiment showing the viologen labelling of lysine residues on SHIRT. (Red) unmodified SHIRT protein (100 µM). (Green) viologen labelled SHIRT (10 µM). SHIRT was expressed from E coli. grown in 15N enriched media and NMR experiments were done in pH 6.2, 20 mM phosphate buffer, 0.05% NaN_3, H_2O:D_2O (9:1 v/v). Experiments and figures provided by Dr N. Baranska.

2.3.3.3 Analysis of the extent of viologen-SHIRT labelling using digestion MALDI

Preliminary experiments which I carried out using tandem mass spectroscopy (MS/MS) to analyse the bioconjugation SHIRT.EV product was unsuccessful, presumably because of the charge associated with viologen molecules attached to the SHIRT (the spectra could not be deconvoluted). Therefore, the SHIRT.EV samples were instead submitted to the Bioscience Technology Facility at the University of York for analysis. The technical team used trypsin digestion to break down SHIRT into shorter polypeptide sequences which were then analysed using LCMS. Comparative sequence analysis then provided a map of lysine residue modification, as shown in ***Figure 22***.

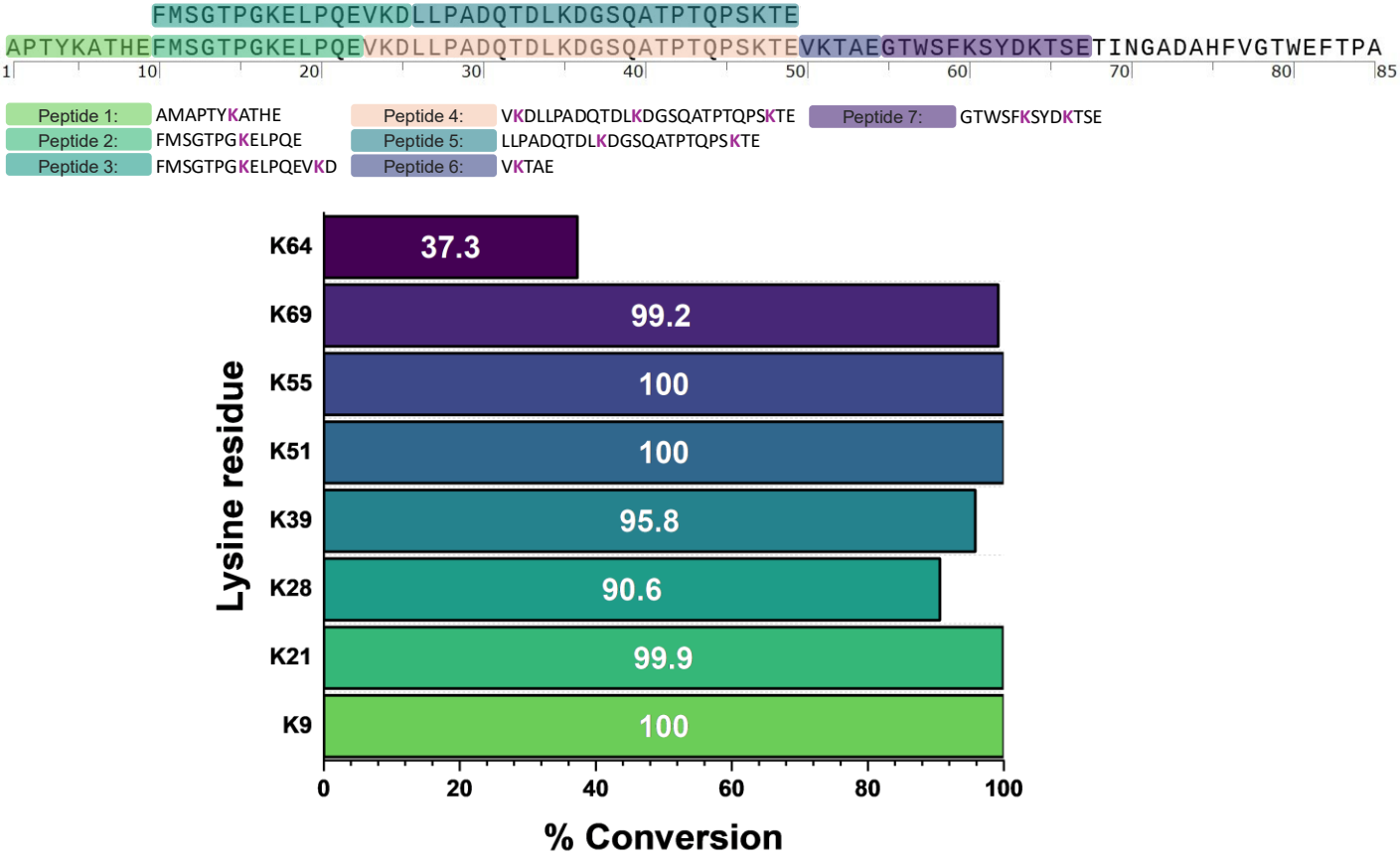

Figure 22 Plotted results from trypsin digestion MALDI analysis. (A) Protein sequence with labels underneath displaying resulting peptides sequences observed from trypsin digestion, lysines are highlighted by purple text. (B) Bar chart displaying percentage conversion of lysine residues present in SHIRTr3.

As shown in ***Figure 22***, a total of nine peptides containing viologen molecules were separated and assigned. Most lysines had a >95% conversion except K28 (conversion of 90.6%) and K64 (only 37.3% ligated with viologen). This result demonstrated that near complete ligation had occurred, resulting in a near-homogenous SHIRT.EV product. Thus, when bioconjugation

reactions are carried out employing a 100-fold EV-NHS to SHIRT, the ratio of EV-NHS to lysine targets has been approximately 14:1.

In the literature, excess amounts of NHS esters are commonly used to achieve near total substitution of all lysine amino acid residues on a peptide sequence, and a reaction ratio of 10- to 20-fold activated ester to lysine would be typically used in a protocol to ensure rapid and efficient labelling.[100–102] Lower amounts of activated ester equivalents are used when trying to achieve selective modification of a single lysine residue.[68,103–105] In the literature, differences in the labelling efficiency of different lysine residues are attributed to variations in solvent accessibility and neighbouring residue effects. From looking at the SHIRT structure, it is speculated that poor conversion of K64 may be caused by the residue not being surface exposed, unlike the other lysine residues in the structure (***Figure 23***). Later work utilises this analysis, as I attempt to remove prospective 'problem' residues to achieve a homogenous viologen-labelled SHIRT product.

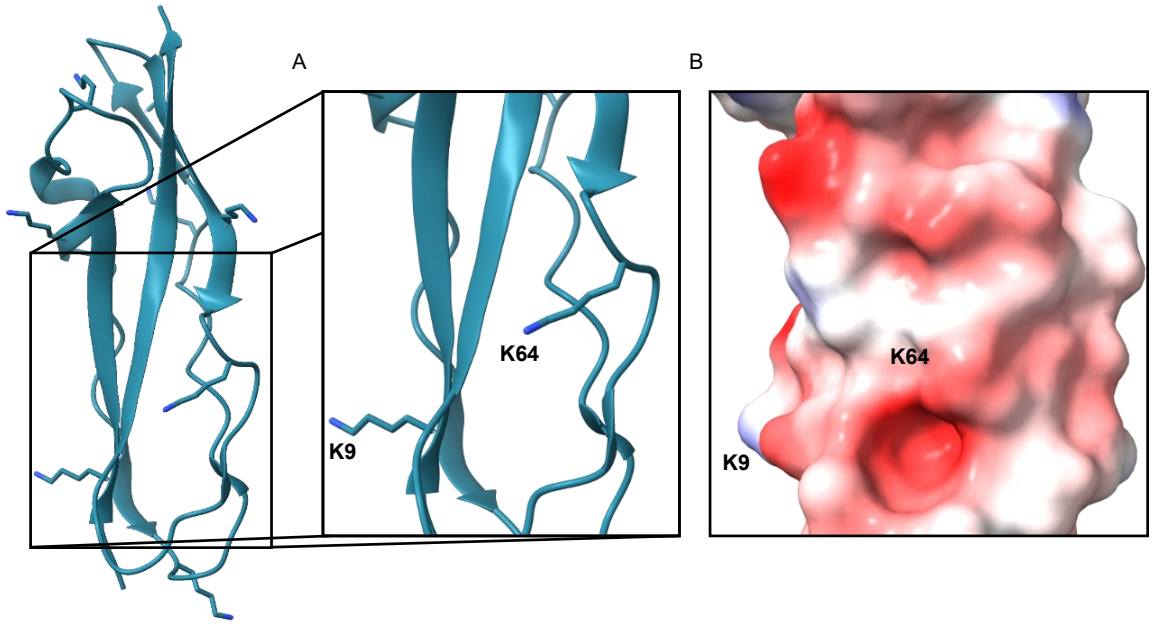

Figure 23 Structure of SHIRTr3 with lysine residues depicted. (A) Zoomed in image of residues K9 and K64 labelled. (B) Zoomed in image of electrostatic potential of residues K9 and K64.

2.3.3.4 nano-DSF determination of the melting point of viologen modified SHIRT

SDS-PAGE analysis of the SHIRT.EV conjugate in ***Section 2.3.3*** showed a band at a different position compared to unmodified SHIRT indicating that viologen labelling effects the proteins properties. Similarly, while wild type SHIRT is amenable to MS/MS, this analytical technique did not yield meaningful results for SHIRT.EV. To therefore determine if the viologen-labelling had disrupted the structural stability of the protein nano-DSF was carried out. Comparisons of 'wild type' SHIRT and the bioconjugation product, SHIRT.EV, identified that the melting temperature (T_m) only decreased by 1.5 °C from 75.8°C to 74.3 °C following viologen labelling (***Figure 24***). Thus, redox marker bioconjugation does not substantially destabilise the high conformational stability of SHIRT, meaning it is still a sensible scaffold on which to develop new biosensing biorecognition elements.

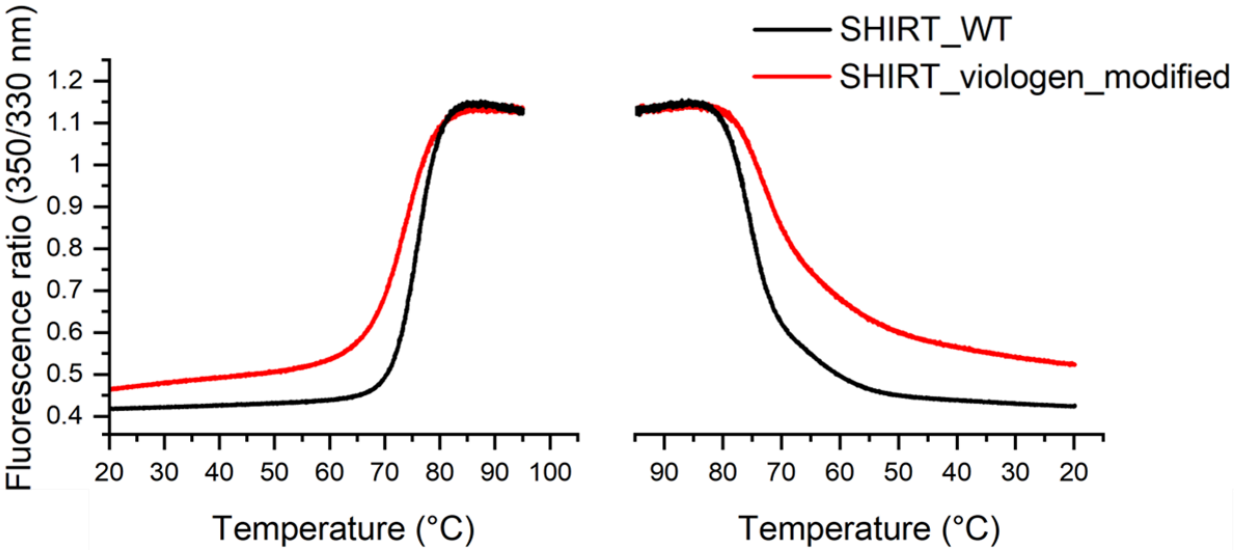

Figure 24 nano-DSF data for both unmodified 'WT' (black) and viologen modified (red) SHIRT. Shown is the thermal unfolding and folding curves. Figures provided by Dr R. Cooper.

2.3.4 Electrochemical measurement of viologen-labelled SHIRT immobilised *via* a C-terminal di-Cys motif

Having established a 100-fold labelling protocol that introduced ethyl viologen functionalities onto a majority of the lysine residues on wild type SHIRT, labelling experiments were repeated using the C-terminal di-Cys SHIRT variant, and protein film electrochemistry experiments were conducted. Following viologen bioconjugation to the CGGC.SHIRT protein, the so called "CGGC.SHIRT.EV" product was immobilised on a gold electrode *via* submersion of the electrode in a 100 μM solution of labelled protein overnight in a nitrogen atmosphere; the electrode surface was then washed in triplicate with DI water and ethanol, before being dried under a stream of nitrogen gas. Control experiments using non viologen labelled Cys containing CGGC.SHIRT and viologen labelled Cys-free wild type protein (SHIRT.EV) were run using an identical electrode-immobilisation protocol.

As shown in ***Figure 25***, a simple polynomial baseline can be used to extract the electron-transfer signals for CGGC.SHIRT.EV. Repeating the baseline subtraction process on CV measurements made at a variety of scan rates confirms the surface confinement of CGGC.SHIRT.EV (presumably through gold-thiol bond formation between the electrode and cysteine residues) because the peak current is proportional to the scan rate (***Figure 26***).[106] Two reduction peaks can be observed in ***Figure 25A*** around -450 mV and –250 mV, these are expected to be associated with surface roughness of the electrode surface.

The electrode which had been soaked in wild-type, viologen-labelled but cysteine-free SHIRT.EV protein did not show any viologen electron transfer signals, meaning any non-specifically bound protein had been removed from the gold electrode in subsequent washing steps. Equally, measurements on an electrode exposed to the Cys-containing but non-viologen labelled CGGC.SHIRT were also free of any Faradaic current peaks, confirming that viologen labelling is necessary to confer reversible redox-reactivity upon the SHIRT protein.

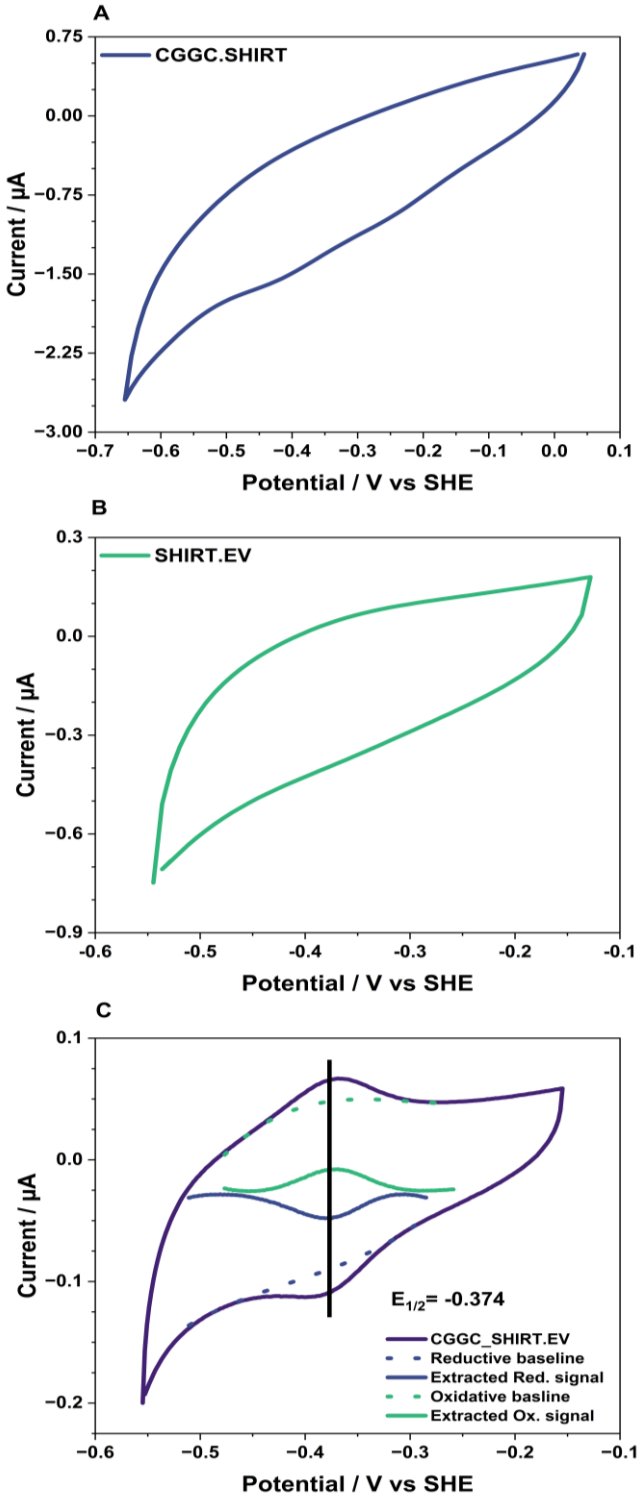

Figure 25 Gold disk working electrode cyclic voltammograms showing (A) the response of unmodified CGGC.SHIRT, (B) the response of viologen labelled 'WT' SHIRT without a surface binding mutation and (C) the response, baseline, and extracted redox peaks from an ethyl viologen conjugated modified CGGC.SHIRT.EV protein, the midpoint potential is labelled at -374 mV. Experiments were conducted at 50 mVs^{-1} in pH 7.4 buffer (100 mM sodium phosphate, 150 mM NaCl) at 25 °C under a N_2 atmosphere. A platinum wire counter electrode and Ag/AgCl (3 M KCl) reference electrode were used. All experiments were started from the most negative potential.

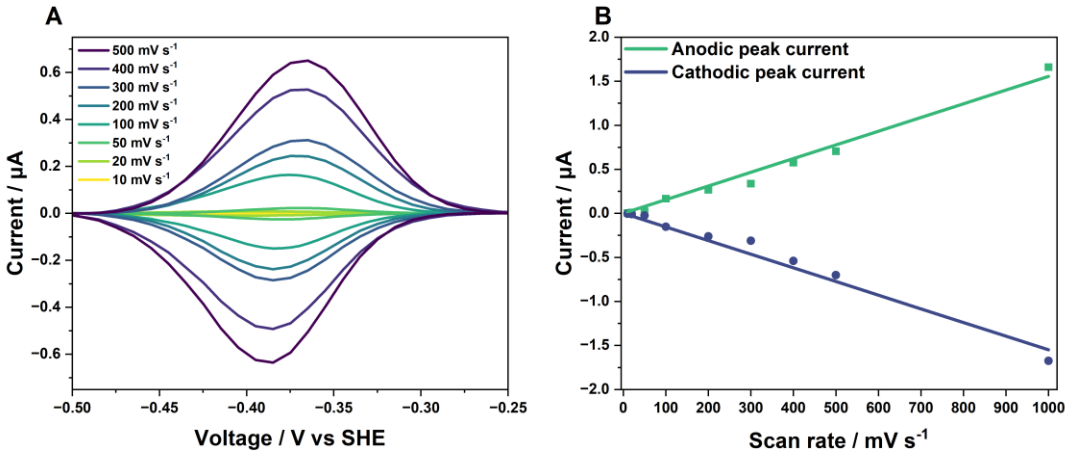

Figure 26 (A) Faradaic only peak signals extracted from differing scan rate CV measurements of CGGC.SHIRT.EV (B) Peak current of the redox signals versus scan rate. The peak current is directly proportional to scan rate, characteristic of a surface bound species. At lower scan rates polynomial peak extraction proves more difficult due to the broadness of the Faradaic signals and the current is likely underestimated.

A CV of CGGC.SHIRT.EV measured at slow scan rate (50 mVs^{-1}) was further modelled using R code written by Dr Nicholas Yates which fits the extracted electron-transfer peak current data to the Nernst-derived equation shown in ***Section 1.4.1.1*** (***Equation 6***). As shown in ***Figure 25C*** the analysis for the redox couple fits to a one-electron transfer process, suggesting that the multiple viologen molecules conjugated to each SHIRT all act in a near-identical manner. Surface coverage was calculated using the integration of the extracted anodic electron-transfer signal and was found to be ~ 126.7 pmol viologen cm^{-2}; assuming eight appended viologen molecules per SHIRT, and that each viologen is electrochemically detectable *via* CV gives a value of ~ 15.8 pmol CGGC.SHIRT.EV cm^{-2} for the data in ***Figure 25***. Notably, as this project progressed, smaller viologen electron transfer peak signals (corresponding to a lower protein coverage on the electrode) were seen when using older CGGC.SHIRT.EV aliquots for protein film electrochemistry measurements. This suggests that despite the high T_m of SHIRT.EV some degradation still occurs over long-term storage of the labelled protein in the freezer.

Parameter	Value
A / cm^2	0.03
Anodic peak potential / $\boldsymbol{mV\ v\ SHE}$	-368
Cathodic peak potential / $\boldsymbol{mV\ v\ SHE}$	-378
$\boldsymbol{E^0_{(Ox/Red)}}$ / $\boldsymbol{mV\ v\ SHE}$	-373
n_s *cathodic*	1
n_s *andoic*	1
n_{app} *cathodic*	0.885
n_{app} *anodic*	0.861
Γ *cathodic* / *pmol*	77.9
Γ *anodic* / *pmol*	126.7

*Table 1: Parameters fitted to the extracted signals in **Figure 25C**, utilising **Equation 6**, displaying the redox signal of SHIRT is characteristic of a one-electron process.*

The stability of CGGC.SHIRT.EV films immobilised on the gold electrode surface was determined by extraction of surface coverage from CVs taken hourly over a twelve-hour period (***Figure 27***). In the experiments, a CGGC.SHIRT.EV protein film displayed good stability with a zero change in coverage value within the error of the analysis (126 → 128 pmol cm^{-2}).

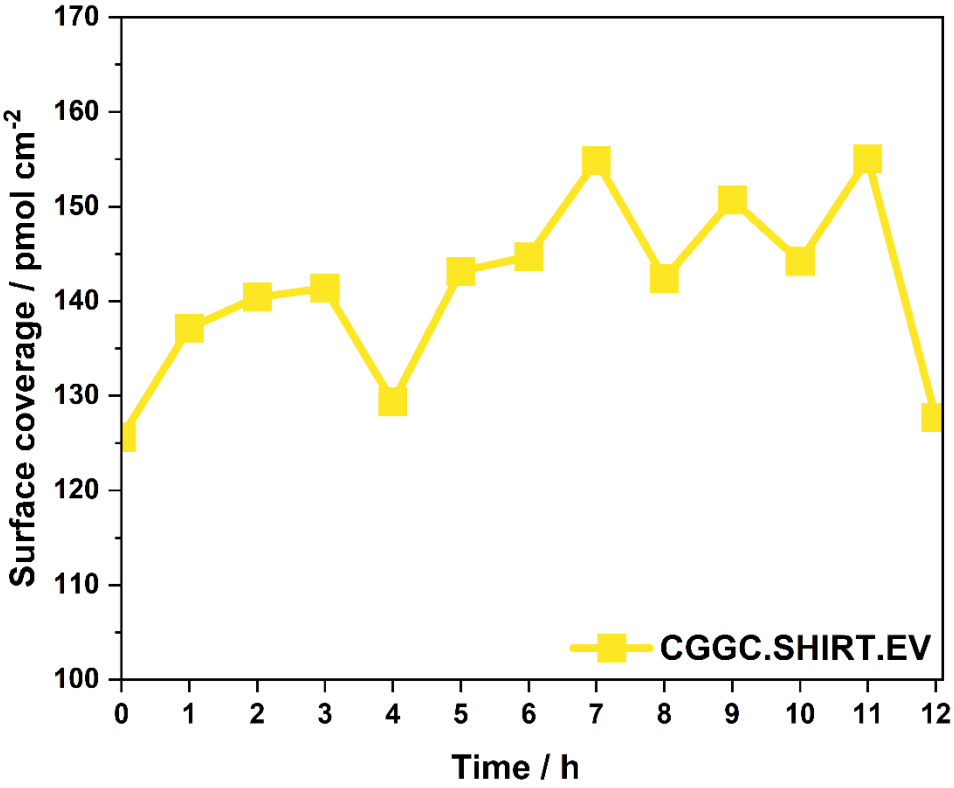

Figure 27 Plot of surface coverage against time for CGGC.SHIRT.EV. Scans at 100 mVs^{-1} were taken hourly and the third scan was used to calculate surface coverage. Experiments were conducted in pH 7.4 buffer (100 mM sodium phosphate, 150 mM NaCl) at room temperature under a N_2 atmosphere. A platinum wire counter electrode and Ag/AgCl (3 M KCl) reference electrode were used.

Measurements of CGGC.SHIRT.EV at a variety of scan rates could also be further analysed to yield a trumpet plot, as outlined in ***Section 1.4.1.2*** (***Equation 7***). This estimates the rate of electron transfer as 27 s^{-1} (***Figure 28***).

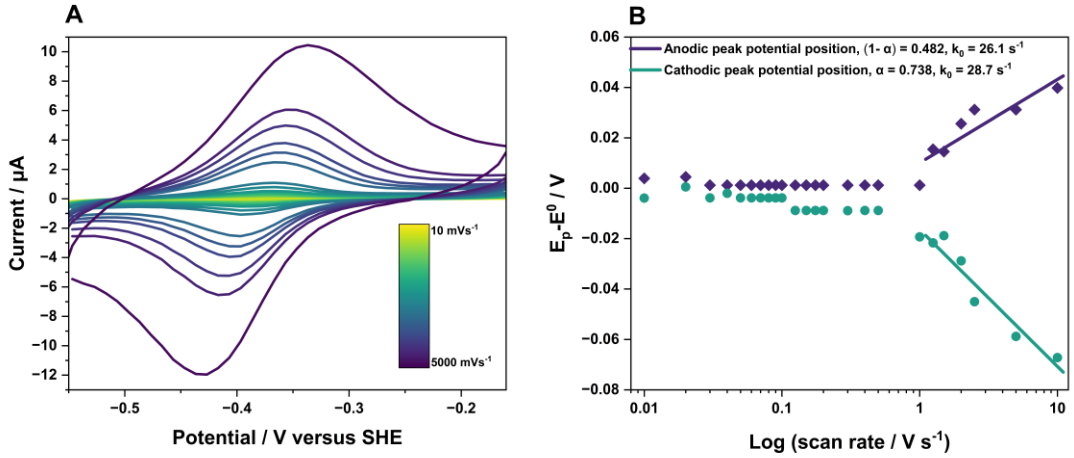

Figure 28 (A) Recorded CV response of CGGC.SHIRT.EV at a variety of scan rates. (B) Trumpet plot displaying the relationship between the natural logarithm of scan rate and the anodic (purple) and cathodic (green) peak potential. Scans were recorded at room temperature and pH 7.4 (100 mM sodium phosphate, 150 NaCl) under a N_2 atmosphere.

FTacV was also used to interrogate the CGGC.SHIRT.EV on gold disk electrode protein "films". As expected, higher order harmonics allowed for resolution of Faradaic-only current without the requirement for baseline subtraction (***Figure 29***). These measurements elicited a response that suggested a faster rate of electron-transfer than elucidated from trumpet plot analysis; the observation of signal up to the 12th harmonic of a 9.54 Hz experiment is equivalent to electron transfer proceeding at a rate of 114.48 s^{-1}. This is consistent with previous studies comparing CV trumpet plot analysis and other voltametric methods. Due to the heavy reliance on baseline subtraction, trumpet plot analysis often underestimates electron transfer rates.[55,107]

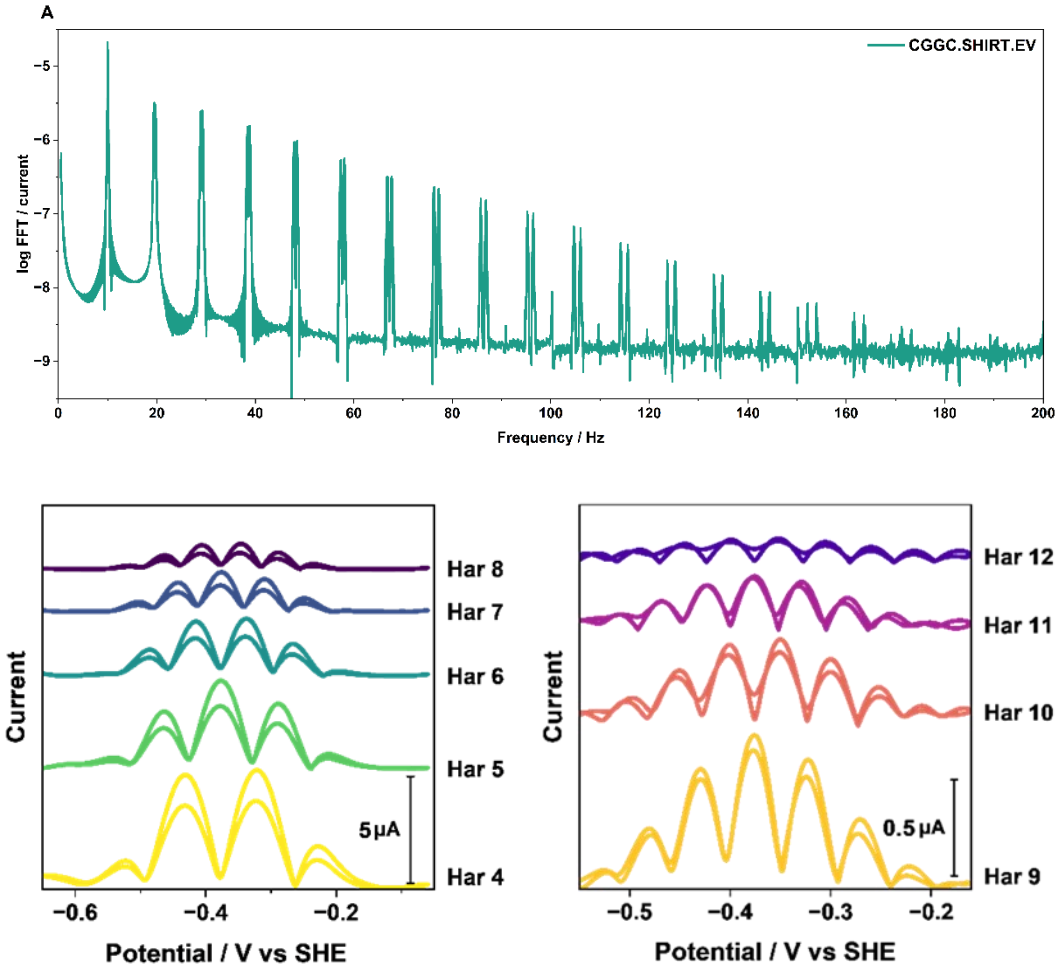

Figure 29 Fourier transform alternating current voltammetry for CGGC.SHIRT.EV immobilised on a gold disk electrode (A) Absolute Fourier "power" spectrum and (B,C) the 4^{th}-12^{th} harmonic for CGGC.SHIRT.EV, obtained by inverse fast Fourier transform. The measurements were recorded on a "home-build" instrument; ω = 9.54 Hz, ΔE = 150 mV, ν = 59.60 mV s^{-1}, DC potential range = -0.4 – 0.8 V vs SHE Experiments were conducted at room temperature and pH 7.4 (100 mM sodium phosphate, 150 nM NaCl) under a N_2 atmosphere.

2.3.5 Immobilisation of viologen labelled SHIRT *via* the N-terminus

2.3.5.1 Synthesis of a 2PCA lipoic acid reagent and N-terminal SHIRT modification

With a strategy for the immobilisation of SHIRT via the C-terminus onto a gold electrode, an alternative approach for immobilisation via the N-terminus was investigated. The lipoic acid 2PCA derivative 2PCA-LP was synthesised in two steps starting from 2,6-pyridinedimethanol (***Scheme 3***), which underwent oxidation to an aldehyde followed by a Steglich esterification with α-lipoic acid. The isolation of the 2PCA-LP reaction product was confirmed by MS, NMR and FT-IR, as detailed in ***Section 5.1.3***. From searching in literature 2PCA-LP has never previously been synthesised.

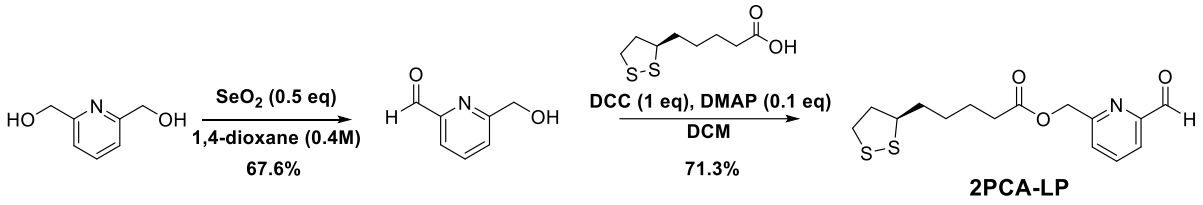

Scheme 3 Synthetic scheme for 2PCA-LP

Published 2PCA bioconjugation studies provide the general conditions for using 2PCA molecules to label a protein N-termini; however, work in the Spicer group has proved that further optimisation is required to maximise conversion between specific 2PCA reagents and proteins.[92,108]

Initial N-terminal modification of SHIRT with 2PCA-LP was therefore achieved utilising the conditions provided in ***Section 5.3.3***, with liquid chromatography mass spectroscopy (LC-MS) used to identify the product. A subsequent reaction condition screen was then carried out. 2PCA-LP proved to be a challenging bioconjugation reagent to use due to its extreme hydrophobicity with a minimum of 30% v/v organic solvent solution required for the compound to not aggregate in bioconjugation reactions. The high organic solvent stability of SHIRT therefore proved to be of enormous value in this reaction optimisation process.

The screening of the bioconjugation conditions was done sequentially, starting at 25°C, 100 equivalents of 2PCA-LP to SHIRT, 50% v/v DMF:PBS, reacting overnight. The reaction parameters (temperature, equivalents, solution composition and time) were then changed sequentially with the best conditions found taken forward, as shown in ***Table 3***, which summarises every reaction and the conversion percentage of 2PCA.SHIRT. Conversion was determined by the comparison of the starting material and product peak areas as obtained by LC-MS (***Figure 30***). ***Figure 31*** visually summarises the results of the reaction screening.

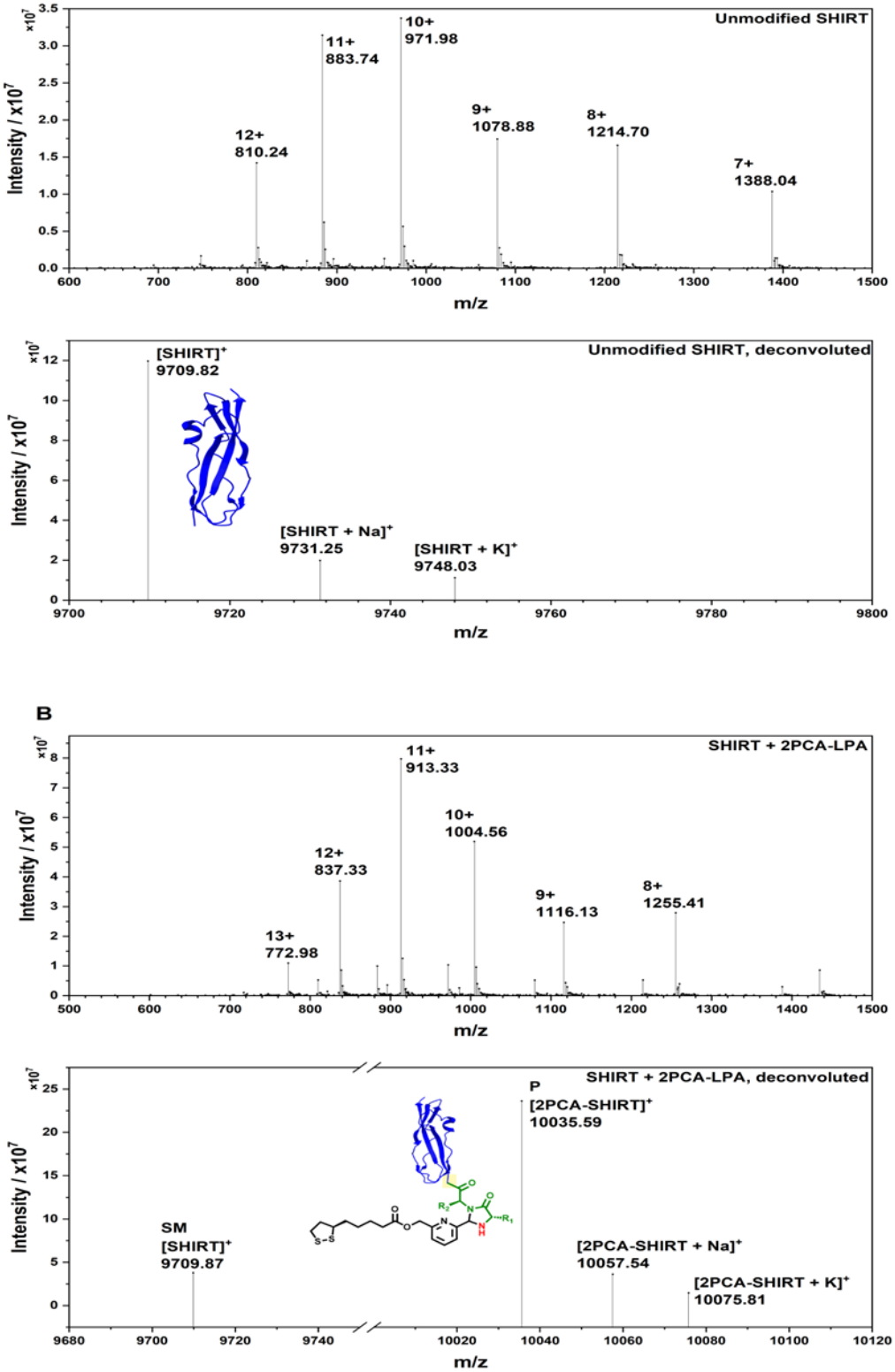

Figure 30 Positive ion ESI-LC/MS analysis of 2PCA-LPA modification of SHIRT. (A) (Top) Negative control SHIRT reacted in same conditions as (B) with absence of 2PCA-LPA reagent. (Bottom) Deconvoluted mass spectra, peak for unmodified SHIRT found at expected m/z (9709.82) with salt adducts seen at m/z of 9731.25 and 9748.03. (B) (Top) Sample of SHIRT reacted with 100 eq of 2PCA-LPA @ 25°c for 18 hours. (Bottom) Deconvoluted mass spectra, modified peak corresponding to SHIRT labelled with 2PCA-LPA is seen at m/z 10035.59, +326.72 m/z above unmodified SHIRT (m/z 9709.87), corresponding to 2PCA-LPA = 325.08 Da.

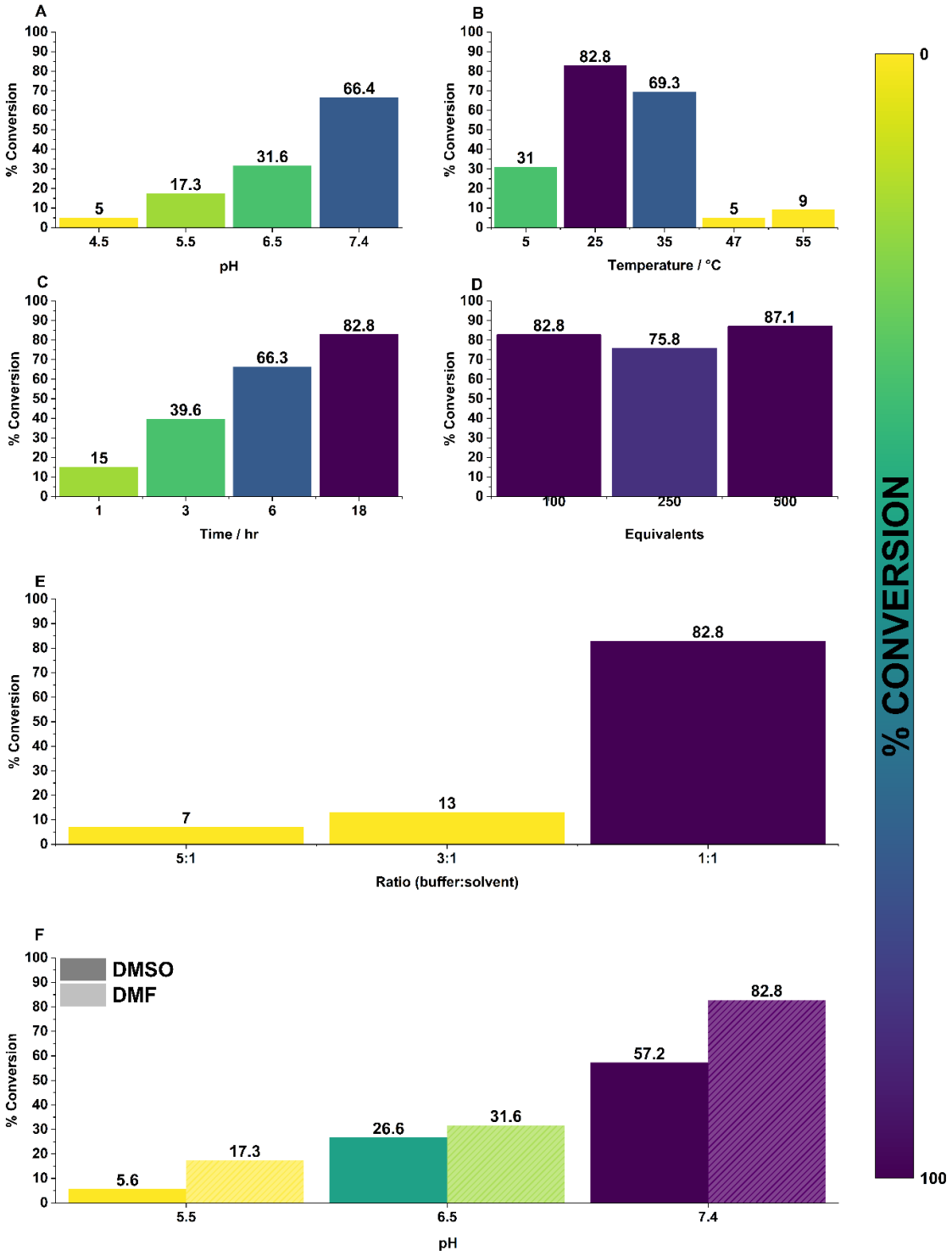

Figure 31 Bar charts displaying the optimisation of parameters for the conversion of the N-terminus of SHIRT with 2PCA-LP. The reaction screening waws carried out sequentially (A → F), with the most efficient condition being taken forward. The starting bioconjugation reaction conditions were: 100 equivalents of 2PCA-LP to SHIRT, a 1:1 ratio of PBS:DMF, 25°C, overnight. (A) Effect of PBS pH on bioconjugation. (B) Temperature dependence. (C) Time dependence for bioconjugation reaction. (D) Equivalents of 2PCA-LP to protein. (E) Ratio of organic solvent to inorganic buffer. (F) Comparison of conversion depending on organic solvents, DMSO (left) and DMF (right) at three different pH's. Conjugation was monitored by LC-MS.

DMF and DMSO were the selected organic solvents due to their prevalence in the bioconjugation literature.[109] pH 7.5 corresponded with the greatest conversion at 66%. The temperature was determined to be optimal at 25 °C, with minimal conversion at temperatures above 37 °C, thought to be due to the hydrolysis of the 2PCA reagent being a competing side reaction that dominated at higher temperatures as shown in ***Figure 32***.

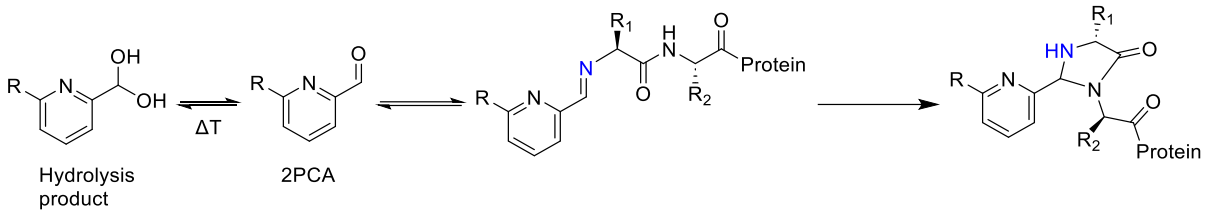

Figure 32 Equilibrium between the aldehyde form of the 2PCA reagent, and the diol hydrolyse form. At temperatures ≥ 37°C it was assumed the hydrolysis product made up nearly all the 2PCA reagent.

The optimal 2PCA bioconjugation to SHIRT that was achieved represented a ~80% protein conversion. 6 to 18 hours of reaction time resulted in acceptable conversion with more time resulting in marginal increases in conversion. 100 equivalents of 2PCA-LPA proved sufficient for achieving optimal conversion, and higher percentages of organic solvent gave better yields, likely driven by the hydrophobicity of 2PCA-LPA. Following the 2PCA screening process, for subsequent electrochemical analysis, 2PCA.SHIRT.EV was produced using the viologen-labelling method detailed in ***Section 2.3.3.***

Given that control protein film electrochemistry experiments shown previously (***Figure 25***) confirmed that the viologen-labelled thiol-free wild-type shirt (SHIRT.EV) could not be immobilised on a gold electrode, it did not matter that optimised 2PCA bioconjugation reactions yielded approximately 20% lipoic acid-free SHIRT. Initially, it was not possible to form a protein film using the same electrode soaking conditions used for CGGC.SHIRT.EV. Instead, it was found that a reducing agent (TCEP initially and later DTT) was required, presumably due to the electrode surface not reducing the lipoic acid. Following this method development, the electrochemical investigation of 2PCA.SHIRT.EV was conducted. In CV, a shift in formal potential was observed, with the 2PCA.SHIRT.EV protein film displaying a midpoint potential value of -387 mV vs SHE relative to a value of -374 mV vs SHE from the equivalent measurements on CGGC.SHIRT.EV (***Figure 33 vs Figure 25***).

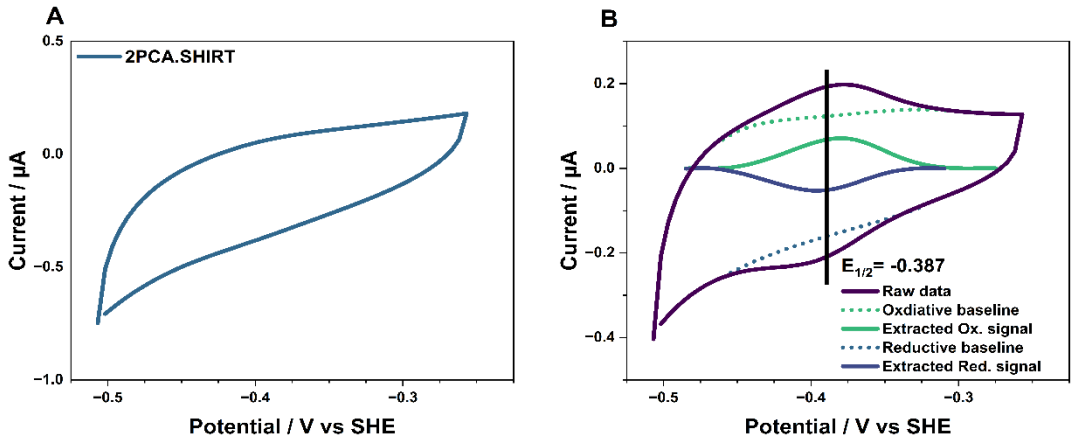

Figure 33 Gold disk working electrode CV measurements showing (A) the response of non-viologen labelled 2PCA.SHIRT and (B) the processed voltammogram for an ethyl viologen conjugate modified 2PCA.SHIRT protein, 2PCA.SHIRT.EV. The midpoint potential of -387 mV vs SHE is denoted by the vertical black line. Scans were measured at 100 mVs^{-1} Experiments were conducted in pH 7.5 buffer (100 mM sodium phosphate, 150 mM NaCl) at room temperature under a N_2 atmosphere. A platinum wire counter electrode and Ag/AgCl (3 M KCl) reference electrode were used. All experiments were started from the most negative potential.

An Ellman's assay was done to investigate the need for reducing agent in the electrode immobilisation step. A 250 µM sample of 2PCA.SHIRT had a concentration of 34.8 µM free sulfhydryl groups, with the theoretical maximum concentration being 500 µM. In comparison a 100 µM sample of CGGC.SHIRT had a free sulfhydryl concentration of 141 µM, showing the C-terminal CGGC motif preserves the Cys groups in the free thiol form.

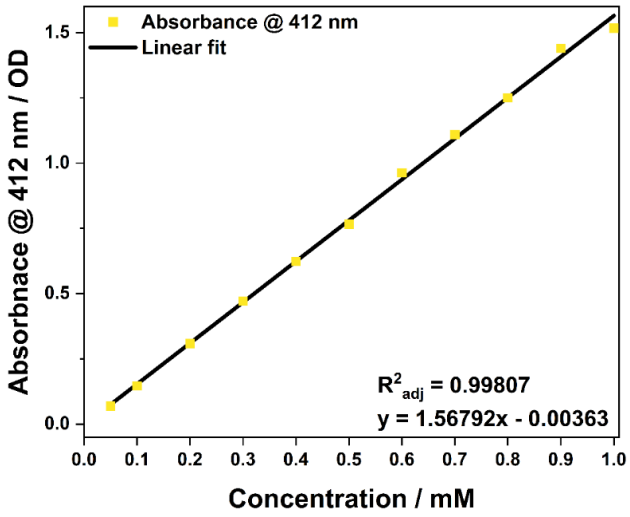

Figure 34 Ellman's assay calibration curve. The assay is used to detect the amount of free sulfhydryl groups detected in solution.

The need for a reducing agent when using lipoic acid is unusual and not observed in literature suggesting bioconjugation to SHIRT is the cause, preventing surface immobilisation.

From ***Figure 33***, 2PCA.SHIRT.EV had a coverage of ~ 8.5 pmol cm^{-2} which is over ten-fold lower than that of CGGC.SHIRT.EV's coverage value, the stability of 2PCA.SHIRT.EV on the electrode was far lower than CGGC.SHIRT.EV; ***Figure 35*** shows a film of 2PCA.SHIRT.EV suffering from a degradation of 28% in surface coverage over twelve hours.

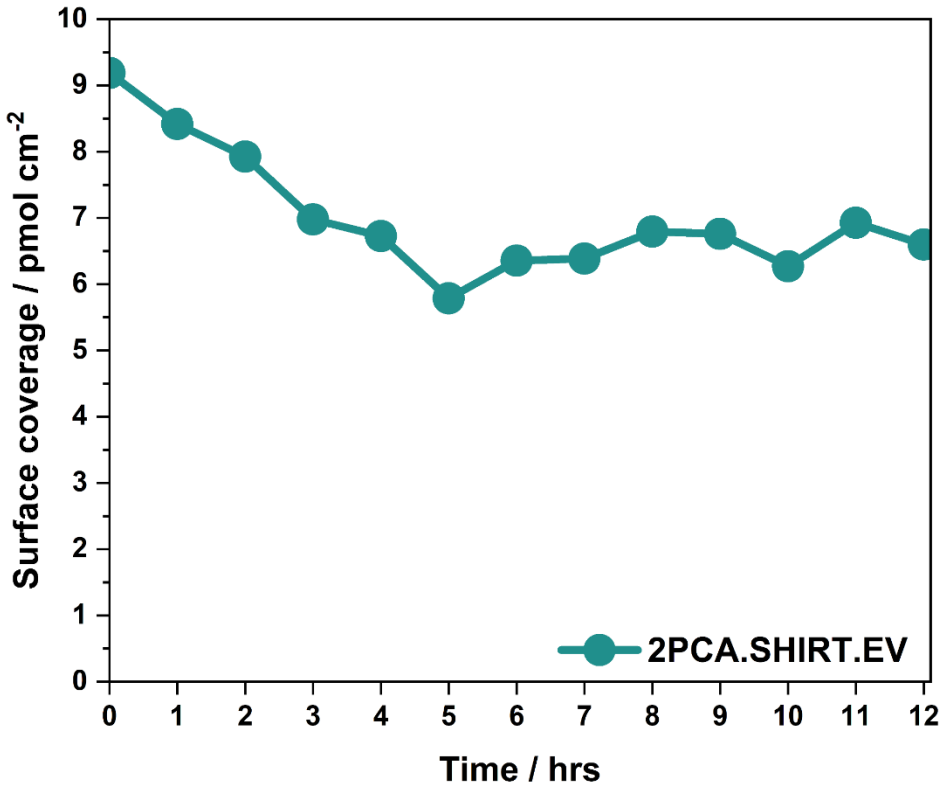

Figure 35 Plot of surface coverage against time for 2PCA.SHIRT.EV. Scans at 100 mV s^{-1} were taken hourly with the third scan being used to calculate surface coverage. Experiments were conducted in pH 7.5 buffer (100 mM sodium phosphate, 150 mM NaCl) at 25 °C under a N_2 atmosphere. A platinum wire counter electrode and Ag/AgCl (3 M KCl) reference electrode were used.

2.3.6 Electrochemical comparison of C- and N-terminus immobilised viologen-labelled SHIRT

2.3.6.1 Experimentation in N_2

The effect of pH on viologen labelled SHIRT CV data was first probed in a N_2 atmosphere. Under sufficiently reducing potentials, the gold electrode surface can catalyse the reduction of protons to form hydrogen ($2H^+ + 2e^- \rightarrow H_2$), as observed by a steep negative current at low potentials in "blank" (i.e. SHIRT-free) experiments in *Error! Reference source not found.*. As expected, this formation of H_2 is more prominent under more acidic conditions because the reduction potential for the proton/hydrogen couple ($E(2H^+/H_2)$) increases at lower pH, as predicted by the Nernst equation.[110] Because this H_2 generating electrocatalytic process will occur at the same speed regardless of experimental scan rate, the amount of current due to this electrocatalysis will remain the same in CVs measured at increasing scan rates. Conversely, the Faradaic current from electron transfer to/from surface confined viologen-labelled SHIRT and the non-Faradaic current from double layer charging scales linearly with scan rate, as shown above (***Figure 28***). Therefore, as shown in *Error! Reference source not found.**C*** **and** ***D***, it is possible to outpace the current contributions from proton reduction in CGGC.SHIRT.EV experiments at low pH, provided they are conducted at sufficiently fast scan rates.

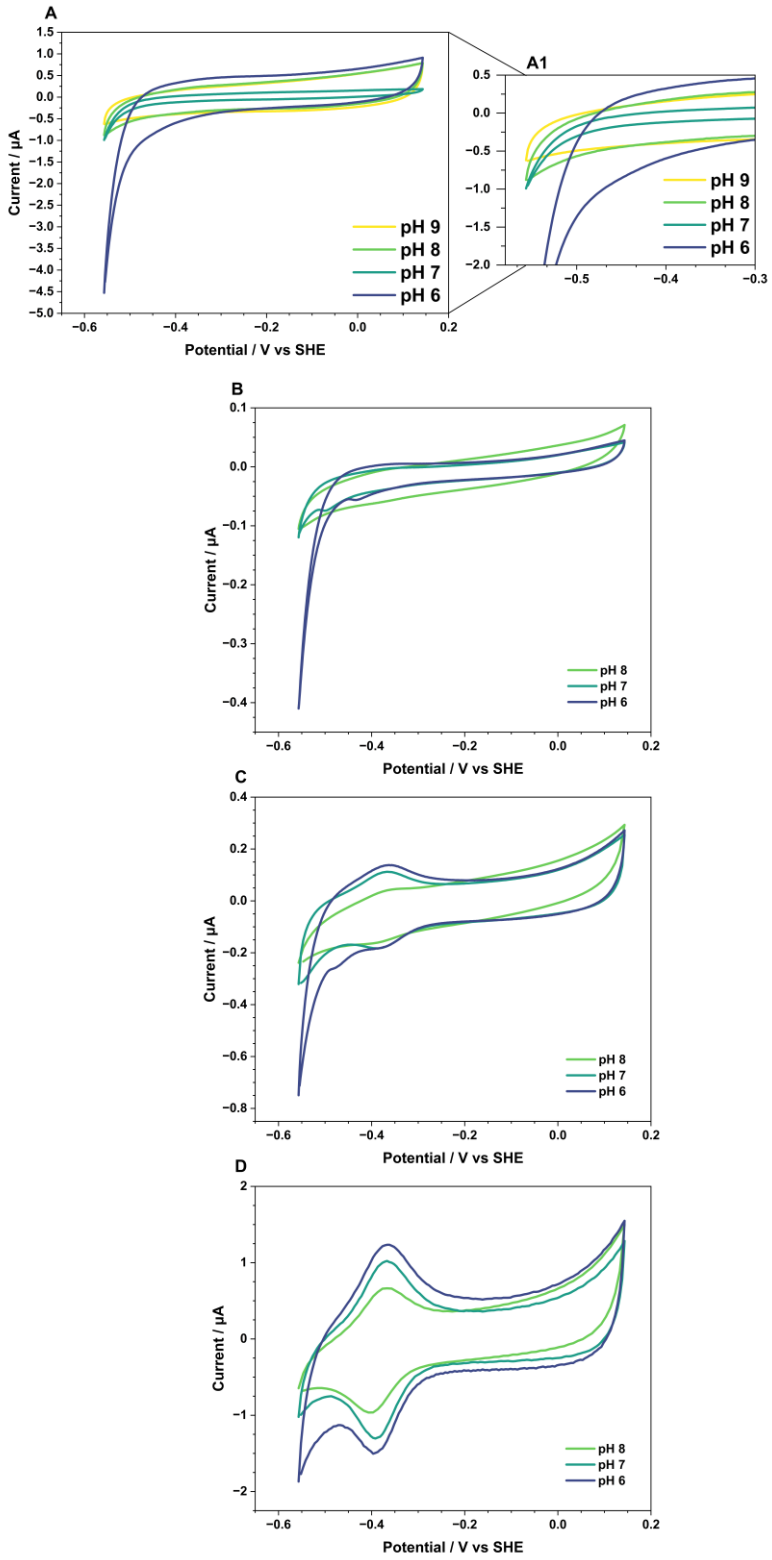

Figure 36 (A) CVs recorded for a blank (protein-free) gold disk electrode at 100 mV s^{-1} at four different pH's (6,7,8,9). Adjacent (A1) zoomed in region to emphasise the pH related hydrogen reduction onset (B-D) CV overlays of CGGC.SHIRT.EV at three different scan rates (B: 10 mV s^{-1}, C: 100 mV s^{-1}, D: 1000 mV s^{-1}) and pH (6, 7, 8). Experiments were conducted in PBS buffer (100 mM sodium phosphate, 150 mM NaCl) at room temperature under a N_2 atmosphere. A platinum wire counter electrode and a SCE reference electrode were used.

Figure 36 shows that relative to a bare gold electrode, the proton reduction current is smaller when CGGC.SHIRT.EV is attached. The same observation is made for 2PCA.SHIRT.EV (data not shown). This suggests that the bare gold surface is a better proton-reduction electrocatalyst that the SHIRT-EV system. However, as shown in *Error! Reference source not found.* at 10 mV s^{-1} there is little to no reversible peak-like viologen redox signal in measurements on CGGC.SHIRT.EV. It is speculated that at slower scan rates the immobilised viologen facilitates the process of proton reduction *via* $2H^+ + 2EV^{\bullet+} \rightarrow H_2 + 2EV^{2+}$; because the reduced viologen is constantly re-oxidised by reaction with protons the reduction peak is transformed into a reduction catalytic wave while the oxidation peak disappears from the CV. Worth also noting is that in appearance there seems to be an increase in the full width at maximum height (FWMH) when scan-rate is increased, however the FWMH for is near identical for all scan-rates.

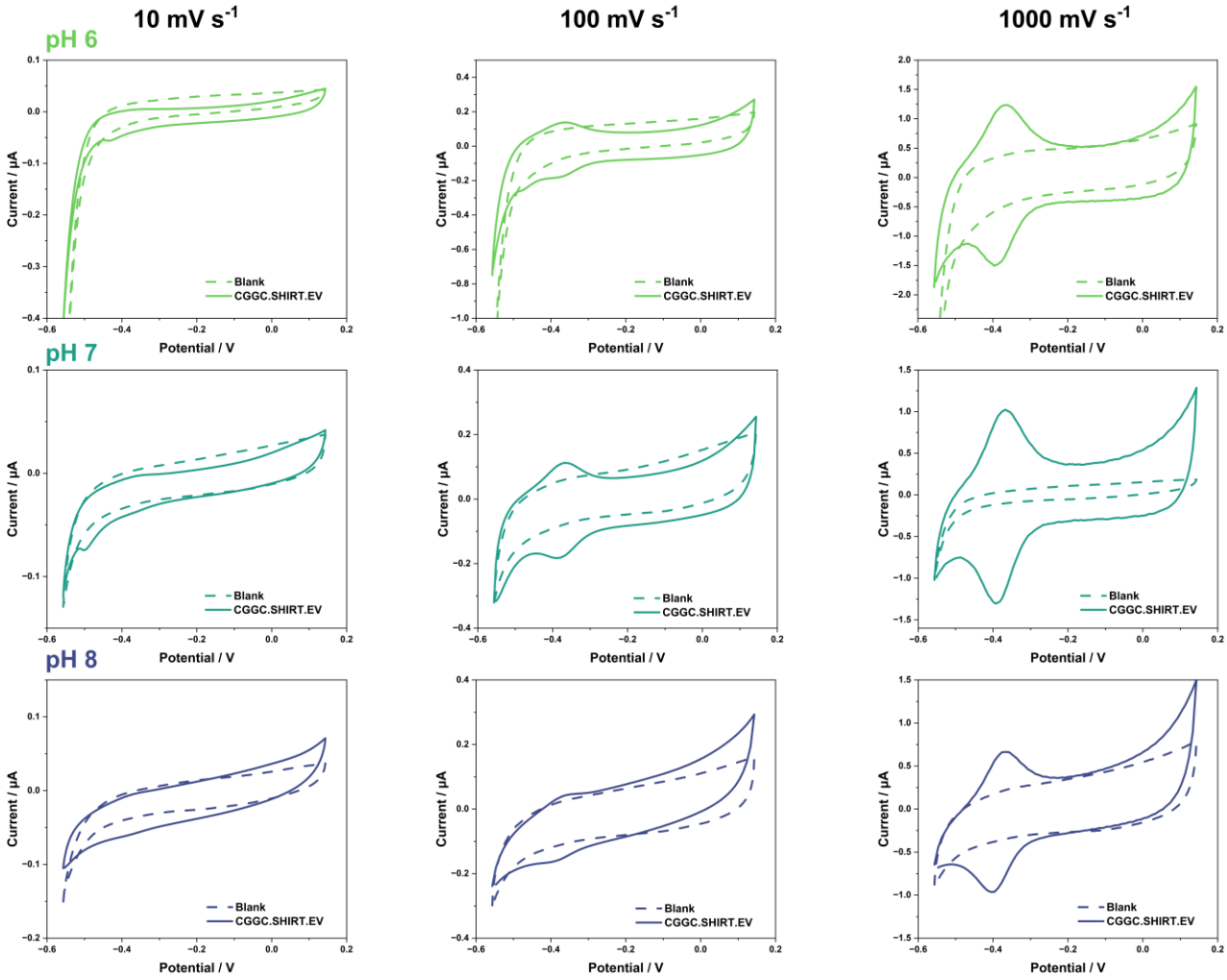

Figure 37 Gold disk electrode blank (protein-free) and CGGC.SHIRT CV's recorded at different pH (6, 7, 8) and scan rates: (left) 10 mV s^{-1}, (middle) 100 mV s^{-1}, (right) 1000 mV s^{-1}. Experiments were conducted in a PBS buffer (100 mM sodium phosphate, 150 mM NaCl) at room temperature under a N_2 atmosphere. A platinum wire counter electrode and a SCE were used. Experiments were started from the most negative potential.

2.3.6.2 Experimentation in open air

Experiments in air were conducted to determine the practicality of building a biosensor that could be used under normal atmospheric conditions. The buffer pH was again varied. As shown in ***Figure 38*A**, experiments on a bare gold disk electrode in air show clear evidence of oxygen reduction, as evidenced by the onset of negative current below approximately 0 V vs SHE, a process which is not observed under N_2.

Oxygen reduction can also be observed for a gold disk electrode functionalised with CGGC.SHIRT.EV. For both bare and CGGC.SHIRT.EV functionalised electrodes, the onset of oxygen reduction occurs at a higher potential with lower pH, as expected due to Nernstian changes in the midpoint potential of the oxygen/water reduction potential ($E(O_2/H_2O)$). Compared to direct oxygen reduction at the bare gold electrode surface, viologens allow for oxygen reduction at a higher potential (in **Figure *38***, oxygen reduction onset at pH 8 occurs at ~350 mV vs SHE on a blank electrode compared to ~210 mV for an electrode functionalised with CGGC.SHIRT.EV).

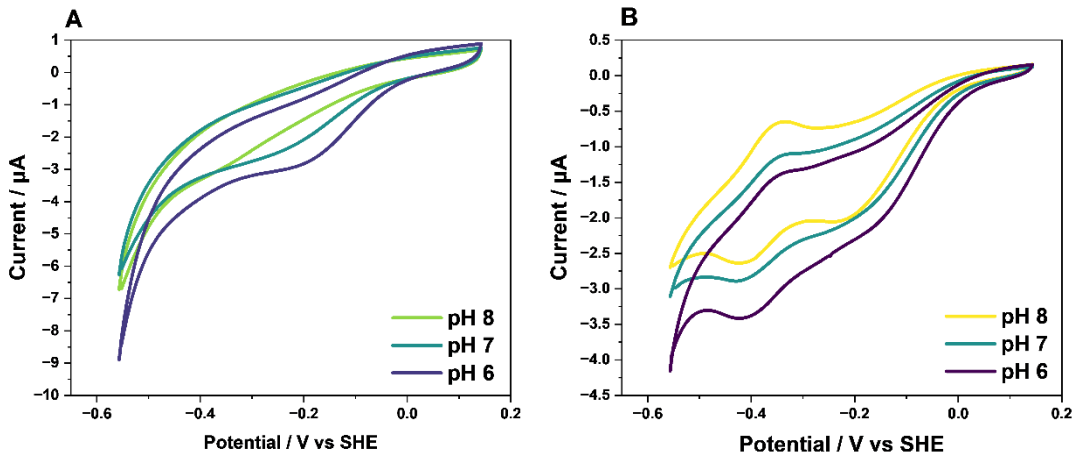

Figure 38 (A) Voltammogram of a blank gold electrode in air within the expected viologen redox window (B) Voltammetric response of CGGC.SHIRT.EV functionalised gold electrode in air. Experiments were conducted at 100 mVs^{-1} in PBS (100 mM sodium phosphate, 150 mM NaCl) at room temperature in the laboratory atmosphere. A platinum wire counter electrode and SCE were used.

Viologen modified surfaces have been previously investigated by researchers seeking to understand their electrocatalytic oxygen reduction properties.[111–113] The CV shape of the CGGC.SHIRT.EV data in ***Figure 38*B** is therefore described as arising from the following processes: first, as the potential is decreased from the most positive value, it reaches a level where reduction of oxygen can occur, resulting in a negative current. O_2 is consumed within the vicinity of the electrode and the process is so rapid that diffusion from the bulk solution becomes rate-limiting, so the current starts to rise as the potential decreases, resulting in an

apparent first “peak”. A subsequent negative current peak at more negative potential is then associated with $EV^{2+} \rightarrow EV^{\bullet+}$. The reduced viologen form, $EV^{\bullet+}$, in turn reduces oxygen, becoming re-oxidised to EV^{2+} (***Equation 8***). Due to the requirement for protons in the oxygen reduction reaction, when the scan direction changes the viologen oxidation peak is far more attenuated in pH 6 and 7 experiments relative to pH 8.

$$2\mathrm{EV}^{\bullet+} + O_2 + 2H^+ \rightarrow 2EV^{2+} + 2H_2O_2 \qquad \textbf{Equation 8}$$

Equation 8 Reaction for viologen mediated oxygen reduction.

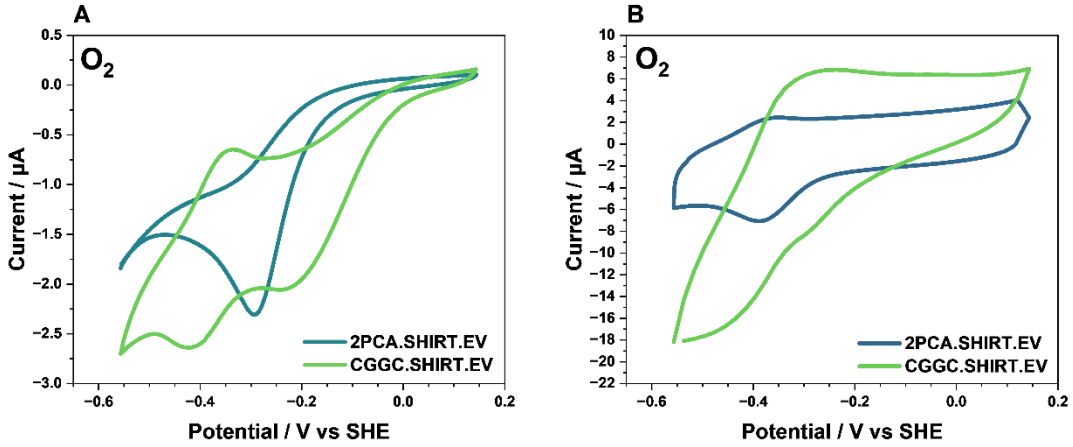

Figure 39 Voltammograms of 2PCA.SHIRT.EV and CGGC.SHIRT.EV on gold disk electrodes in air. (A) Experiment at 10 mV s^{-1}. (B) Experiment at 1000 mV s^{-1}. Experiments were conducted using a standard three electrode set-up in pH 8.0 PBS (100 mM sodium phosphate, 150 mM NaCl) at room temperature in the laboratory atmosphere. A platinum wire counter electrode and SCE were used.

As shown in ***Figure 39***, the CV of CGGC.SHIRT.EV and 2PCA.SHIRT.EV in air displayed different responses. The separation of the two peaks associated with oxygen reduction and viologen redox is reportedly dependent on the ratio of [Viologen]/[O_2] species.[114,115] The results shown in ***Figure 39*** therefore suggest that the surface coverage of the 2PCA.SHIRT.EV is low compared to CGGC.SHIRT.EV, in agreement with the surface coverage experiments reported above. CGGC.SHIRT.EV’s higher concentration of viologen at the electrode surface means the rate of formation of $EV^{\bullet+}$ is greater than the rate of oxygen diffusion through the buffer, yielding two distinct peaks. The difference in voltammograms between slow and fast scan rate

is attributed to the process of hydrogen production being relatively slow, allowing for the viologen to out-pace the process at faster scan rates.

2.4 Summary and conclusions

The functionalisation of SHIRT with viologen molecules *via* an activated-ester lysine targeting methodology proved to be a viable strategy for generating an artificial SHIRT redox protein. Trypsin digestion MALDI elucidated a near-total coverage (>90%) of viologen to lysine residues, with the recalcitrance of a single residue to labelling being attributed to the surface inaccessibility of this one amino acid residue. nanoDSF reported a small decrease in melting point for the SHIRT protein post viologen labelling suggesting conformational retention after bioconjugation.

The immobilisation of viologen labelled SHIRT to a gold electrode surface *via* C-temrinal Cys residues introduced *via* site-directed mutagenesis was successful, with a formal potential of - 374 mV vs SHE at pH 7.5, room temperature being determined *via* electrochemical analysis of CGGC.SHIRT.EV. Bioconjugation at the N-terminus also proved successful with the lipoic acid labelled 2PCA.SHIRT generated with a conversion of >80%. This species was also successfully modified with viologen and immobilised onto a gold electrode yielding a formal potential of - 387 mV vs SHE at pH 7.5, room temperature for 2PCA.SHIRT.EV.

The two strategies are illustratively compared in ***Figure 40***. Immobilisation of viologen-labelled SHIRT onto a gold electrode *via* the C-terminal di-Cys strategy was more effective compared to N-terminal immobilisation using a lipoic acid functionality installed *via* bioconjugation. The diCys immobilised viologen-SHIRT yielded larger electron-transfer signals and a more stable film.

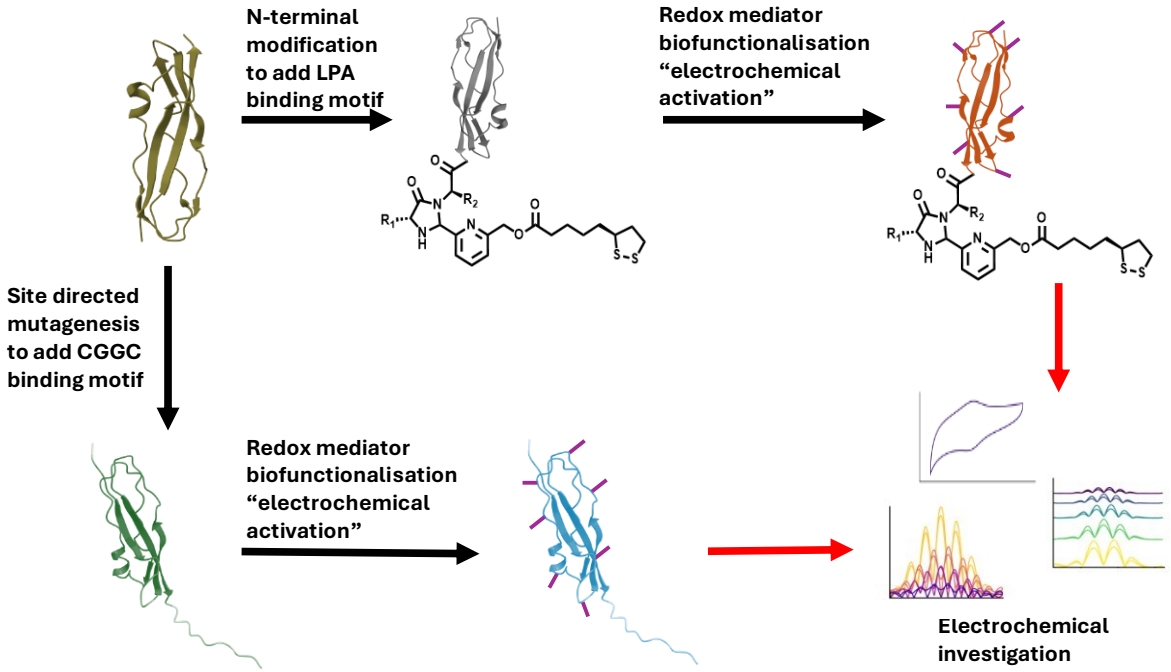

Figure 40 Summary of protein related modification highlight a general scheme including Immobilization method (N-terminal modification, Site directed mutagenesis), Redox mediator functionalisation and measurements showing the functionalised forms of immobilized protein with direct cyclic voltammetry and Fourier transformed alternating current voltammetry.

3 Developing a SHIRT electrochemical biosensor

3.1 SH3 SHIRT bio-electrochemical sensor design

3.1.1 SH3-binding SHIRT construct design

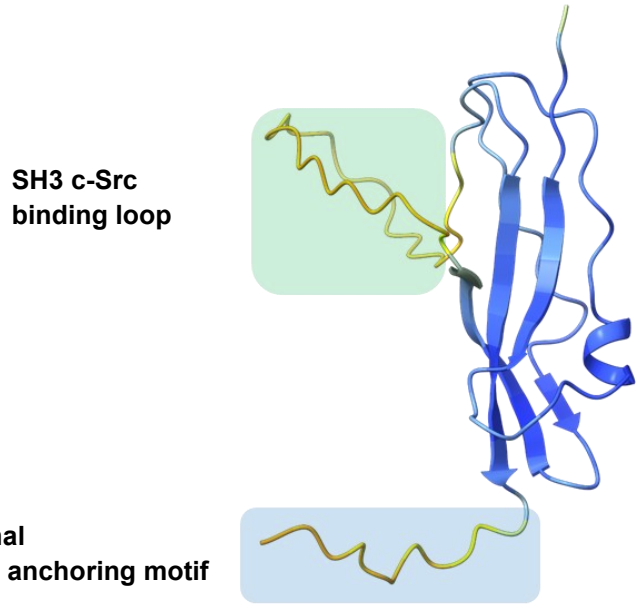

Figure 41 (Top) AlphaFold predicted model for CGGC.SBtSH3. (Bottom) Sequence for CGGC.SBtSH3 showing lysine residues (purple), mutated arginine residues (red), SH3 c-Src binding loop (green), and CGGC binding motif (blue).

As briefly introduced in ***Chapter 1.2.1***. SHIRT constructs have been previously developed which incorporate peptide binding loops to facilitate binding to the protein SH3, specifically through the introduction of a so-called “Vsl12” recognition loop (***Figure 41***). The structure and sequence of SH3 can be seen in ***Figure 42***. The aim of ***Chapter 3*** is to explore using the methods from the previous chapter to make an electrode immobilised, viologen-labelled SH3-binding SHIRT construct that will function as a biorecognition element in a bio-electrochemical SH3 biosensing FTacV experiment.

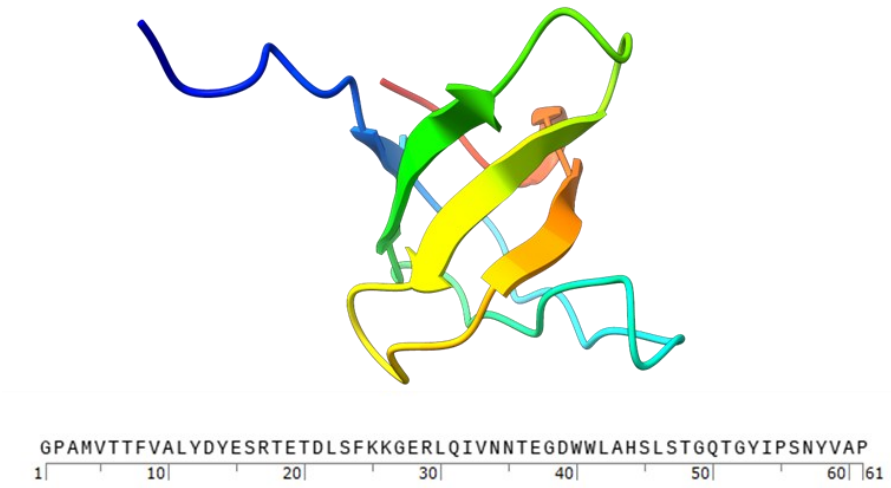

Figure 42 Structure and sequence of SH3 c-Src domain protein supplied by Dr Rachael Cooper

The development of a SHIRT-based biorecognition element for SH3 is medically relevant due to SH3 domain proteins playing a role in multiple signalling and regulatory systems in mammalian cellular pathways, typically acting as a binding partner to proline rich sequences. Mutation to the SH3 sequence has been associated with multiple diseases, cancers[116] and neurological issues,[117] with SH3 (and other *c-Src* protein tyrosine kinases) being investigated as candidates for potential drug targets.[34]

3.1.2 Gold screen-printed electrodes

Screen-printed electrodes are miniature, all-in-one electrochemical cells (***Figure 43***). The advantage of SPEs compared to conventionally used disk electrodes comes from their lower fabrication costs, production scalability and accessibility in operation. Fabrication of SPEs is done by printing different inks on paper, ceramic or plastic substrates. SPEs are a suitable platform for electrochemical biosensor development because they are inexpensive (commercial electrodes typically costing <$5.00 per electrode) and only low volumes of analyte (50-500 µL) are required.[118–121] SPEs suffer from variability between produced electrode batches, typically having “rougher” surfaces compared to disk electrodes. A particular challenge when using gold working electrode SPEs is that the rigorous mechanical and electrochemical steps used to prepare gold disk electrodes for thiol bond formation cannot be applied because this would strip the thin electroplated gold layer.

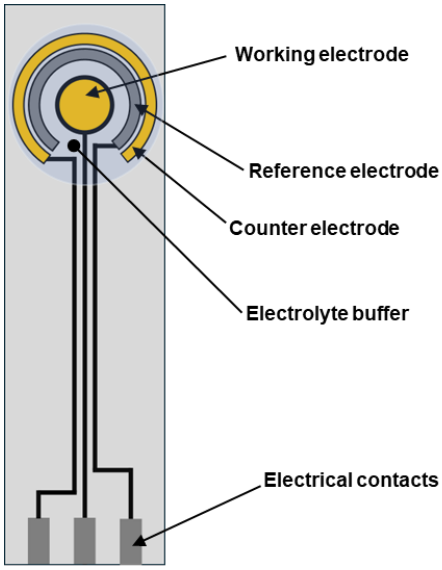

Figure 43 Diagram of a gold screen-printed electrode.

3.2 Aims

The focus of the experiments described in this chapter are to:

- Apply the bioconjugation tools developed in ***Chapter 2*** to the SH3-binding SHIRT scaffold SBtSH3.
- Demonstrate the immobilisation and electrochemical detection of viologen labelled SBtSH3 on a screen-printed electrode surface.
- Prove bio-electrochemical sensing of SH3 *via* FTacV measurements of viologen labelled SBtSH3.

3.3 Results and discussion

3.3.1 di-Cys SH3 binding SHIRT construct (*CGGC.SBtSH3*)

3.3.1.1 Purification of CGGC.SBtSH3

A plasmid for CGGC.SBtSH3 was designed by Dr Natalia Baranska, removing lysine amino acid residue K64 (***Section 2.1.1***), to try and achieve homogenous lysine labelling. The plasmid was used to transform into competent BL21 (DE3) *E. coli via* heat shock and plated onto media containing ampicillin. Colonies were selected and overexpressed using shake-flask conditions, before the CGGC.SBtSH3 protein was purified using immobilised metal affinity chromatography (IMAC) and size exclusion chromatography (SEC) as described in ***Section 5.3.1.1***.

As shown ***Figure 44*****,** an SDS-PAGE gel confirmed the presence of a single, purified protein product in eluted fractions from SEC. The sequence of purified protein was analysed using trypsin digestion and MALDI-MS, which confirmed the correct amino acid sequence of the CGGC.SBtSH3 construct. It is notable that unlike the wild type protein (***Section 2.3.1***), the SHIRT variant runs close to the theoretically correct molecular weight of 12.7 kDa. This is attributed to the introduction of the SH3 binding loop causing the protein to be less stable.

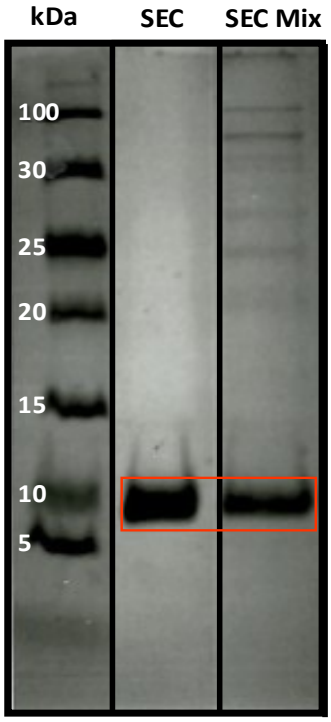

Figure 44 15% bis-acrylmide gel with a PageRuler™ Unstained Range Protein Ladder showing the presence of purified CGGC.SBtSH3 (red box) in pooled fractions.

3.3.1.2 Viologen bioconjugation to CGGC.SBtSH3 and analysis

Bioconjugation to the purified CGGC.SBtSH3 protein with the activated ester viologen was performed using the procedure described in ***Section 5.3.2***. The viologen labelled product, CGGC.SBtSH3.EV, was then immobilised onto a gold SPE and CV confirmed the expected redox functionality as shown in ***Figure 45***.

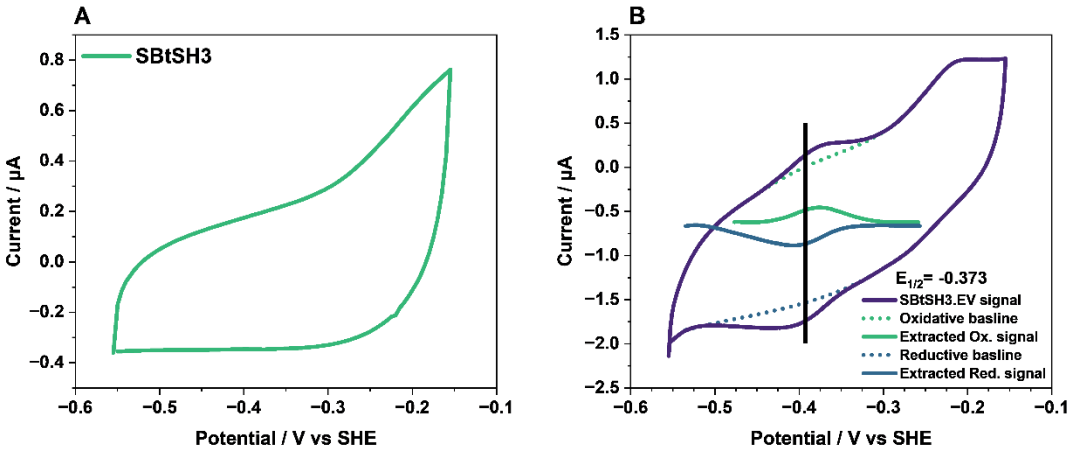

Figure 45 (A) Voltammogram of SBtSH3 immobilised on a gold SPE (B) Voltammetric response and the extracted electron-transfer signal of SBtSH3.EV immobilised on a gold SPE. Experiments were conducted at room temperature pH 7.5 (100 mM sodium phosphate, 150 mM NaCl) and in a N_2 atmosphere.

Analysis of the CV measurement of SBtSH3.EV yields a midpoint potential of –373 mV vs SHE within a similar region to previously immobilised SHIRT.EV proteins (***Section 2.3.4 and 2.3.5***). Peak broadening is observed in both the anodic and cathodic peaks. Next, CV experiments were conducted in air. SBtSH3.EV displayed similar stability to CGGC.SHIRT.EV (***Figure 46***), however the coverage values were approximately a fifth that of CGGC.SHIRT.EV.

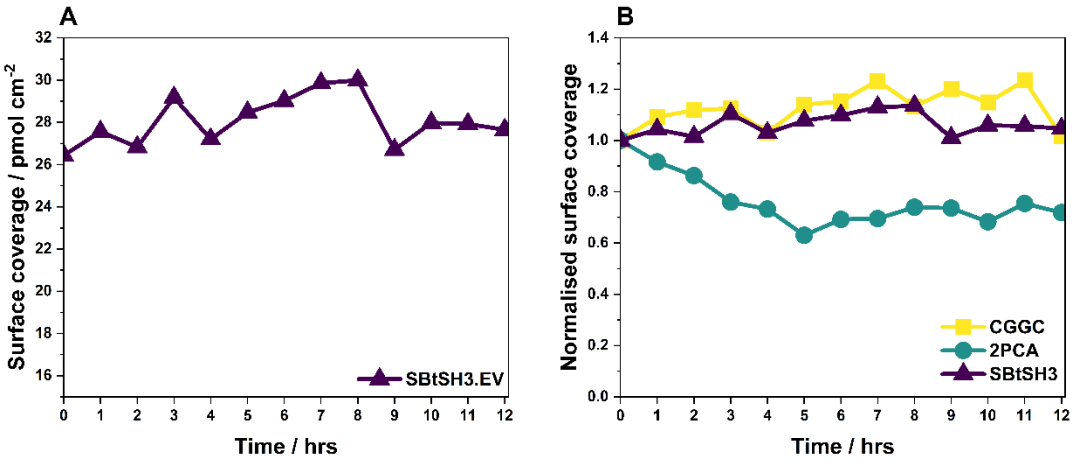

Figure 46 Plot of surface coverage against time (A) SBtSH3.EV, experiments were conducted at room temperature, pH 7.5 (100 mM sodium phosphate, 150 mM NaCl) and in air. (B) Normalised coverage comparing CGGC.SHIRT.EV and 2PCA.SHIRT.EV in a N_2 atmosphere alongside SBtSH3.EV in air, points are normalised by the first recorded point at t = 0.

SBtSH3.EV was analysed by SDS-PAGE and multiple protein bands were observed when using a 16% Tris-Tricine gel. Trypsin digestion and MALDI mass spectroscopy was then carried out. **Figure *47*** shows the results of the mass spectroscopy displaying poor lysine conversion compared to **Section 2.3.3.3**. Lysine's K47, K51, and K60 had zero viologen conjugate present. Lysine K24 had a maximum coverage of 6%, K17 coverage was 63%, and K35 had coverage of 46%.

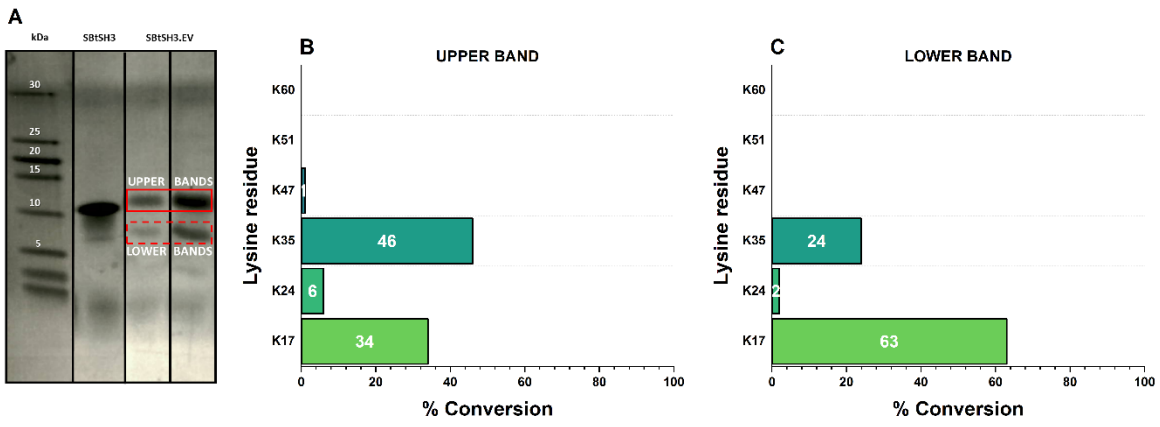

Figure 47 (A) 16.5% Tris-Tricine gel of viologen modification of SBtSH3 and plotted results from trypsin digestion MALDI analysis. (B) Bar chart displaying the conversion of lysine for SBtSH3 (upper gel band), (C) Bar chart displaying the conversion of lysine for SBtSH3 (lower gel band).

The MALDI analysis exemplifies how deletion of the lysine residue with poor coverage was unsuccessful in achieving total viologen coverage on the remaining lysine residues. Poor viologen labelling of the lysine residues on CGGC.SBtSH3 is speculated to be caused by the introduction of the peptide binding blocking the bioconjugation from occurring. Unfortunately,

due to the timescale of the project, it was necessary to proceed with biosensing experiments using aliquots of the heterogeneous CGGC.SBtSH3.EV protein bioconjugation product. It also exemplifies how deletion of lysine residues with poor coverage was unsuccessful in achieving total viologen coverage on the remain lysine residues. The lower labelling efficiency explains the intensity of the viologen peaks in ***Figure 48*** being lower than observed in equivalent CV measurements in ***Chapter 2***.

FTacV was previously proven capable of discriminating between irreversible and reversible electron-transfer processes, in numerous published studies.[59] The response of a SBtSH3.EV modified gold SPE under N_2 and air was compared *via* CV and FTacV. ***Figure 48*** shows that in CV measurements the viologen mediated oxygen reduction is clearly observed in air and dominates the viologen only electron transfer signals observed in a N_2 atmosphere. Conversely, ***Figure 48B*** shows that when FTacV is used the difference between the 4th, 5th and 6th harmonics extracted from scans in air and N_2 is minimal because only the rapid viologen electron transfer processes contribute to these signals.

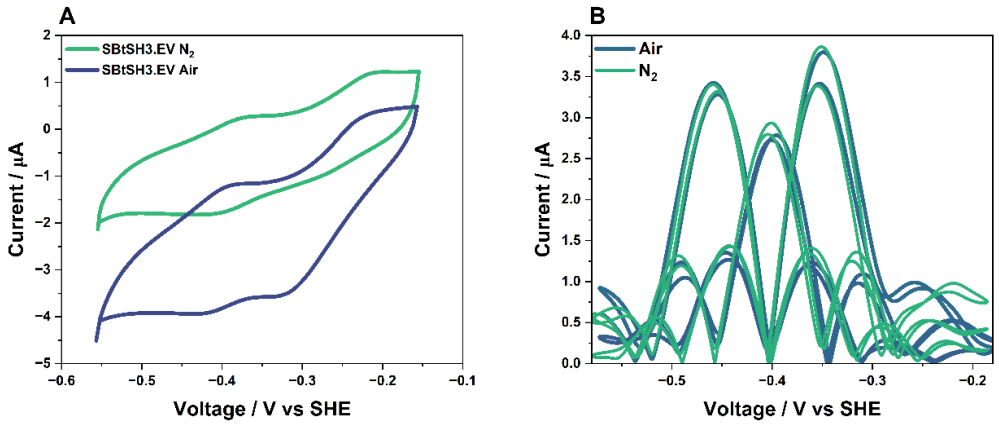

Figure 48 (A) 100 mV s^{-1} CVs of SBtSH3.EV in N_2 atmosphere and air. (B) FTacV of SBtSH3.EV in N2 atmosphere and air, 4th, 5th and 6th harmonics overlaid, the measurements were recorded on a "home-build" instrument; ω = 9.54 Hz, ΔE = 150 mV, v = 59.60 mV s^{-1}, DC potential range = -0.4 – 0.8 V. All experiments were conducted in pH 7.5 buffer (100 mM sodium phosphate, 150 mM NaCl) utilising a gold screen printed electrode with an Ag/AgCl reference electrode. CV experiments were started from the most negative potential

3.3.2 SH3 c-Src domain

3.3.2.1 Purification

The plasmid for the SH3 c-Src domain was provided by Dr Rachael Cooper from the Plevin group. The plasmid was used to transform into competent cells, and the protein was expressed and purified in the same manner described in **Section 3.3.1**.

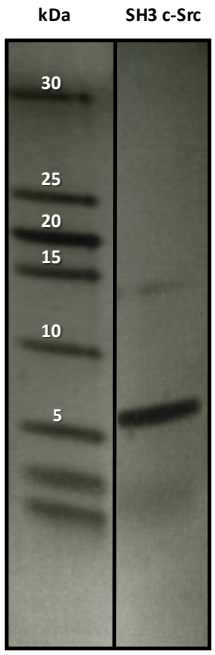

Figure 49 16.5% Tris-tricine SDS-PAGE confirming the purification of SH3 c-Src.

SH3 c-Src has a theoretical mass of 6.8 kDa, and the use of a 16.5% Tris-tricine SDS-PAGE gel reveals a protein band in an appropriate position. The successful purification of SH3 c-Src was further confirmed using trypsin digestion and MALDI-MS (data not shown).

3.3.3 Bio-electrochemical sensing of SH3 binding

SH3 c-Src binding to SBtSH3 would represent a ~50% increase in the molecular mass of the SBtSH3 protein, and it was hoped this would cause a change to the viologen electron transfer process, either blocking the redox mediator from passing electrons to the electrode surface or causing a reorganisation of the SHIRT that altered the electron transfer distance and in turn the associated current.

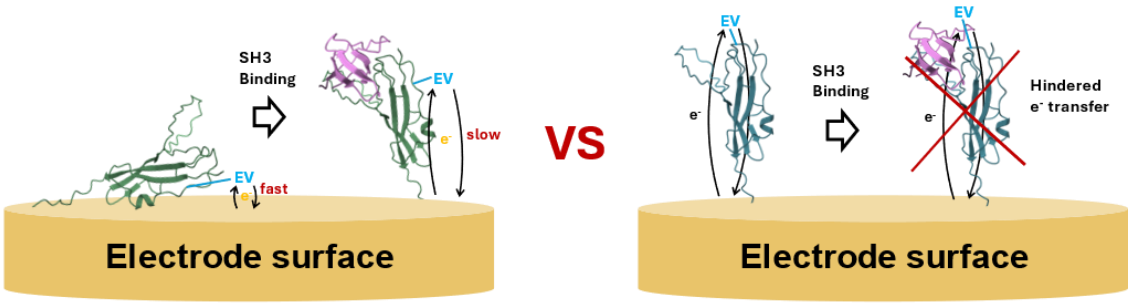

Figure 50 Example of the potential mechanisms which cause the decrease in signal when SH3 binding occurs to CGGC.SBtSH3.EV

Figure 51 shows the results of initial FTacV electrochemical biosensing experiments in air, where a 1 mM SH3 solution was applied for 3 minutes to gold SPEs functionalised with CGGC.SBtSH3.EV. The current response from the 6th harmonic showed a 26–45 % decrease, corresponding to the binding of SH3 to the electrode surface. The same signal loss wasn't seen in control experiments where a CGGC.SBtSH3.EV functionalised SPE was submerged in a phosphate buffer solution. Signal loss was however observed when a functionalised electrode was submerged in a 1 mM BSA solution, where a signal decrease of up to 66% was seen, (***Figure 52***), displaying non-specific binding to the electrode or peptide binding loop.

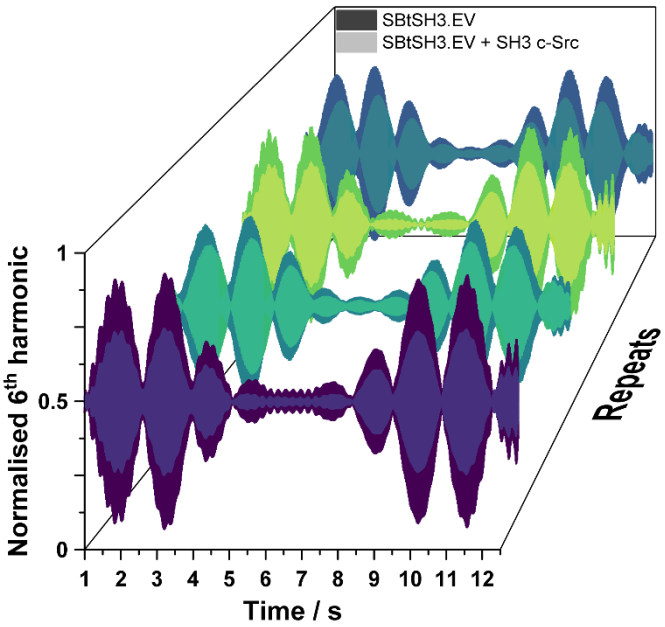

Figure 51 Extracted 6th harmonic from repeated FTacV binding experiments involving four Au-SPE functionalised with SBtSH3.EV and then incubated for 3 minutes with SH3 c-Src (1 mM). The darker plotted data represents the signal from SBtSH3.EV prior to the addtion of SH3 c-Src and lighter data represents the signal post addition of SH3 c-Src after 3 minutes. The measurements were recorded on a "home-build" potentiostat; ω = 9.54 Hz, ΔE = 150 mV, v = 59.60 mV s^{-1}, DC potential range = -0.4 – 0.8 V. Experiments were conducted in a pH 7.5 buffer (100 mM sodium phosphate, 150 mM NaCl), in air at room temperature.

The 6th harmonic was selected due to its consistency in response to the presence of SH3 binding to the SBtSH3.EV modified electrode, as shown in **Figure 53** which charts the change in the maximum current (i_{max}) of different harmonics as a function of SH3 incubation time. As expected, harmonics 1-3 yield a complex response because of the contributions from non-Faradaic processes and oxygen reduction.

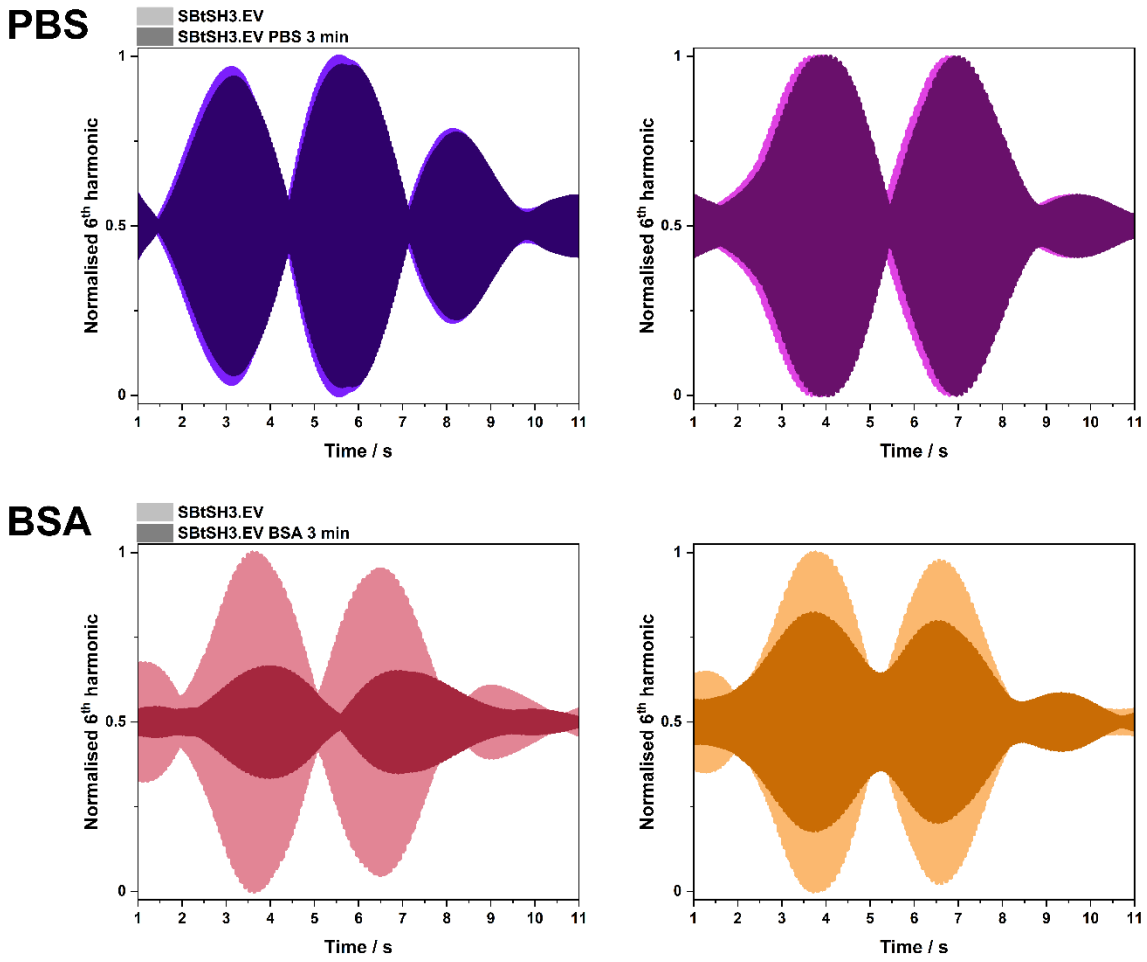

Figure 52 Extracted 6th harmonic from repeated FTacV binding experiments involving four Au-SPE functionalised with SBtSH3.EV and then incubated for 30 minutes with either BSA (1 mM) or PBS buffer. The lighter plotted data represents the signal from SBtSH3.EV prior to the addtion of BSA/PBS and the darker data represents the signal post 3 minutes of incubation. The measurements were recorded on a "home-build" potentiostat; ω = 9.54 Hz, ΔE = 150 mV, v = 59.60 mV s^{-1}, DC potential range = -0.4 – 0.8 V. Experiments were conducted in a pH 7.5 buffer (100 mM sodium phosphate, 150 mM NaCl), in air at room temperature.

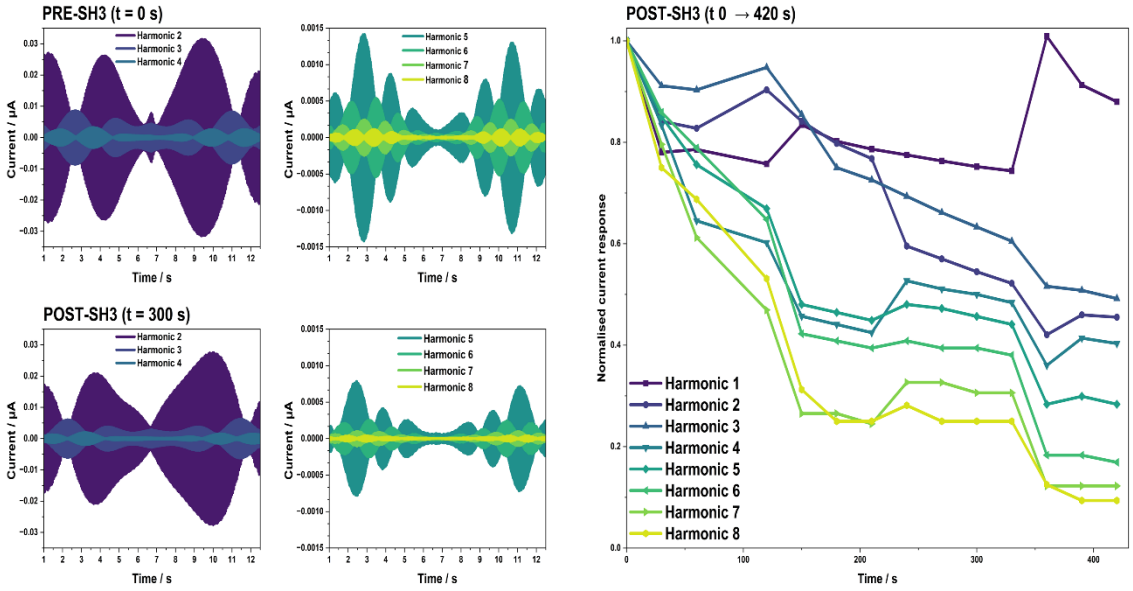

Figure 53 (Left) Overlaid voltammograms of the total currents extracted from harmonics 2-8 in FTacV experiments before (top) and three minutes after (bottom) the addition of SH3. (Right) The normalised peak currents extracted from harmonics 2-8 over five minutes of SH3 binding with measurements recorded every thirty seconds. The measurements were recorded on a "home-build" potentiostat; ω = 9.54 Hz, ΔE = 150 mV, v = 59.60 mV s^{-1}, DC potential range = -0.4 – 0.8 V. Experiments were conducted in a pH 7.5 buffer (100 mM sodium phosphate, 150 mM NaCl), in air at room temperature.

Next an electrochemical titration experiment using different concentrations of SH3 was conducted by the addition of increasing concentrations of SH3 which were then allowed to bind for five minutes after which a measurement was taken. The equilibrium dissociation constant was calculated using a variation of the Hill equation.[122] [SH3] is the concentration of SH3, n is the Hill coefficient, and K_A is the equilibrium association constant. The K_d was extracted from a simulated fitting of the Hill equation, where K_d was calculated to be 0.0056 µM. This K_d is significantly lower compared to literature for similar binding loops, where K_d values are reported to range between 0.3-145 µM.[123–125] This is speculated to be due to a lack of resolution at lower concentrations.

$$R = \frac{1}{1 + \left(\frac{K_A}{[SH3]}\right)^n}$$

$R =$	Fraction of bound receptor protein (relative response).
$[SH3] =$	Substrate (SH3) concentration / µM
$K_A =$	Association constant
$n =$	Hill coefficient

Equation 9 Hill equation for the calculation of the association constant of SH3.

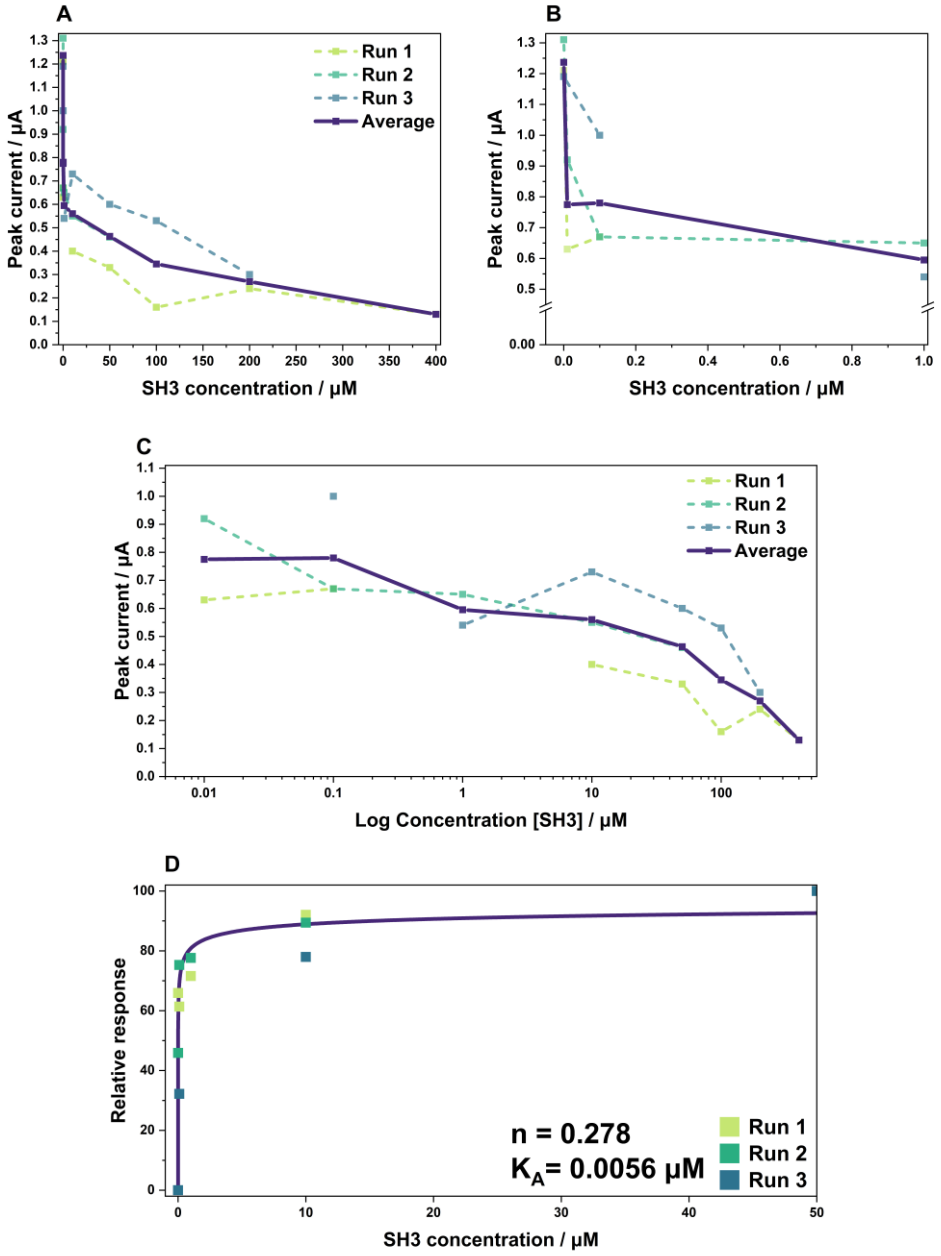

Figure 54 Extracted peak currents from 5th harmonic from three runs (dotted line) of SBtSH3.EV modified Au-SPEs titrated against increasing concentrations of SH3. The average of all three runs is shown as a solid line. (A) Full titration concentration range of 10 nM – 400 µM SH3. (B) Titration concentration range of 10 nM – 1000 nM SH3. Experiments were conducted in a pH 7.4 buffer (100 mM sodium phosphate, 150 mM NaCl), in air at room temperature. (C) Logarithmic plot of the extracted peak current from the 5th harmonic against the titration concentration range of 10 nM – 400 µM (D) Fitted Hill plot analysis of the binding of SH3. The solid line represents a best fit for an average of values. Fitting was done using Microsoft excel, utilising the solver program.

Finally, to try and probe the kinetics of SH3 binding to the SHIRT biosensor, experiments were conducted using a 100 nM solution of SH3 in PBS buffer. A SBtSH3.EV functionalised electrode was initially electrochemically cycled in SH3-free PBS until a stable signal was seen, before being submerged in the SH3 solution and measured using consecutive FTacV measurements. The SPE was finally resubmerged in blank PBS to see if SH3 unbinding could be observed. More detailed information for the experimental protocol is provided in **Section 5.4.1.2**.

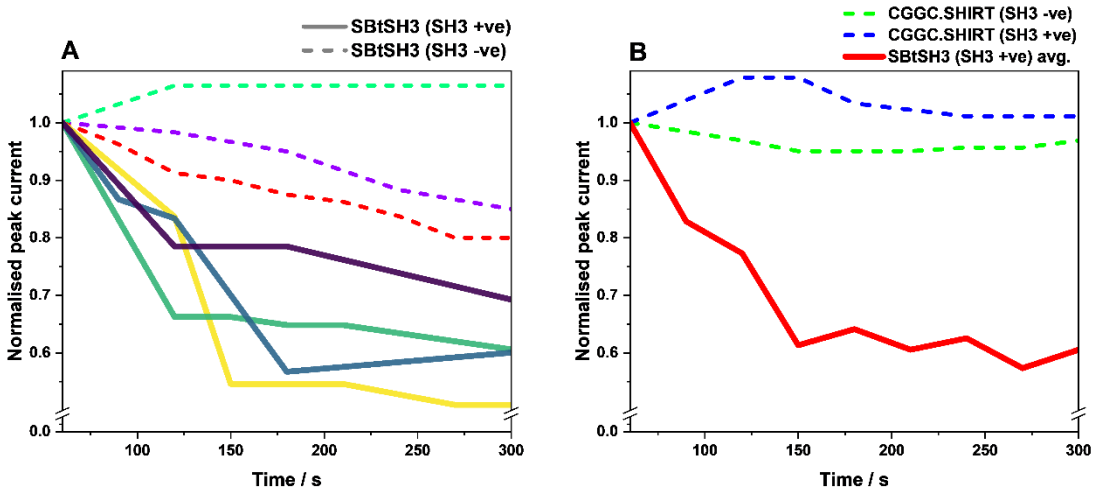

Figure 55 Peak potentials of the 6th harmonic from FTacV normalised relative to the measurement at t = 0 (A) Solid lines represent data from +SH3 c-Src experiments where SBtSH3.EV functionalised Au-SPE was placed in a 100 nM SH3 (pH 7.5, 100 mM sodium phosphate, 150 mM NaCl) solution. Dotted lines show data from -SH3 c-Src control experiments where SBtSH3.EV functionalised Au-SPE was left in pH 7.5 PBS (100 mM sodium phosphate, 150 mM NaCl). (B) Solid line showing the average of experiments in (A) and data from a control experiment using the peptide-loop free CGGC.SHIRT.

It was observed that when measuring consecutive FTacV measurements in 100 nM SH3, the electrochemical response stabilised after five minutes. Rate analysis for “on” binding was not attempted, with the kinetic resolution of the FTacV measurement deemed to be too slow for accurate determination. Post SH3-binding, when SPEs were transferred from SH3 solution to SH3-free PBS there was little change after 30 min (data not shown). It was therefore not possible to determine a k_{off} value.

3.4 Summary and conclusions

Detection of SH3 c-Src binding to SBtSH3.EV was successful even with less-than-ideal conjugation of viologen on the protein. Electrochemical detection of SH3 binding using the 6th harmonic extracted from FTacV was a robust strategy even in air. Unlike in CV, contributions from oxygen reduction current were invisible in the 6th harmonic from FTacV, and a consistent decrease in current was observed upon SH3 binding. SBtSH3.EV seemingly displays a high binding strength to SH3, with signal equilibration from a 100 nM solution being seen within minutes and a of K_d 0.006 μM was estimated. This is in comparison to literature values of 17.7 μM determined *via* isothermal titration calorimetry for the same binding loop. Unfortunately, BSA also binds to the gold SPE CGGC.SBtSH3.EV biosensor, suggesting future experiments to quantify the selectivity for SH3.

4 Conclusions and potential future work

4.1 Summary

The aim of this thesis was to probe the feasibility of developing an artificial redox active protein for detecting analyte binding. I believe this has been successful. The design and concept of an in-air working biosensor is seen in **Chapter 3**, time-based experiments were able to determine that SH3 binding to the loop occurs rapidly (within five minutes), and preliminary titration data suggests a k_d within the nanomolar range for SBtSH3.EV. This was determined using FTacV, utilising the peak current of the 6^{th} harmonic. Unfortunately, introduction of the SH3 binding loop caused a decrease in the viologen-lysine labelling efficiency.

4.2 Future considerations/outlook

Achieving a homogenous coverage of viologen molecules attached to the SH3-binding loop SHIRT construct proved more challenging than expected. Future work should consider whether viologen-labelling of multiple amino acid residues is the best path to follow. Instead, alternative bioconjugation strategies to modify a single specific amino acid residue may be more successful. With the rise of structural prediction AI tools it seems inevitable that a program will be developed to assist in designing such protein engineering approaches.

In **Section 3.3.3**, the electrochemical detection of SH3 binding to immobilised SBtSH3.EV was done towards the end of the project and extensive repeats, controls and alternative verification of SH3 binding using methods such as QCM-D, SPR or EIS couldn't be conducted due to time

constraints. The use of spectroscopic methods to elucidate the mechanism of what occurs during and after SH3 binding, and why this leads to decreased 6th harmonic FTacV viologen current, would be helpful for understanding the optimal position of viologen labels to detect analyte binding.

Finally, another natural extension to the work reported in this Thesis would be to apply the viologen-labelling, surface immobilisation and electrochemical testing methods to a SHIRT variant designed to possess small molecule binding capabilities. If a viologen label is within close enough proximity of a small molecule binding site, detection of binding could be possible, as hypothesised in ***Figure 56***. If successful, this could provide a powerful tool for detection of small molecules such as pharmaceuticals or environmental residues which could require the uniquely high solvent stability of SHIRT.

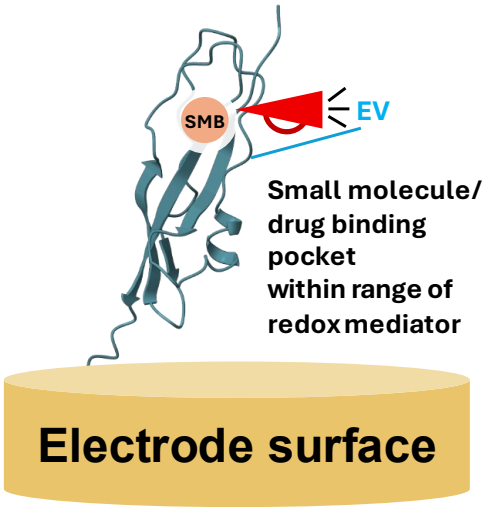

Figure 56 Graphic representation of a potential internal small molecule binding pocket "communicating" with a viologen molecule.

5 Experimental

5.1 Chemical Synthesis

5.1.1 Materials

All chemicals and solvents were bought from commercial suppliers (Fischer Scientific, Thermo Sigma-Aldrich, Flourochem, Merck) and used without purification unless said otherwise. When used, solvents were dried over activated 4Å molecular sieves or obtained from a PureSolv MD 7 solvent purification system, which dries the solvent through two drying columns filled with molecular sieves.

CGGC.SBtSH3 plasmid was designed and obtained from Dr Natalia Baranska (Department of Chemistry, University of York). SHIRT and CGGC.SHIRT plasmids were obtained from Dr Racheal Cooper (Department of Biology, University of York). Trypsin digestion and tandem MALDI-MS was performed by the Bioscience Technology Facility (Department of Biology, University of York).

5.1.2 Instruments

Proton nuclear magnetic resonance ^{1}H-NMR (400 MHz) and Carbon nuclear magnetic resonance ^{13}C-NMR (101 MHz) experiments were done using a JEOL ECX-400 (400 MHz) instrument at ambient temperature, unless stated otherwise. Data is reported in the manner of: Multiplicity is reported as singlet (s), doublet (d), triplet (t), quartet (q) or multiplet (m). Broad (br) is used as a prefix for a broad signal (e.g. br s). Chemical shifts (δ) were reported in ppm using residual solvent as a standard and coupling constants (*J*) in Hz. Spectra was processed using MestReNova ver. 14.3.3 software. FT-IR spectra experiment's for molecules were recorded in the range of 4000 – 400 cm^{-1} using a PerkinElmer AUTR Two FT-IR spectrometer at ambient temperature. High resolution mass spectra (HRMS) of molecules were done using Electrospray ionisation (ESI) mass spectra experiments were recorded using a Bruker compact TOF spectrometer coupled with a MS-Agilent 1260 Infinity series LC system. Measurement of mean error (m/z values) are reported with a mean error in ppm. Experiments were conducted by Karl Heaton at the University of York.

Liquid chromatography-mass spectrometry (LC-MS) analysis of proteins was done using a Dionex UltiMate 3000 RSLC system utilizing an Ultimate 3000 photodiode array detecting UV adsorption at 220, 270 and 280 nm using a C4 (150 x 2.1 mm, 1.9 µm) column. Coupled with a HCTultra ETD II ion trap spectrometer. HPLC water + 0.1% formic acid (solvent A) and

acetonitrile + 0.1% formic acid (solvent B), were used as a mobile phase at a flowrate of 300 µL min^{-1} using the multistep gradient: (**A:B** minutes (start-end)): **90:10** 0-5 → **10:90** 5-6.5 → **90:10** 6.5-7. Spectra were analysed using Bruker Data Analysis 4.4.2. Prior to LCMS analysis protein samples were exchanged into HPLC grade water using dialysis and diluted to a concentration of 50 µM.

Thin layer chromatography was performed on silica gel 60 F_{254} aluminium backed plates (Merck). Plates were visualised under a UVItec LF-204.S lamp visualising at 254 nm.

16.5% Mini-PROTEAN© tris-tricine gels were purchased from Bio-Rad and 15% bis-acrylamide gels were made in-house using a Bio-Rad Handcast system and the recipe used for the resolving and stacking gels is in Table below.

15% bis-acrylamide (resolving gel)	
Component	Volume
H_2O	2.4 mL
1.5 M Tris-HCl, 0.4% SDS, pH 8.8	2.5 mL
30% Acrylamide/bis solution	5.0 mL
20% Ammonium persulfate solution	50 µL
TEMED	10 µL

15% bis-acrylamide (stacking gel)	
Component	Volume
H_2O	3.2 mL
0.5 M Tris-HCl, 0.4% SDS, pH 6.8	1.3 mL
30% Acrylamide/bis solution	0.5 mL
20% Ammonium persulfate solution	12.5 µL
TEMED	8.0 µL

Table 2 Composition of 15% bis-acrylamide SDS-PAGE resolving and stacking gels.

TEMED and APS were the final component added to the mixture before being thoroughly mixed and cast into a cassette. Resolving gel was allowed to set and stacking buffer was put on top, with a sample lane comb inserted. After electrophoresis gels were stained using a quick Coomassie stain overnight.

5.1.3 Synthetic procedures

1-Ethyl-4,4'-dipyridinyl iodide **(MAW01/EV)**

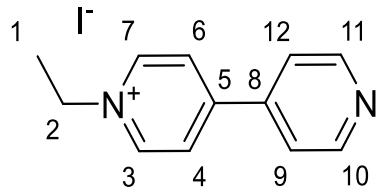

$C_{12}H_{13}N_2I$

MW: 312.15 g mol^{-1}

4,4'-bipyridine (3.35 g, 21.5 mmol, 1.0 equiv) was dissolved in acetone (30 mL) and under a N_2 atmosphere iodoethane (4.10 mL, 51.0 mmol, 2.4 equiv) was added dropwise. The reaction was heated to reflux and reacted for 18 h under a N_2 atmosphere. The reaction mixture was cooled to room temperature, filtered, and washed using excess acetone and dried collecting a yellow/orange product 1-Ethyl-4,4'-dipyridinyl iodide; **5.680 g, 18.2 mmol, 85.1%**.

HRMS: (EIS): Calculated for $C_{12}H_{13}N_2$ $[M]^+$ 185.1073 found 185.1073. (mean error -1.2 ppm)

^{1}H NMR: **(400 MHz, CDCl3)** δ 9.51 (d, *J* = 6.8 Hz, 2H,***H3,7***), 8.88 (dd, *J* = 6.36 Hz, 2H,***H10,11***), 8.37 (d, *J* = 6.8 Hz, 2H,***H9,12***), 7.70 (dd, *J* = 6.01 Hz, 2H,***H4,6***), 5.05 (q, *J* = 7.4 Hz, 2H,***H2***), 1.77 (t, *J* = 7.4 Hz, 3H,***H1***).

^{13}C NMR: (101 MHz, CHLOROFORM-*D*) δ 151.54 (C**12,11**), 145.23 (C**3,7**), 139.12 (C**5,8**) ,126.03 (C**9,12**), 126.03 (C**6,14**), 57.43(C**2**), 17.01 (C**1**)

IR (ATR) (cm^{-1}): 2969 (C-H), 1644 (C=N), 1176 (C-N)

1-(Carboxypentyl)-1‘-ethyl-4,4‘-bipyridinium dibromide **(MAW02)**

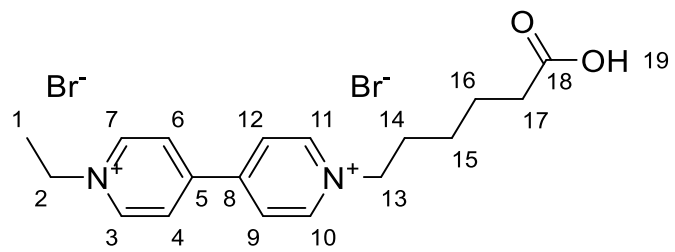

$C_{18}H_{24}N_2O_2Br_2$

MW: 460.21g mol^{-1}

The compound was prepared using a procedure modified by Dr N. Baranska from the literature.[126]

1-Ethyl-4,4’-dipyridinyl iodide (**MAW01**) (0.50 g, 1.60 mmol, 1.0 equiv) was dissolved in anhydrous acetonitrile (5 mL). 6-Bromohexanoic acid (5.01 g 25.7 mmol, excess) was dissolved in anhydrous acetonitrile (15 mL) and added to the reaction mixture and the solution was refluxed under an N_2 atmosphere for 72 h. After cooling to room temperature, the solvent was removed *in vacuo* and the solid was resuspended in acetone. The suspension was filtered and the solid was washed with excess acetone. The remaining solid was recrystalised using hot ethanol. The crystalized product was dissolved in deionised water (5 mL). The solution was filtered through celite, and the filtrate was flash-frozen and lyophilised to yield 1-(Carboxypentyl)-1‘-ethyl-4,4‘-bipyridinium dibromide as a yellow solid; **246 mg, 0.54 mmol, 46%**.

HRMS: (EIS): Calculated for $C_{18}H_{24}N_2O_2$ $[M-H]^+$ 299.1754 found 299.1753. (mean error 3.0 ppm)

1H NMR: (400 MHz, D2O): δ 9.11 (m, *J* = 6.5 Hz, 4H, ***H3,7,10,11***), 8.53 (d, *J* = 6.8 Hz, 4H, ***H4,6,9,12***), 4.74 (q, *J* = 14.9 Hz, 4H, ***H2,13***), 2.38 (t, *J* = 7.3 Hz, 2H, ***H17***), 2.10 (tt, *J* = 7.6 Hz, 2H, ***H16***), 1.72–1.61 (m, 5H, ***H1,14***), 1.48–1.34 (m, 2H, ***H15***).

^{13}C NMR: (101 MHz, D_2O): δ 173.94 (C**18**), 145.64 (C**3,7,10,11**), 127.26 (C**4,6,9,12**), 61.91 (C**13**), 57.79 (C**2**), 32.78 (C**14**), 30.67 (C**17**), 25.01 (C**16**), 23.78 (C**15**), 15.67 (C**1**)

1-(Carboxypentyl)-1‘-ethyl-4,4‘-bipyridinium *N*-hydroxy succinimide ester dibromide **(MAW03/EVC-NHS)**

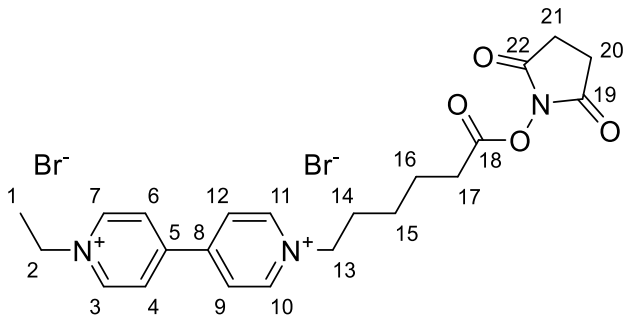

$C_{22}H_{27}N_3O_4Br_2$

MW: 550.04 mol^{-1}

The compound was prepared using procedure modified by Dr N. Baranska from literature.[127] 1-(Carboxypentyl)-1‘-ethyl-4,4‘-bipyridinium dibromide (**MAW02**) (60 mg, 130 µmol, 1.0 equiv), N-hydroxysuccinimide (15 mg, 134 µmol, 1.03 equiv), and N,N’-dicyclohexyl carbodiimide (DCC) (28 mg, 139 µmol, 1.06 equiv) were dissolved in anhydrous dimethylformamide (15 mL). The reaction mixture was stirred for 18 h at room temperature under an inert atmosphere. The solvent was then removed *in vacuo* and the solid was resuspended in in anhydrous acetonitrile (20 mL). The suspension was filtered through celite, and the residue was washed using excess acetonitrile and concentrated. The residue was then dissolved in deionised water, flash frozen, and lyophilized to yield 1-(Casrboxypentyl)-1‘-ethyl-4,4‘-bipyridinium *N*-hydroxy succinimide ester dibromide as an orange solid; **47 mg, 85 µmol, 64%**.

HRMS: (EIS): Calculated for $C_{22}H_{27}N_3O_4$ $[M]^{2+}$ 198.5995; found 198.5991. (mean error 0.3 ppm)

^{1}H NMR: **(400 MHz, ACETONITRILE-*D3*)** δ 8.90 (dd, *J* = 10.2 Hz, 4H, ***H3,7,10,11***), 8.38 (d, *J* = 6.2 Hz, 4H, ***H4,6,9,12***), 4.65 (dq, *J* = 14.6, 7.4 Hz, *J* = 6.2 Hz, 2H, ***H2,13***), 2.75 (s, 4H, ***H20,21***), 2.65 (t, *J* = 7.3 Hz, 2H, ***H17***), 2.01-2.10 (m, 2H, ***H1***), 1.71-1.83 (m, 2H, H***14),*** 1.65 (t, *J* = 7.3 Hz, 2H, H**16**), 1.43-1.52 (m, 2H, H***15)***

IR (ATR) (cm^{-1}): 2927 (C-H), 1703 (C=O), 1625 (C=N), 1217 (C-O), 1184 (C-N)

6-(Hydroxymethyl)-2-pyridinecarboxaldehyde **(MAW04/2PCA)**

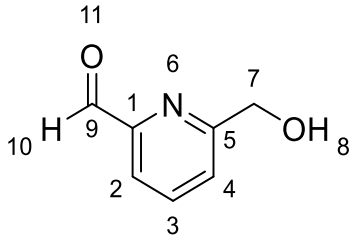

$C_7H_7NO_2$

MW: 137.14 mol^{-1}

The compound was prepared based on procedure from the literature.[128] 2,6-pyridinedimethanol (639 mg, 4.59 mmol) was put into a solution with 1,4-dioxane (20 mL) to which selenium dioxide (351 mg, 3.16 mmol) was added and the mixture was sonicated for five minutes. The reaction mixture was then stirred at 65 °C overnight. The mixture was then cooled to room temperature before being diluted using dichloromethane (50 mL) and filtered through celite. The filtrate was then concentrated under reduced pressure and purified using flash chromatography (DCM:MeOH, 20:1) yielding an oily yellow liquid of the title compound; **427 mg, 3.11 mmol, 68%.**

HRMS: (EIS): Calculated for $C_7H_7NO_2$ $[M-H]^-$ 134.0248; 134.0245 found. (mean error 3.1 ppm)

^{1}H NMR: **(400 MHz, CHLOROFORM-*D*)** δ 10.07 (s, *J* = 8.9 Hz, 1H, ***H10***), 7.92-7.85 (m, 2H, ***H2,4***), 7.49-7.56 (m, 1H, ***H3***), 4.87 (s, 2H, ***H7***), 3.61 (app s, 1H, ***H8***)

13C NMR: (**101 MHz, CHLOROFORM-D**) δ 193.07(C**9**), 160.39(C**5**), 151.55(C**1**), 137.67(C**3**), 124.80(C**4**), 120.38(C**2**), 64.11(C**7**).

IR (ATR) (cm^{-1}): 3338 (O-H), 2850 (C-H), 1710 (C=O),

(6-formylpyridin-2-yl)methyl (R)-5-(1,2-dithiolan-3-yl)pentanoate **(MAW05/2PCA-LPA)**

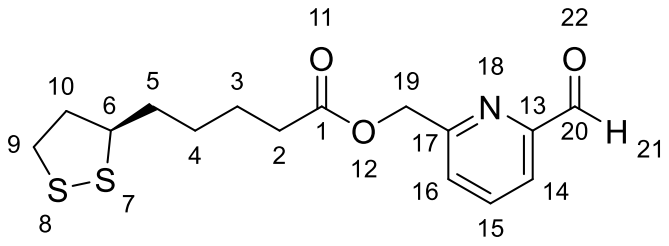

$C_{15}H_{19}NO_3S_2$

MW: 325.08 mol^{-1}

The compound was synthesized using modified procedure from the literature.[129] 6-(Hydroxymethyl)-2-pyridinecarboxaldehyde **(MAW04)** (208 mg, 1.52 mmol) was added to α-lipoic acid (206 mg, 0.99 mmol) in dichloromethane (20 mL) followed by the addition of dimethylaminopyridine (41 mg, 0.34 mmol) and finally N,N'-Dicyclohexylcarbodiimide (242.1 mg, 1.17 mmol). The reaction mixture was then stirred at room temperature for 18 h and then filtered through celite before being concentrated under reduced pressure. The crude was then purified using flash column chromatography (DCM:MeOH, 20:1) to produce a yellow oil of the title compound; **232 mg, 0.71 mmol, 71 %**.

HRMS: (EIS) Calculated for $C_{15}H_{19}NO_3S_2Na$ $[M+Na]^+$ 348.0699; 348.0702 found (mean error 0.9 ppm).

^{1}H NMR: **(400 MHz, CHLOROFORM-*D*)** δ 10.04 (s, 1H, ***H21***), 7.89 (m, *J* = 4.7 Hz, 2H, ***H16,H14***), 7.54-7.60 (m, 1H, ***H15***), 5.31 (s, 2H, ***H19***), 3.61–3.49 (m, 1H, ***H6***), 3.21–3.04 (m, 2H, ***H10***), 2.45 (t, 1H, ***H9***), 1.96–1.82 (m, 1H, ***H5***), 1.81–1.59 (m, 5H, ***H3,H4***), 1.57–1.39 (m, 2H, ***H2***)

13C NMR: (**101 MHz, CHLOROFORM-D**) δ 193.31(C**20**), 173.10(C**1**), 156.91(C**13**), 152.52(C**17**), 137.98(C**15**), 126.01(C**14**), 120.88(C**16**), 66.30(C**19**), 56.42(C**6**), 40.35(C**9**), 38.61(C**10**), 34.70(C**5**), 34.02(C**2**), 28.86(C**4**), 24.74(C**4**).

IR (ATR) (cm^{-1}): 2924 (C-H), 1737 (C=O), 1593 (C=N), 1456 (C-O),

5.2 Electrochemical methods

5.2.1 Potentiostats and software

CV and SWV experiments were done utilising a PocketStat or CompactStat potentiostat (Ivium technologies) using IviumSoft software for windows.

FTacV measurements were done using custom built instruments, which have been described before schematically.[58] These instruments operate utilizing custom software written specifically for the devices known as “pot”.

5.2.2 Electrochemical rig

Electrochemical experiments were done in a three-electrode glass cell made in-house (York Department of Chemistry Glass Workshop), the set-up consists of a disk working electrode (3 mm) (BASi), a platinum wire (Sigma-Aldrich) counter electrode which were made in-house from 1 mm diameter wire, and a reference electrode – either an Ag/AgCl (3 M NaCl) electrode contained within a Luggin capillary (BASi) filled with 3 M NaCl, or a saturated calomel electrode (SCE) using a fritted end (Scientific Laboratory Supplies).

The use of different reference electrodes was due to the fact that Luggin capillaries are not suited for FTaCV measurements, presumed to be unsuitable due to the capillary restricting electrical contact to the electrolyte solution.[130]

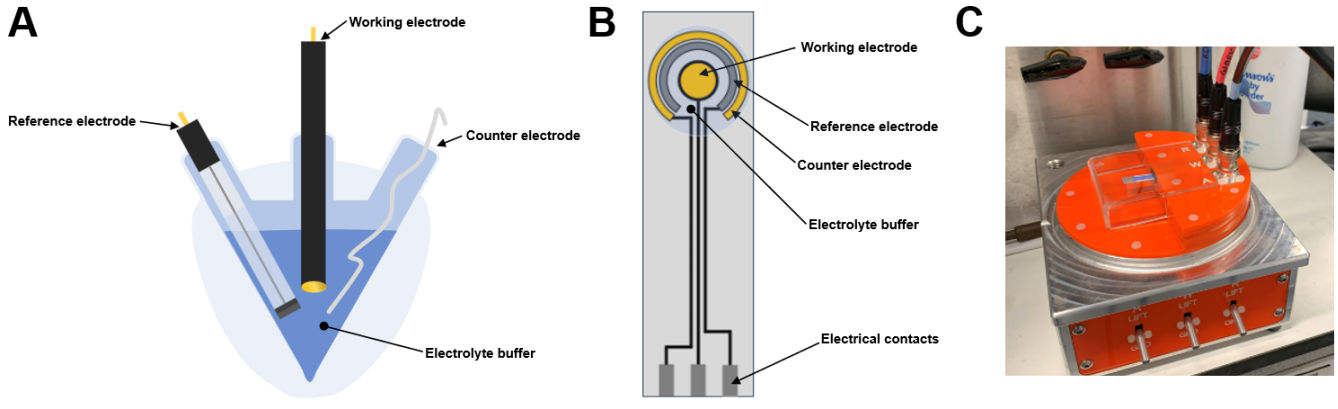

Figure 57 Setup of electrochemical cells for a three-electrode setup as well as diagram of screen-printed electrode (SPE). (A) Electrochemical cell setup used for disk electrodes – reference electrode was switched between a Luggin capillary and a fritted reference electrode depending on the measurement - FTacV requires direct interfacing (fritted reference) with the buffer. (B) Diagram of screen-printed electrode. (C) Photo of the custom SPE connector –used for CV and FTacV measurements due to the ability to unground individual electrodes.

For experiments using SPE's a custom connector was made in-house (York Department of Chemistry Electronics Workshop). The custom device allowed for individual electrodes to be grounded/ungrounded allowing for the use of both Iviumsoft for CV measurements and the custom software "pot" for FTacV measurements.

Experiments conducted inside of a glovebox (in-house design and build) were done under a N_2 atmosphere (O_2 ≤ 25 ppm), buffers were also degassed using N_2 for at least 10 minutes before being left inside of the glovebox overnight. Temperature was controlled using a water-jacket and a thermistor fitted water circulator and experiments were conducted at 25°c, except in SPE experimentation where experiments were done under ambient temperatures. During all experiments rotating electrodes weren't used.

5.2.3 Reference calibration

Potentials are reported versus a standard hydrogen electrode (SHE), when possible. To determine the conversion factor between the reference electrode (Ag/AgCl and Hg/Hg_2Cl_2) used and SHE, experimentation was done to determine the conversion factor (cf). To do so the midpoint potential of ferri/ferrocyanide couple was determined and compared to a literature value of 425 mV.[131] The midpoints for a gold disk electrode using an Ag/AgCl (3M NaCl) reference was determined to be ~182 mV and for a calomel reference electrode ~181 mV. For gold screen printed electrodes (BVT Technologies) using an Ag/AgCl reference a midpoint of ~103 mV was determined.

Using the relationship:

$$E\ (V\ versus\ SHE) = E\ (V\ versus\ Reference) + cf$$

cf was determined by:

$$cf = E\ (V\ versus\ SHE) - E\ (V\ versus\ Reference)$$

Equation 10/11 Equations relating the literature and reference midpoint potentials for a redox couple (ferri/ferrocyanide) for the determination of the conversion factor (cf) for a reference electrode. Below is the rearranged form for cf.

The determined midpoints allowed for the calculation of each conversion factor for a unique reference electrode. This was (for a gold disk electrode) +243 mV for Ag/AgCl (3M NaCl) and +244 mV for a calomel reference electrode. For gold screen printed electrodes a *cf* of +322 mV. Experimental values were determined using cyclic voltammetry of 10 mM $K_3[Fe(CN)^6]$ in 200 mM phosphate buffer, pH 7.0.

5.2.4 Disk electrode preparation

When using working disk electrodes in electrochemical experiments, the electrodes were mechanically polished and electrochemically cleaned immediately before use (> 24 hrs prior to use). Mechanical polishing was done using WhiteFelt polishing pads (Buehler) using alumina suspensions (MetPrep) of decreasing particle sizes: 1.0 (α), 0.3 (α) and 0.05 (γ) μm, polishing for 1 minute per direction (clockwise and anticlockwise). Electrodes were then rinsed with Milli-Q water and sonicated in Milli-Q water and ethanol, for 3 minutes each to remove any residual alumina particles. Electrodes were then dried under N_2. Electrochemical polishing was done using cyclic voltammetry, mechanically polished electrodes were polished using: 50 scans at 100 mV s^{-1} in 0.5 M NaOH (-1.25 to +0.65 V versus Ag/AgCl 3M NaCl) before being rinsed with Milli-Q water and 50 scans at 100 mV s^{-1} in 0.5 M H_2SO_4 (-0.25 to +1.55 V versus Ag/AgCl 3 M NaCl). The mechanical and electrochemical polishing was repeating until a stable voltammogram with the characteristic shape indicative of a gold monolayer surface (***Figure 58***) was seen.

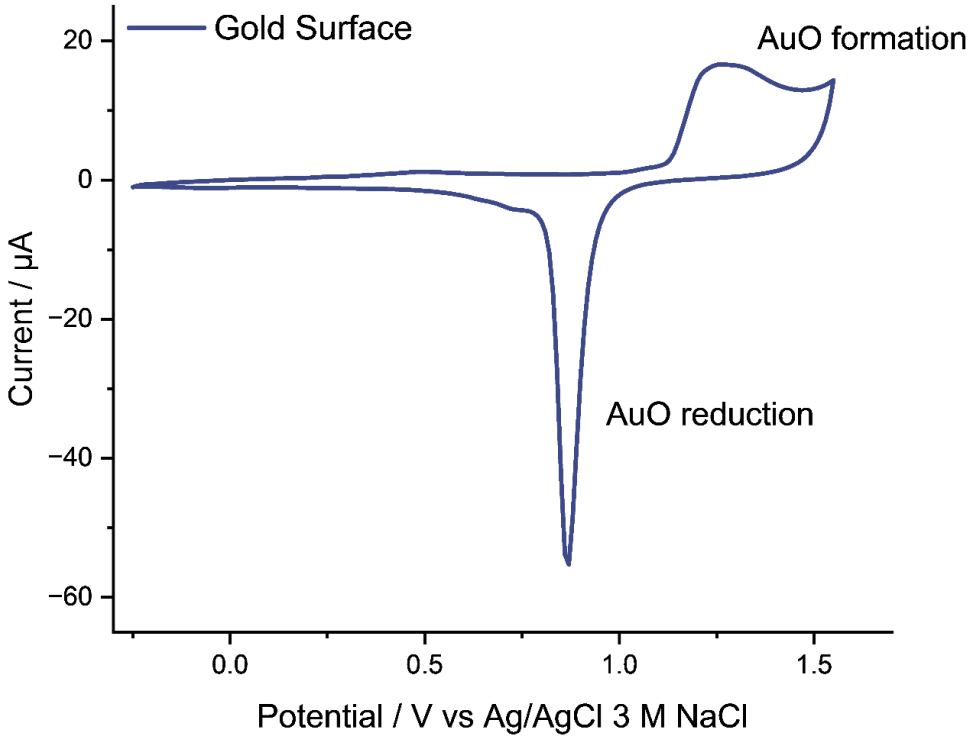

Figure 58: Example voltammogram of polished gold surface in 0.5 M H_2SO_4 at 100 mV s^{-1}. Characteristic areas seen of a polished gold surface are seen in the single cathodic peak representing a reducing AuO monolayer surface.

Immobilisation of the protein onto gold electrode surfaces was the same throughout. Polished and dried surfaces were immersed in a 100 µM solution of the functionalised protein in buffer for 24 hours at ambient temperature, under N_2. Functionalised surfaces were then washed in triplicate pairs, alternating between Milli-Q water and ethanol, before being dried under N_2 gas and used for electrochemical experiments.

5.2.5 Cyclic Voltammetry and Fourier transform alternating current voltammetry measurements

Conditions for cyclic voltammetry (CV) and Fourier transform alternating current voltammetry (FTacV) experiments varied between experiments and details of parameters can be found under relevant figures. In cyclic voltammetry (and FTacV) experiments potential was cycled between limiting potentials, starting at the most positive potential and sweeping to the most negative, this was done at a fixed scan rate unless stated overwise. An equilibration period of 10 seconds was conducted where the potential is held at the starting voltage prior to the scan being recorded. For cyclic voltammetry three scans were recorded as standard; however, the third scans are presented unless stated overwise. For FTacV a single measurement was taken and thus presented.

5.3 Protein related methods

5.3.1 Protein purification

Protein purifications using nickel-affinity chromatography utilising protein His-tags used a HisTrap HP column (Cytiva) using an ÄKTA go (Cytiva). Purification utilising size exclusion chromatography used a Superdex S75 gel filtration column using an ÄKTA pure (Cytiva).

5.3.1.1 Expression and preparation of SHIRT constructs

WT and Di-Cysteine versions of the protein were expressed and purified by Dr Rachael Cooper using an already established protocol. The K64R version of the protein was expressed and purified by Dr Natalia Baranska.

His-tagged versions of the SBtSH3 and any other constructs were prepared, expressed and purified in-house. Plasmids with the custom sequence for SBtSH3 were ordered from GenScript and designed by Dr Natalia Baranska. The custom plasmid was transformed into *E coli*. BL21 DE3 competent cells and glycerol stocks were prepared for later expression.

The transformed *E. coli* was grown aerobically in Lauria-Bertani with 50 μg mL-1 of kanamycin at 37 °C, 180 rpm. Protein expression was induced once the cells had reached an OD_{600} = 0.6 – 0.8 using 1 mM Isopropyl β-D-1-thiogalactopyranoside (IPTG). Cells were then re-incubated overnight at 20 °C, 180 rpm. Cells were then centrifuged (5000 g, 20 mins, 4 °C) and the pellet was re-suspended in 35 mL of buffer A (20 mM Tris, 500 mM NaCl, 20 mM imidazole, pH 7.5) with a EDTA-free protease inhibitor tablet, DNase I (20 μg mL^{-1}), RNase A (20 μg mL^{-1}) and

lysed by sonication on ice. The lysate was centrifuged (30000 g, 40 mins, 4 °C) and the supernatant was purified using three step procedure.

First the SBtSH3 was purified using a HisTrap HP column equilibrated with buffer A. After washing with buffer A. SBtSH3 was extracted over a linear 1-100% imidazole gradient of buffer B (20 mM Tris, 500 mM NaCl, 500 mM imidazole, pH 7.5) over twenty column volumes. Fractions containing the His-tagged SBtSH3 were then collected and monitored using a 15% bis-acrylamide SDS PAGE – as was done after each purification step. The fractions containing His-tag was then cleaved using bovine thrombin at a ratio of 1 unit for every 1 mg of the protein, being dialysed using 3.5 kDA MWCO dialysis tubing in 2 L of buffer A (overnight, 4 °C). Next the his-tag cleaved SBtSH3 was re-purified using a HisTrap HP column using the same procedure as the first step instead collecting the flow through. Finally, the collected fractions were purified using a S75 size exclusion column using buffer C (20 mM Tris, 150 mM NaCl, pH 7.5). Purified SBtSH3 was then concentrated using 5 kDa MWCO protein spin concentrators until the desired concentration was reached, determining concentration using a Bradford assay. The remaining protein was then aliquoted, flash-frozen and stored at -70 °C.

SHIRT is highly soluble and can be stored to concentrations up to 10 mM (~100 mg mL^{-1})

5.3.1.2 Expression and preparation of SH3 c-Src

The plasmid for SH3 domain of c-Src was obtained from Dr Rachael Cooper and was transformed into *E coli*. BL21 DE3 competent cells from which glycerol stocks were prepared for later expression.

A His-tagged construct of SH3 c-Src was prepared, expressed and purified in-house. The transformed plasmid was grown aerobically in Lauria-Bertani with 50 μg mL-1 of kanamycin at 37 °C, 180 rpm. Protein expression was induced once the cells had reached an OD_{600} = 0.6 – 0.8 using 1 mM Isopropyl β-D-1-thiogalactopyranoside (IPTG) where the cells were then incubated overnight at 20 °C, 180 rpm. Cells were then centrifuged (5000 g, 20 mins, 4 °C) and the pellet was re-suspended in 35 mL of buffer A (20 mM Tris, 500 mM NaCl, 20 mM imidazole, pH 7.5) with an EDTA-free protease inhibitor tablet, DNase I (20 μg mL^{-1}), RNase A (20 μg mL^{-1}) and lysed by sonication on ice. The lysate was centrifuged (30000 g, 40 mins, 4 °C) and the supernatant was purified using three step procedure.

First the SH3 c-Src was purified using a HisTrap HP column equilibrated with buffer A. After washing with buffer A. SH3 c-Src was extracted over a linear 1-100% imidazole gradient of buffer B (20 mM Tris, 500 mM NaCl, 500 mM imidazole, pH 7.5) over twenty column volumes. Fractions containing the His-tagged SH3 c-Src were then collected and monitored using a

15% bis-acrylamide SDS PAGE – as was done after each purification step. The fractions containing His-tag was then cleaved using HRV 3C protease in a ratio of 1:500 to the protein, being dialysed using 3.5 kDA MWCO dialysis tubing in 2 L of buffer A (overnight, 4 °C). Next the his-tag cleaved SH3 c-Src was re-purified using a HisTrap HP column using the same procedure as the first step instead collecting the flow through. Finally, the collected fractions were purified using a S75 size exclusion column using buffer C (20 mM Tris, 150 mM NaCl, pH 7.5). Purified SH3 c-Src was then concentrated using 3 kDa MWCO protein spin concentrators until the desired concentration was reached, determining concentration using a Bradford assay. The remaining protein was then aliquoted, flash-frozen and stored at -70 °C.

5.3.2 Protein bioconjugation (Redox mediator)

The modification of proteins using viologen molecule EVC-NHS using methodology described by Thermofisher Scientific.[132]

Typically, ratios of DMF to buffer was 10% and concentration of EV NHS in DMF was 10x that of the of protein. Most reactions were carried out with 250 μM solutions of protein.

Viologen modified proteins were produced by the addition of 100 equivalents of EV NHS (0.25 mM) in DMF to the protein (250 μM) in 100 mM sodium phosphate, 150 mM sodium NaCl, pH 7.5. The reaction mixture was then shaken at 25°c for an hour, before adding hydroxylamine to a final concentration of 10 mM to quench any excess NHS ester. Once again, the mixture was shaken at 25°c for an hour, before being buffer exchanged using a 3k MWCO protein spin concentrator (1200xg, 15min, 4°c) into 100 mM sodium phosphate, 150 mM sodium NaCl, pH 7.5 and isolated using a desalting column. Concentration was measured using a BCA assay (Pierce BCA Assay Kit, Thermo Scientific) before being aliquoted, flash frozen and stored at –70°C.

Variation in the equivalents of EV NHS was tested and apparent 100% modification was observed at values >25 by SDS-PAGE, however 100 equivalents was used to ensure total modification of lysine residues on the protein.

5.3.3 Protein bioconjugation (N-terminus)

The original conditions for targeted N-terminal modification were designed by Lydia Barber described in their doctoral dissertation. A variety of conditions was screened and the most effective described below.

200 µL of 100 µM SHIRT in PBS (100 mM sodium phosphate, 150 mM NaCl) was mixed with 200 µL of 500 mM 2PCA-LPA in DMF. The reaction was allowed to react at 25˚c for 18 hours (overnight). The mixture was then transferred into a dialysis setup using PBS and allowed to dialyse at 4˚c. After, samples were taken for LC-MS to quantify the conversion of N-terminus and for electrode immobilisation multiple reactions were pooled together and concentrated using a 3k MWKO spin concentrator. Increasing the concentration of 2PCA-LPA caused the molecule to aggregate using the reaction conditions stated.

5.3.4 Plate reader assay

A CLARIOstar Plus (BMG Labtech) plate reader was used in plate reader assays and data was analysed using MARS data analysis software (BMG Labtech). Assays used 96 well, PS, U-bottom, clear microplates from Greiner.

Bicinchoninic acid (BCA) assays were done by making standards of bovine serum albumin (BSA) prepared between 0 and 2000 µg mL^{-1} using serial dilution in the same buffer as the relevant protein storage buffer. Working reagent was prepared using a Pierce™ BCA protein assay kit purchased from Thermoscientific using a 50:1 ratio of reagents A:B. 25 µL of each sample was mixed with 200 µL of working reagent and incubated for thirty minutes at 37°c. The samples were allowed to cool to room temperature and absorbance at 562 nm recorded. Protein concentration was calculated using a standard curve produced using the BSA standards.

Ellman's assays were conducted by making standards of cysteine prepared between 0 and 1500 µM using serial dilution in a pH 8.0 sodium phosphate (100 mM) containing EDTA (1 mM). Ellman's reagent solution was made by dissolving 4 mg of DTNB in 1 mL of reaction buffer. 250 µL of each sample was added to solution containing 50 µL of Ellman's reagent solution and 250 µL of reagent buffer. The reaction solutions were then incubated for fifteen minutes at 25°c, and then samples absorbances were measured at 412 nm. Free sulfhydryl concentration was determined by plotting a standard curve using the cysteine standards and comparing protein samples concentrations.

5.4 Chapter 2 experimental procedures

5.4.1 Electrochemical binding experiments involving SBtSH3.EV and SH3 c-Src.

Measurements were done in air utilising a custom SPE connector allowing for the ungrounding of individual electrodes. SPE's were submerged in an Eppendorf filled with buffer with a custom lid, made in-house, allowing for the fitting of SPE's without the loss of buffer due to evaporation.

5.4.1.1 SBtSH3.EV titration experiment

The minimum concentration for SH3 c-Src binding to SBtSH3.EV was done by initially cycling SBtSH3.EV functionalised electrodes in PBS (100 mM sodium phosphate, 150 mM NaCl) until stability was seen in the scans before taking the electrode and submerging in low concentration SH3 c-Src for thirty minutes. The electrode was washed off and response recorded with FTacV before re-submerging in SH3 c-Src, increasing concentration with each subsequent experiment and was done in a range of 10 nm – 400 μM.

5.4.1.2 SBtSH3.EV rate experiment

Rate experiments were done by submerging redox protein assembled electrodes into PBS (100 mM sodium phosphate, 150 mM NaCl) and FTacV scans were cycled until stabilisation of the observed signal. The electrode was then submerged into a solution of PBS with 100 nM SH3 c-Src and FTacV measurements were taken every thirty seconds for five minutes, before then taking measurements at minute intervals until fifteen minutes. The electrode was then transferred into a fresh PBS solution and measurements were taken every minute for fifteen minutes then every five minutes until thirty minutes had elapsed in PBS.

6 Appendix

6.1 N-terminal 2PCA-LP conversion rate table

Solvent	pH	Temperature (°C)	Equivalents	Time (hr)	Ratio (buffer:solvent)	% conversion
DMF	7.5	25	500	18	1:1	**87.1**
DMF	7.5	35	300	18	1:1	**84.3**
DMF	7.5	35	400	18	1:1	**84.2**
DMF	7.5	35	500	18	1:1	**83.5**
DMF	7.5	25	100	18	1:1	**82.8**
DMF	7.5	35	600	18	1:1	**82.7**
DMF	7.5	25	250	6	1:1	**77.6**
DMF	7.5	25	250	18	1:1	**75.8**
DMF	7.5	35	100	18	1:1	**69.3**
DMF	7.5	35	250	18	1:1	**69.2**
DMF	7.5	25	100	18	1:1	**66.4**
DMF	7.5	25	100	6	1:1	**66.3**
DMF	7.5	25	500	6	1:1	**43.8**
DMF	7.5	25	100	3	1:1	**39.6**
DMF	6.5	25	100	18	1:1	**31.6**
DMF	7.5	5	100	18	1:1	**31**
DMF	7.5	25	500	18	3:1	**22.2**
DMF	5.5	25	100	18	1:1	**17.3**
DMF	7.5	25	100	1	1:1	**15**
DMF	7.5	25	100	18	3:1	**13**
DMF	7.5	5	100	6	1:1	**9.8**
DMF	7.5	55	100	18	1:1	**9**
DMF	7.5	5	100	3	1:1	**7.3**
DMF	7.5	25	100	18	5:1	**7**
DMF	7.5	25	500	18	5:1	**5.9**
DMF	7.5	5	100	1	1:1	**<5**
DMF	7.5	5	250	18	1:1	**<5**
DMF	4.5	25	100	18	1:1	**<5**
DMF	7.5	47	100	18	1:1	**<5**

DMF	6.5	47	100	18	1:1	**<5**
DMF	5.5	47	100	18	1:1	**<5**
DMSO	7.5	25	100	18	1:1	**57.2**
DMSO	6.5	25	100	18	1:1	**26.6**
DMSO	7.5	55	100	18	1:1	**9.8**
DMSO	5.5	25	100	18	1:1	**5.6**
DMSO	7.5	47	100	18	1:1	**<5**
DMSO	6.5	47	100	18	1:1	**<5**
DMSO	5.5	47	100	18	1:1	**<5**

Table 3 N-terminal conversion rates for 2PCA-LP screened over different reaction condition, sorted by solvent type and % conversion.

Reference list

1 X. Wang, Y. Luo, K. Huang and N. Cheng, *Advanced Agrochem*, 2022, **1**, 3–6.

2 Y. Huang, J. Xu, J. Liu, X. Wang and B. Chen, *Sensors (Basel)*, 2017, **17**, 2375.

3 A. Servati, L. Zou, Z. J. Wang, F. Ko and P. Servati, *Sensors (Basel)*, 2017, **17**, 1622.

4 J. Budd, B. S. Miller, N. E. Weckman, D. Cherkaoui, D. Huang, A. T. Decruz, N. Fongwen, G.-R. Han, M. Broto, C. S. Estcourt, J. Gibbs, D. Pillay, P. Sonnenberg, R. Meurant, M. R. Thomas, N. Keegan, M. M. Stevens, E. Nastouli, E. J. Topol, A. M. Johnson, M. Shahmanesh, A. Ozcan, J. J. Collins, M. Fernandez Suarez, B. Rodriguez, R. W. Peeling and R. A. McKendry, *Nat Rev Bioeng*, 2023, **1**, 13–31.

5 ACT Team, *The ACT-Accelerator: Two years of impact*, World Health Organization, 2022.

6 L. C. Clark Jr and C. Lyons, *Ann. N. Y. Acad. Sci.*, 1962, **102**, 29–45.

7 N. Bhalla, P. Jolly, N. Formisano and P. Estrela, *Essays Biochem.*, 2016, **60**, 1–8.

8 V. Naresh and N. Lee, *Sensors (Basel)*, 2021, **21**, 1109.

9 S. A. Spring, S. Goggins and C. G. Frost, *Molecules*, 2021, **26**, 2130.

10 D. Grieshaber, R. MacKenzie, J. Vörös and E. Reimhult, *Sensors* , 2008, **8**, 1400–1458.

11 M. L. Chiu, D. R. Goulet, A. Teplyakov and G. L. Gilliland, *Antibodies (Basel)*, 2019, **8**, 55.

12 A. Bogomolova, E. Komarova, K. Reber, T. Gerasimov, O. Yavuz, S. Bhatt and M. Aldissi, *Anal. Chem.*, 2009, **81**, 3944–3949.

13 A. Burrows, J. Holman, S. Lancaster, T. Overton, A. Parsons, G. Pilling and G. Price, in *Chemistry3*, Oxford University Press, 2021.

14 R. K. Tyagi, N. Garg, R. Shukla and P. S. Bisen, *Role of novel drug delivery vehicles in nanobiomedicine*, IntechOpen, London, England, 2020.

15 Y. Liu, N. Tuleouva, E. Ramanculov and A. Revzin, *Anal. Chem.*, 2010, **82**, 8131–8136.

16 B. Byrne, E. Stack, N. Gilmartin and R. O'Kennedy, *Sensors (Basel)*, 2009, **9**, 4407–4445.

17 D. Mann, C. Reinemann, R. Stoltenburg and B. Strehlitz, *Biochem. Biophys. Res. Commun.*, 2005, **338**, 1928–1934.

18 J. Hidding, .

19 Z. Chen, L. Hu, B.-T. Zhang, A. Lu, Y. Wang, Y. Yu and G. Zhang, *Int. J. Mol. Sci.*, 2021, **22**, 3605.

20 B. Sequeira-Antunes and H. A. Ferreira, *Biomedicines*, 2023, **11**, 3201.

21 X. Ni, M. Castanares, A. Mukherjee and S. E. Lupold, *Curr. Med. Chem.*, 2011, **18**, 4206–4214.

22 A. V. Lakhin, V. Z. Tarantul and L. V. Gening, *Acta Naturae*, 2013, **5**, 34–43.

23 C. Y. Loo, D. A. Corliss and N. Ganeshkumar, *J. Bacteriol.*, 2000, **182**, 1374–1382.

24 I. M. Tleyjeh, J. M. Steckelberg, H. S. Murad, N. S. Anavekar, H. M. K. Ghomrawi, Z. Mirzoyev, S. E. Moustafa, T. L. Hoskin, J. N. Mandrekar, W. R. Wilson and L. M. Baddour, *JAMA*, 2005, **293**, 3022–3028.
25 Y. Takahashi, E. Takashima, K. Shimazu, H. Yagishita, T. Aoba and K. Konishi, *Infect. Immun.*, 2006, **74**, 740–743.
26 Å. Nylander, G. Svensäter, D. B. Senadheera, D. G. Cvitkovitch, J. R. Davies and K. Persson, *PLoS One*, 2013, **8**, e63768.
27 A. V. Kajava, *J. Struct. Biol.*, 2012, **179**, 279–288.
28 F. Whelan, A. Lafita, J. Gilburt, C. Dégut, S. C. Griffiths, H. T. Jenkins, A. N. St John, E. Paci, J. W. B. Moir, M. J. Plevin, C. G. Baumann, A. Bateman and J. R. Potts, *Proc. Natl. Acad. Sci. U. S. A.*, 2021, **118**, e2101349118.
29 R. Cooper, PhD, University of York, 2021.
30 A. Borgia, K. R. Kemplen, M. B. Borgia, A. Soranno, S. Shammas, B. Wunderlich, D. Nettels, R. B. Best, J. Clarke and B. Schuler, *Nat. Commun.*, 2015, **6**, 8861.
31 M. Plevin, .
32 M. V. Rodionova, R. S. Poudyal, I. Tiwari, R. A. Voloshin, S. K. Zharmukhamedov, H. G. Nam, B. K. Zayadan, B. D. Bruce, H. J. M. Hou and S. I. Allakhverdiev, *Int. J. Hydrogen Energy*, 2017, **42**, 8450–8461.
33 A. C. Gray, A. R. M. Bradbury, A. Knappik, A. Plückthun, C. A. K. Borrebaeck and S. Dübel, *Nat. Methods*, 2020, **17**, 755–756.
34 M. Mehrabipour, N. S. K. Jasemi, R. Dvorsky and M. R. Ahmadian, *Cells*, 2023, **12**, 2054.
35 M. H. Ahmed, M. S. Ghatge and M. K. Safo, *Subcell. Biochem.*, 2020, **94**, 345–382.
36 R. Höhner, M. Pribil, M. Herbstová, L. S. Lopez, H.-H. Kunz, M. Li, M. Wood, V. Svoboda, S. Puthiyaveetil, D. Leister and H. Kirchhoff, *Proc. Natl. Acad. Sci. U. S. A.*, 2020, **117**, 15354–15362.
37 I.-G. Lee and B.-J. Lee, *Antioxidants (Basel)*, 2021, **10**, 502.
38 J. C. Lewis, *ACS Catal.*, 2013, **3**, 2954–2975.
39 A. J. Thomson and H. B. Gray, *Curr. Opin. Chem. Biol.*, 1998, **2**, 155–158.
40 J. Finkelstein, *Nature*, 2009, **460**, 813.
41 K. Yaku, K. Okabe, M. Gulshan, K. Takatsu, H. Okamoto and T. Nakagawa, *Sci. Rep.*, 2019, **9**, 13102.
42 S. Prabhulkar, H. Tian, X. Wang, J.-J. Zhu and C.-Z. Li, *Antioxid. Redox Signal.*, 2012, **17**, 1796–1822.
43 H. Wei and E. Wang, *Chem. Soc. Rev.*, 2013, **42**, 6060–6093.
44 Z. Dong, Q. Luo and J. Liu, *Chem. Soc. Rev.*, 2012, **41**, 7890–7908.
45 C. E. Valdez, Q. A. Smith, M. R. Nechay and A. N. Alexandrova, *Acc. Chem. Res.*, 2014, **47**, 3110–3117.

46 A. Y. Chen, R. N. Adamek, B. L. Dick, C. V. Credille, C. N. Morrison and S. M. Cohen, *Chem. Rev.*, 2019, **119**, 1323–1455.
47 A. J. Bard and L. R. Faulkner, *Electrochemical Methods: Fundamentals and Applications*, Wiley, 2001.
48 E. Laviron, *J. Electroanal. Chem. Interfacial Electrochem.*, 1979, **101**, 19–28.
49 K. Oldham, J. Myland and A. Bond, *Electrochemical Science and Technology: Fundamentals and Applications*, Wiley, 2011.
50 K. Bano, G. F. Kennedy, J. Zhang and A. M. Bond, *Phys. Chem. Chem. Phys.*, 2012, **14**, 4742–4752.
51 H. Adamson, A. M. Bond and A. Parkin, *Chem. Commun. (Camb.)*, 2017, **53**, 9519–9533.
52 J. Zhang, S.-X. Guo, A. M. Bond and F. Marken, *Anal. Chem.*, 2004, **76**, 3619–3629.
53 A. M. Bond, D. Elton, S.-X. Guo, G. F. Kennedy, E. Mashkina, A. N. Simonov and J. Zhang, *Electrochem. Commun.*, 2015, **57**, 78–83.
54 H. O. Lloyd-Laney, M. J. Robinson, A. M. Bond, A. Parkin and D. J. Gavaghan, *J. Electroanal. Chem. (Lausanne Switz)*, 2021, **894**, 115204.
55 H. O. Lloyd-Laney, N. D. J. Yates, M. J. Robinson, A. R. Hewson, J. Branch, G. R. Hemsworth, A. M. Bond, A. Parkin and D. J. Gavaghan, *J. Electroanal. Chem. (Lausanne Switz)*, 2023, **935**, 117264.
56 A. R. Dale-Evans, M. J. Robinson, H. O. Lloyd-Laney, D. J. Gavaghan, A. M. Bond and A. Parkin, *Front. Chem.*, 2021, **9**, 672831.
57 H. O. Lloyd-Laney, N. D. J. Yates, M. J. Robinson, A. R. Hewson, J. D. Firth, D. M. Elton, J. Zhang, A. M. Bond, A. Parkin and D. J. Gavaghan, *Anal. Chem.*, 2021, **93**, 2062–2071.
58 A. M. Bond, N. W. Duffy, S.-X. Guo, J. Zhang and D. Elton, *Anal. Chem.*, 2005, **77**, 186A-195A.
59 N. G. Baranska, B. Jones, M. R. Dowsett, C. Rhodes, D. M. Elton, J. Zhang, A. M. Bond, D. Gavaghan, H. O. Lloyd-Laney and A. Parkin, *ACS Meas. Sci. Au*, 2024, **4**, 418–431.
60 Z. Zhuo, Y. Yu, M. Wang, J. Li, Z. Zhang, J. Liu, X. Wu, A. Lu, G. Zhang and B. Zhang, *IJMS*, 2017, **18**, 2142.
61 Y. Biniuri, G.-F. Luo, M. Fadeev, V. Wulf and I. Willner, *J. Am. Chem. Soc.*, 2019, **141**, 15567–15576.
62 C. S. McKay and M. G. Finn, *Chem. Biol.*, 2014, **21**, 1075–1101.
63 O. Koniev and A. Wagner, *Chem. Soc. Rev.*, 2015, **44**, 5495–5551.
64 C. D. Spicer and B. G. Davis, *Nat. Commun.*, 2014, **5**, 4740.
65 J. Kalia and R. T. Raines, *Curr. Org. Chem.*, 2010, **14**, 138–147.
66 N. Stephanopoulos and M. B. Francis, *Nat. Chem. Biol.*, 2011, **7**, 876–884.
67 C. Zhang, E. V. Vinogradova, A. M. Spokoyny, S. L. Buchwald and B. L. Pentelute, *Angew. Chem. Int. Ed Engl.*, 2019, **58**, 4810–4839.

68 M. J. Matos, B. L. Oliveira, N. Martínez-Sáez, A. Guerreiro, P. M. S. D. Cal, J. Bertoldo, M. Maneiro, E. Perkins, J. Howard, M. J. Deery, J. M. Chalker, F. Corzana, G. Jiménez-Osés and G. J. L. Bernardes, *J. Am. Chem. Soc.*, 2018, **140**, 4004–4017.

69 G. T. Hermanson, *Bioconjugate Techniques*, Academic Press, San Diego, CA, 3rd edn., 2013.

70 R. Shemesh, A. Novik and Y. Cohen, *Genomics Proteomics Bioinformatics*, 2010, **8**, 180–189.

71 B. Hardt and E. Bause, *Biochem. Biophys. Res. Commun.*, 2002, **291**, 751–757.

72 D. M. Anstrom, L. Colip, B. Moshofsky, E. Hatcher and S. J. Remington, *Acta Crystallogr. Sect. F Struct. Biol. Cryst. Commun.*, 2005, **61**, 1069–1074.

73 A. J. Lomant and G. Fairbanks, *J. Mol. Biol.*, 1976, **104**, 243–261.

74 J. V. Staros, R. W. Wright and D. M. Swingle, *Anal. Biochem.*, 1986, **156**, 220–222.

75 J.-R. Deng, N. C.-H. Lai, K. K.-Y. Kung, B. Yang, S.-F. Chung, A. S.-L. Leung, M.-C. Choi, Y.-C. Leung and M.-K. Wong, *Commun. Chem.*, 2020, **3**, 67.

76 H. Jiang, G. D. D'Agostino, P. A. Cole and D. R. Dempsey, *Methods Enzymol.*, 2020, **639**, 333–353.

77 A. G. Reid and C. W. Machan, *J. Am. Chem. Soc.*, 2023, **145**, 2013–2027.

78 T. Zhang, Q. Chen, X. Li, J. Liu, W. Zhou, B. Wang, Z. Zhao, W. Li, D. Chao and D. Zhao, *CCS Chem*, 2022, **4**, 2874–2887.

79 K. Tsukahara and H. Todorobaru, *Chem. Lett.*, 1992, **21**, 1181–1184.

80 M. Berville, J. Richard, M. Stolar, S. Choua, N. Le Breton, C. Gourlaouen, C. Boudon, L. Ruhlmann, T. Baumgartner, J. A. Wytko and J. Weiss, *Org. Lett.*, 2018, **20**, 8004–8008.

81 S. Ašpergěr, *Trans. Faraday Soc.*, 1952, **48**, 617–624.

82 E. M. Fell, D. De Porcellinis, Y. Jing, V. Gutierrez-Venegas, T. Y. George, R. G. Gordon, S. Granados-Focil and M. J. Aziz, *J. Electrochem. Soc.*, 2023, **170**, 070525.

83 M. Quan, D. Sanchez, M. F. Wasylkiw and D. K. Smith, *J. Am. Chem. Soc.*, 2007, **129**, 12847–12856.

84 R. J. Mortimer, *Annu. Rev. Mater. Res.*, 2011, **41**, 241–268.

85 W. Wu, S. Guo, J. Bian, X. He, H. Li and J. Li, *J. Energy Chem.*, 2024, **93**, 453–470.

86 Macdonald A. M. G., Pardue Harry L., Townshend Alan, Clerc J. T., Ed., *Analytica Chimica Acta*, Elsevier, 1982, vol. 140.

87 N. G. Baranska, phd, University of York, 2023.

88 F. J. M. Hoeben, I. Heller, S. P. J. Albracht, C. Dekker, S. G. Lemay and H. A. Heering, *Langmuir*, 2008, **24**, 5925–5931.

89 M. Li, P. He, Y. Zhang and N. Hu, *Biochim. Biophys. Acta*, 2005, **1749**, 43–51.

90 W. Sun, R. Gao and K. Jiao, *J. Phys. Chem. B*, 2007, **111**, 4560–4567.

91 R. Gulaboski, V. Mirčeski, I. Bogeski and M. Hoth, *J. Solid State Electrochem.*, 2012, **16**, 2315–2328.
92 L. Barber and C. Spicer, *ChemRxiv*, 2024.
93 H. N. Bridge, W. Leiter, C. L. Frazier and A. M. Weeks, *Cell Chem. Biol.*, 2024, **31**, 534-549.e8.
94 J. M. Abad, S. F. L. Mertens, M. Pita, V. M. Fernández and D. J. Schiffrin, *J. Am. Chem. Soc.*, 2005, **127**, 5689–5694.
95 K. Bandyopadhyay, S.-G. Liu, H. Liu and L. Echegoyen, *Chemistry*, 2000, **6**, 4385–4392.
96 N. Anand, P. Ramudu, K. H. P. Reddy, K. S. R. Rao, B. Jagadeesh, V. S. P. Babu and D. R. Burri, *Appl. Catal. A Gen.*, 2013, **454**, 119–126.
97 L. Michaelis and E. S. Hill, *J. Gen. Physiol.*, 1933, **16**, 859–873.
98 A. G. Mauk and G. R. Moore, *J. Biol. Inorg. Chem.*, 1997, **2**, 119–125.
99 D. A. Moffet, J. Foley and M. H. Hecht, *Biophys. Chem.*, 2003, **105**, 231–239.
100 D. A. Koomson, J. H. Nicholson, A. P. S. Brogan and L. Aldous, *Chem. Sci.*, 2024, **15**, 9325–9332.
101 J. F. Stargardt and F. M. Hawkridge, *Anal. Chim. Acta*, 1983, **146**, 1–8.
102 T. Watanabe and K. Honda, *J. Phys. Chem.*, 1982, **86**, 2617–2619.
103 M. Haque, N. Forte and J. R. Baker, *Chem. Commun. (Camb.)*, 2021, **57**, 10689–10702.
104 S. M. Sarrett, C. Rodriguez, G. Rymarczyk, M. M. Hosny, O. Keinänen, S. Delaney, S. Thau, B. A. Krantz and B. M. Zeglis, *Bioconjug. Chem.*, 2022, **33**, 1750–1760.
105 A. Tantipanjaporn and M.-K. Wong, *Molecules*, 2023, **28**, 1083.
106 A. L. Eckermann, D. J. Feld, J. A. Shaw and T. J. Meade, *Coord. Chem. Rev.*, 2010, **254**, 1769–1802.
107 H. Adamson, A. N. Simonov, M. Kierzek, R. A. Rothery, J. H. Weiner, A. M. Bond and A. Parkin, *Proc. Natl. Acad. Sci. U. S. A.*, 2015, **112**, 14506–14511.
108 L. J. Barber, N. D. J. Yates, M. A. Fascione, A. Parkin, G. R. Hemsworth, P. G. Genever and C. D. Spicer, *RSC Chem Biol*, 2023, **4**, 56–64.
109 L. De Rosa, R. Di Stasi, A. Romanelli and L. D. D'Andrea, *Molecules*, 2021, **26**, 3521.
110 P. S. Lamoureux, A. R. Singh and K. Chan, *ACS Catal.*, 2019, **9**, 6194–6201.
111 K. Cho, S. Park, J. Chang and S.-H. Han, *J. Electroanal. Chem. (Lausanne Switz)*, 2016, **764**, 71–78.
112 S. Hu, C. Xu, Y. He, L. Meng and D. Cui, *Microchem. J.*, 2000, **65**, 311–317.
113 N. Oyama, N. Oki, H. Ohno, Y. Ohnuki, H. Matsuda and E. Tsuchida, *J. Phys. Chem.*, 1983, **87**, 3642–3647.
114 Q. Lin, Q. Li, C. Batchelor-McAuley and R. G. Compton, *Phys. Chem. Chem. Phys.*, 2013, **15**, 7760–7767.

115 Q. Lin, Q. Li, C. Batchelor-McAuley and R. G. Compton, *J. Electrochem. Sci. Technol.*, 2013, **4**, 71–80.
116 Y. Yan, L. Zhang, T. Xu, J. Zhou, R. Qin, C. Chen, Y. Zou, D. Fu, G. Hu, J. Chen and Y. Lu, *PLoS One*, 2013, **8**, e81905.
117 N. Kurochkina and U. Guha, *Biophys. Rev.*, 2013, **5**, 29–39.
118 S. Singh, J. Wang and S. Cinti, *ECS Sens. Plus*, 2022, **1**, 023401.
119 G. Liang, Z. He, J. Zhen, H. Tian, L. Ai, L. Pan and W. Gong, *Environ. Technol. Innov.*, 2022, **28**, 102922.
120 R. D. Crapnell and C. E. Banks, *ChemElectroChem*, 2024, **11**, e202400370.
121 A. E. F. Oliveira, A. C. Pereira and M. A. C. de Resende, *Electroanalysis*, 2022, **35**, e202200093.
122 A. Hill, A. Hill and A. Paganini-Hill, *The Journal of Physiology*, 1910, **40**, 4–7.
123 M. Harkiolaki, M. Lewitzky, R. J. C. Gilbert, E. Y. Jones, R. P. Bourette, G. Mouchiroud, H. Sondermann, I. Moarefi and S. M. Feller, *EMBO J.*, 2003, **22**, 2571–2582.
124 R. J. Rickles, M. C. Botfield, X. M. Zhou, P. A. Henry, J. S. Brugge and M. J. Zoller, *Proc. Natl. Acad. Sci. U. S. A.*, 1995, **92**, 10909–10913.
125 J. Gemperle, R. Hexnerová, M. Lepšík, P. Tesina, M. Dibus, M. Novotný, J. Brábek, V. Veverka and D. Rosel, *Sci. Rep.*, 2017, **7**, 8057.
126 H. Yamaguchi and A. Harada, *Biomacromolecules*, 2002, **3**, 1163–1169.
127 M. Passon, A. Ruff, P. Schuler, B. Speiser and W. Leis, *J. Solid State Electrochem.*, 2015, **19**, 85–101.
128 J. I. MacDonald, H. K. Munch, T. Moore and M. B. Francis, *Nat. Chem. Biol.*, 2015, **11**, 326–331.
129 R. Kodela, M. Chattopadhyay and K. Kashfi, *ACS Med. Chem. Lett.*, 2012, **3**, 257–262.
130 N. D. J. Yates, PhD, University of York, 2021.
131 J. E. O'Reilly, *Biochim. Biophys. Acta*, 1973, **292**, 509–515.
132 Thermofisher, *Bioconjugation and crosslinking technical handbook*, Thermofisher Scientific, 2022.